Physics of Radioactive Beams[1]

Chapter 6

Coulomb Excitation

Carlos A. Bertulani, Texas A&M University-Commerce, TX 75429, USA

[1]These notes consist of a series of lectures presented by the author at the Geselschaft für Schwerionenforschung, Darmstadt, Germany in the Spring of 1994. GSI-Report 1994-11. This material was latter extended and published in the book "Physics of Radioactive Beams", C.A. Bertulani, M. Hussein and G. Muenzenberg, Nova Science, Hauppage, NY, 2002, ISBN: 1-59033-141-9

0.1 Introduction

In relativistic heavy ion collisions, the wavelength associated with the projectile-target separation is much smaller than the characteristic length of system. It is, therefore, a reasonable approximation to treat $\mathbf{r}$ as a classical variable $\mathbf{r}(t)$, given at each instant by the trajectory followed by the relative motion. At high energies, is also a good approximation to replace this trajectory by a straight line. The intrinsic dynamics can then be handled as a quantum mechanics problem with a time dependent Hamiltonian. This treatment is discussed in full details by Alder and Winther in Refs. [1, 2, 3].

The intrinsic state $|\psi(t)>$ satisfies the Schrödinger equation

$$[h \ + \ V(\mathbf{r}(t))] \ |\psi(t)>= i\hbar \frac{\partial |\psi(t)>}{\partial t}. \tag{1}$$

In the equation above, h is the intrinsic Hamiltonian and V is the channel-coupling interaction.

Expanding the wave function in the set $\{|m>; \ m = 0, N\}$ of eigenstates of h, where N is the number of excited states included in the Coupled-Channels problem, we obtain

$$|\psi(t)>= \sum_{m=0}^{N} \ a_m(t) \ |m> \ \exp\left(-iE_m t/\hbar\right), \tag{2}$$

where E_m is the energy of the state $|m>$. Taking scalar product with each of the states $< n|$, we get the set of coupled equations

$$i\hbar \ \dot{a}_n(t) = \sum_{m=0}^{N} \ < n|V|m> \ e^{i(E_n - E_m)t/\hbar} \ a_m(t), \qquad\qquad n = 0 \text{ to } \ N\,. \tag{3}$$

It should be remarked that the amplitudes depend also on the impact parameter b specifying the classical trajectory followed by the system. For the sake of keeping the notation simple, we do not indicate this dependence explicitly. We write, therefore, $a_n(t)$ instead of $a_n(b,t)$. Since the interaction V vanishes as $t \to \pm\infty$, the amplitudes have as initial condition $a_n(t \to -\infty) = \delta(n,0)$ and they tend to constant values as $t \to \infty$. Therefore, the excitation probability of an intrinsic state $|n>$ in a collision with impact parameter b is given as

$$P_n(b) = |a_n(\infty)|^2. \tag{4}$$

The total cross section for excitation of the state $|n>$ can be approximated by the classical expression

$$\sigma_n = 2\pi \ \int \ P_n(b) \ bdb. \tag{5}$$

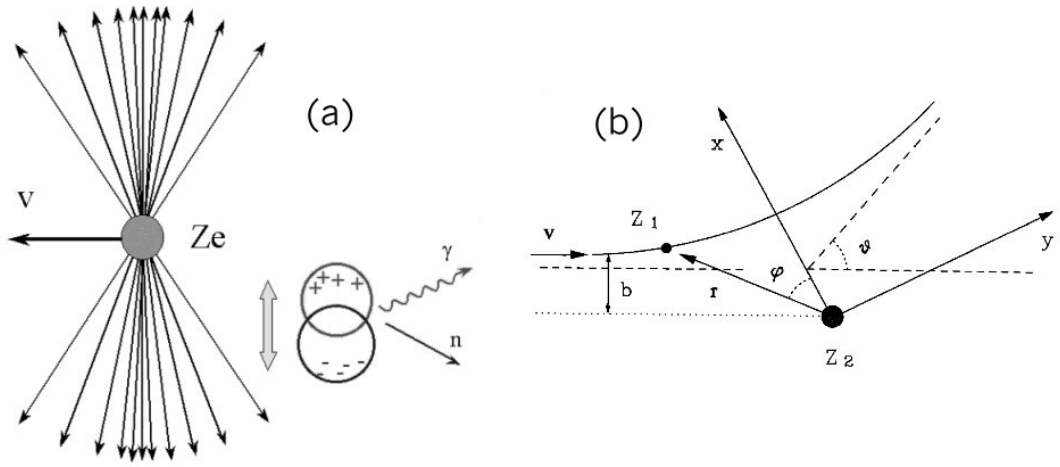

Figure 1: (a) The Coulomb field of a fast moving particle (nucleus) excites another nucleus as it passes by in a peripheral collision. The process involves the excitation followed by gamma- or particle-decay of stable and unstable nuclei. (b) A nuclear target is Coulomb excited by a projectile moving along a modified Rutherford trajectory. The coordinates used in text are shown.

Since we are interested in the excitation of specific nuclear states, with good angular momentum and parity quantum numbers, it is appropriate to develop the time-dependent coupling interaction $V(t)$ into multipoles. In Ref. [3], a multipole expansion of the electromagnetic excitation amplitudes in relativistic heavy ion collisions was carried out. This work used first order perturbation theory and the semiclassical approximation. The time-dependence of the multipole interactions was not explicitly given. This was accomplished in Ref. [4] (see also [5, 6]), which we describe after Supplement A.

We will discuss the methods used for the description of Coulomb excitation, specially at intermediate and high energy collisions ($E_{lab} \gtrsim 100$ MeV/nucleon). We will also show some applications of the theory for reactions involving stable nuclei. In particular, most of the applications will invoke the excitation of giant resonances in Coulomb excitation of stable nuclei (see Fig. 1).

Supplement A

0.2 The electromagnetic interaction

The equation of motion of a charge in an electromagnetic field is given by

$$\frac{d}{dt}\frac{m\mathbf{v}}{\sqrt{1-\mathrm{v}^2/c^2}} = q(\mathbf{E}+\frac{\mathbf{v}}{c}\times\mathbf{B}\ ). \tag{6}$$

Since one can write

$$\mathbf{B}=\nabla\times\mathbf{A}\ ; \qquad \mathbf{E}=-\nabla\phi-\frac{1}{c}\frac{\partial\mathbf{A}}{\partial t}, \tag{7}$$

we get

$$\begin{aligned}\frac{d}{dt}\frac{m\mathbf{v}}{\sqrt{1-\mathrm{v}^2/c^2}} &= q\left[-\nabla\phi-\frac{1}{c}\frac{\partial\mathbf{A}}{\partial t}+\frac{\mathbf{v}}{c}\cdot(\nabla\times\mathbf{A})\right]\\ &= \nabla\left(-q\phi+q\frac{\mathbf{v}}{c}.\mathbf{A}\right)-\frac{q}{c}\left(\frac{\partial}{\partial t}+\mathbf{v}.\nabla\right)\mathbf{A}\\ &= \nabla\left(-q\phi+q\frac{\mathbf{v}}{c}.\mathbf{A}\right)-\frac{q}{c}\frac{d\mathbf{A}}{dt}\end{aligned} \tag{8}$$

where we have used

$$\frac{d\mathbf{A}\left[\mathbf{r}(t),t\right]}{dt}=\left(\frac{\partial}{\partial t}+\mathbf{v}.\nabla\right)\mathbf{A}\left[\mathbf{r}(t),t\right]. \tag{9}$$

We can rewrite 8 as

$$\frac{d}{dt}\left(\frac{m\mathbf{v}}{\sqrt{1-\mathrm{v}^2/c^2}}+\frac{q}{c}\mathbf{A}\right)+\nabla\left(q\phi-\frac{q}{c}\mathbf{v}\cdot\mathbf{A}\right)=0. \tag{10}$$

In terms of the Lagrangian equation

$$\frac{d}{dt}\left(\nabla_{\mathbf{r}}\mathcal{L}\right)-\nabla_{\mathbf{r}}\mathcal{L}=0$$

the suitable Lagrangian for 10 is

$$\mathcal{L}\left(\mathbf{r},\mathbf{v}\right)=-\ mc^2\sqrt{1-\mathrm{v}^2/c^2}+\frac{q}{c}\mathbf{v}\cdot\mathbf{A}(r,t)-q\phi(r,t). \tag{11}$$

The canonical momentum is

$$\mathbf{p}=\nabla_{\mathbf{v}}\mathcal{L}=\frac{m\mathbf{v}}{\sqrt{1-\mathrm{v}^2/c^2}}+\frac{q}{c}\mathbf{A}(\mathbf{r},t)=\mathbf{P}+\frac{q}{c}\mathbf{A}(\mathbf{r},t) \tag{12}$$

where

$$\mathbf{P}\ =m\mathbf{v}/\sqrt{1-\mathrm{v}^2/c^2} \tag{13}$$

is the kinetic momentum and $q\mathbf{A}/c$ is the momentum carried by the electromagnetic field.

The Hamiltonian is

$$\mathcal{H} = \mathbf{p}.\ \mathbf{v} - \mathcal{L} = \frac{mc^2}{\sqrt{1 - \mathrm{v}^2/c^2}} + q\phi. \tag{14}$$

We rewrite 14 as

$$\mathcal{H}(\mathbf{r}, \mathbf{p}) = c\left\{\left[\mathbf{p} - \frac{q}{c}\ \mathbf{A}(\mathbf{r}, t)\right]^2 + (mc)^2\right\}^{1/2} + q\phi(\mathbf{r}, t). \tag{15}$$

For non-relativistic particles,

$$\mid \mathbf{P} \mid = \mid \mathbf{p} - \ \frac{q}{c}\ \mathbf{A} \mid << \ mc \tag{16}$$

and

$$H\left(\mathbf{r}, \mathbf{p}\right) = mc^2 + \frac{\left(\mathbf{p} - \ q\mathbf{A}/c\right)^2}{2m} + q\phi. \tag{17}$$

The second term has as part of its contribution the quantity

$$\left(q\mathbf{A}\right)^2 \ / \ 2mc^2$$

which is relevant only in processes where two photons are involved and may be ignored. The remaining terms yield the *electromagnetic interaction* Hamiltonian

$$\mathcal{H}_{int} = q\phi - \frac{q}{c}\ \mathbf{v}.\mathbf{A} \tag{18}$$

where the rest + kinetic energy of the particle was subtracted.

For systems involving a charge density $\rho\left(\mathbf{r}, t\right)$, H can be generalized to

$$\mathcal{H}_{int} = \int \left[\rho\phi - \frac{1}{c}\ \mathbf{j}.\mathbf{A}\right] d^3r. \tag{19}$$

0.3 Relativistic Coulomb excitation

0.3.1 Time-dependent electromagnetic interaction

We consider a nucleus 1 which is at rest and a relativistic nucleus 2 which moves along the z-axis and is excited from the initial state $|I_iM_i >\equiv |i >$ to the state $|I_fM_f >\equiv |f >$ by the electromagnetic field of nucleus 1. The nuclear states are specified by the spin quantum numbers I_i, I_f and by the corresponding magnetic quantum numbers M_i, M_f, respectively. We assume that the relativistic nucleus 1 moves along a straight-line trajectory with impact

parameter b, which is therefore also the distance of the closest approach between the center of mass of the two nuclei at the time $t = 0$. We shall consider the situation where b is larger than the sum of the two nuclear radii, such that the charge distributions of the two nuclei do not strongly overlap at any time.

The Coulomb field for a particle moving in a straight-line is given by

$$\phi\left(\mathbf{r},t\right)=\frac{Ze}{\mid\mathbf{r}-\mathbf{R}(t)\mid}=\frac{Ze}{\sqrt{(x-b)^2+y^2+(z-\mathrm{v}t)^2}} \tag{20}$$

where it is assumed that the trajectory lies in the plane $x - z$, and $\mathbf{R}(t) = (b, 0, \mathrm{v}t)$.

If the charge velocity is comparable to c, one has to account for the retardation. As shown in Ref. [7] the correct potential, called by *Liénard-Wiechert potential* is given by

$$\phi(\mathbf{r},t)=\frac{\gamma Ze}{\sqrt{(x-b)^2+y^2+\gamma^2(z-\mathrm{v}t)^2}}. \tag{21}$$

The vector potential is given by

$$\mathbf{A}(\mathbf{r},t)=\frac{\mathbf{v}}{c}\phi(\mathbf{r},t). \tag{22}$$

We know consider the excitation of the target from an initial rate $\mid i >$ to a final state $\mid f >$. We summarize the results obtained by Bertulani and collaborators [4, 5]. In first order perturbation theory the transition amplitude is given by

$$a_{fi}=\frac{1}{i\hbar}\int_{-\infty}^{\infty}dt\;e^{i(E_f-E_i)t/\hbar}<\;f\mid\mathcal{H}_{int}\mid i> \tag{23}$$

where

$$<f\mid\mathcal{H}_{int}\mid i>=\int\;\left[\rho_{fi}\phi(\mathbf{r},t)-\frac{1}{c}\,\mathbf{j}_{fi}(\mathbf{r})\cdot\mathbf{A}(\mathbf{r},t)\right]d^3r \tag{24}$$

with

$$\rho_{fi}(\mathbf{r}) = \varphi_i(\mathbf{r})\varphi_f^*(\mathbf{r}) \tag{25}$$

$$\mathbf{j}_{fi}(\mathbf{r}) = \frac{\hbar}{2im}\left[\varphi_i^*(\mathbf{r})\nabla\varphi_f(\mathbf{r})-\varphi_f(\mathbf{r})\nabla\varphi_i^*(\mathbf{r})\right]. \tag{26}$$

Thus,

$$a_{fi}=\frac{1}{i\hbar}\int_{-\infty}^{\infty}dt\;e^{i\omega t}\left[\rho_{fi}(\mathbf{r})-\frac{\mathbf{v}}{c^2}\cdot\mathbf{j}_{fi}(\mathbf{r})\right]\phi\left(\mathbf{r},t\right)d^3r. \tag{27}$$

Assuming that the internal coordinate $\mathbf{r}$ is much smaller in magnitude than $|\mathbf{R}(t)|$ we can approximate $\phi\left(\mathbf{r},t\right)$ in lower orders of $|\mathbf{r}|\,/\,|\mathbf{R}(t)|$. For example, in dipole approximation we only take the two lowest terms in the expansion, i.e.,

$$\phi\cong\frac{\gamma Ze}{\left[b^2+\gamma^2\mathrm{v}^2t^2\right]^{1/2}}+\frac{\gamma Ze(xb+\gamma^2\mathrm{v}tz)}{\left[b^2+\gamma^2\mathrm{v}^2t^2\right]^{3/2}}. \tag{28}$$

Using $\int d^3r\ \rho_{fi}\left(\mathbf{r}\right)=0$, we get to lowest order

$$< f \mid \mathcal{H}_{int} \mid i >= \int \left\{ \rho_{fi}(\mathbf{r}) \frac{\gamma Ze(xb+\gamma^2 \mathrm{v}tz)}{\left[b^2+\gamma^2\mathrm{v}^2t^2\right]^{3/2}} - \ j_{fi}^{(z)}(\mathbf{r}) \frac{\mathrm{v}}{c^2} \frac{\gamma Ze}{\left[b^2+\gamma^2\mathrm{v}^2t^2\right]^{1/2}} \right\} d^3r \qquad (29)$$

in which terms proportional to $\int d^3r\ \mathbf{r}\cdot\mathbf{j}_{fi}(\mathbf{r})$, or higher, were neglected since they contribute to quadrupole excitations.

The current interaction of Eq. 24 can be treated in a similar way as for the scalar interaction. This interaction cannot be neglected, since it yields appreciable corrections in collisions at intermediate and high energies (i.e., $\mathrm{v}/c \sim 0.2$, and higher). For practical purposes, it is also important to write this part of the interaction in terms of a spherical basis operator.

Since the velocity $\mathbf{v}$ in Eq. 27 is along the z-axis, we can write

$$< f \mid \mathcal{H}_{int} \mid i >= \int d\mathbf{r}\ \phi\ \rho_{fi} - \frac{\mathrm{v}}{c^2} \int\ d\mathbf{r}\ \phi\ \nabla(z)\cdot\mathbf{j}_{fi}\ . \qquad (30)$$

Using $\nabla\cdot(f\mathbf{j}) = f(\nabla\cdot\mathbf{j}) + \mathbf{j}\cdot\nabla f$ and the *continuity equation* $\nabla\cdot\mathbf{j} = -i\omega\rho$, we get

$$< f \mid \mathcal{H}_{int} \mid i >= \int d\mathbf{r}\ \phi\ \rho_{fi} - i\frac{\mathrm{v}\omega}{c^2} \int d\mathbf{r}\ \phi\ z\ \rho_{fi}\ - \frac{\mathrm{v}}{c^2} \int d\mathbf{r}\ \phi\ \nabla\cdot(z\mathbf{j}_{fi})\,, \qquad (31)$$

where $\hbar\omega = E_f - E_i$ is the energy difference between the states $|f>$ and $|i>$.

In the third integral we can use $\phi_0 \equiv \phi(\mathbf{r}=0)$, i.e., the first term in 28. Since ϕ_0 does not depend on $\mathbf{r}$ it can be taken out of the integral and it vanishes due to Gauss theorem. Thus, Eq. 29 becomes

$$< f \mid \mathcal{H}_{int} \mid i >= \gamma Ze \int \rho_{fi}(\mathbf{r}) \left\{ \frac{(xb+\gamma^2\mathrm{v}tz)}{\left[b^2+\gamma^2\mathrm{v}^2t^2\right]^{3/2}} - i\frac{(\mathrm{v}\omega/c^2)\,z}{\left[b^2+\gamma^2\mathrm{v}^2t^2\right]^{1/2}} \right\} d^3r. \qquad (32)$$

Defining

$$\mathcal{M}(E1,-\mu) = \frac{i}{\omega}\ \int d^3r\mathbf{J}(\mathbf{r})\cdot\nabla\left(rY_{1\mu}\right) = \int d^3r\ \rho(\mathbf{r})\ r\ Y_{1\mu}(\mathbf{r}) \qquad (33)$$

we get for the electric dipole potential

$$\begin{aligned} \left(\mathcal{H}_{int}\right)_{fi}^{(E1)}(t) \ &= \ \sqrt{\frac{2\pi}{3}}\ \gamma \left\{ \mathcal{E}_1(\tau)\ \left[\mathcal{M}_{fi}(E1,-1) - \mathcal{M}_{fi}(E1,1)\right] \right. \\ &+ \ \left. \sqrt{2}\ \gamma\ \left[\tau\mathcal{E}_1(\tau) - i\frac{\omega v}{\gamma c^2}\ \mathcal{E}_2(\tau)\right]\ \mathcal{M}_{fi}(E1,0) \right\}, \end{aligned} \qquad (34)$$

where $\tau = \gamma \mathrm{v}/b$, and

$$\mathcal{E}_1(\tau) = \frac{Z_1 e}{b^2\ [1+\tau^2]^{3/2}} \qquad \text{and} \quad \mathcal{E}_2(\tau) = \frac{Z_1 e}{b\ [1+\tau^2]^{1/2}}. \tag{35}$$

A similar derivation can be carried out for the M1 and the E2 multipolarities. More details are found in Ref. [4] (see also [5])

$$(\mathcal{H}_{int})_{fi}^{(M1)}(t) = i\ \sqrt{\frac{2\pi}{3}}\ \frac{v}{c}\gamma\ \mathcal{E}_1(\tau)\ \left[\mathcal{M}_{fi}(M1,1) + \mathcal{M}_{fi}(M1,-1)\right]\ , \tag{36}$$

where

$$\mathcal{M}(M1,\mu) = -\frac{i}{2c}\ \int d^3r\ \mathbf{J}(\mathbf{r}).\mathbf{L}\Big(rY_{1\mu}\Big)\ . \tag{37}$$

The current $\mathbf{J}$ in Eq. 37 is made up of the usual convective part and a magnetization part, proportional to the intrinsic (Dirac and anomalous) magnetic moment of the nucleons.

For the E2 multipolarity one finds [4, 5]

$$\begin{aligned}(\mathcal{H}_{int})_{fi}^{(E2)}(t) &= -\sqrt{\frac{\pi}{30}}\ \gamma\ \Big\{3\ \mathcal{E}_3(\tau)\ \Big[\mathcal{M}_{fi}(E2,2) + \mathcal{M}_{fi}(E2,-2)\Big] \\ &+ \gamma\Big[6\ \tau\mathcal{E}_3(\tau) - i\ \frac{\omega v}{\gamma c^2}\ \mathcal{E}_1(\tau)\Big]\ \Big[\mathcal{M}_{fi}(E2,-1) + \mathcal{M}_{fi}(E2,1)\Big] \\ &+ \sqrt{6}\ \gamma^2\ \Big[\Big(2\tau^2-1\Big)\ \mathcal{E}_3(\tau) - i\ \frac{\omega v}{\gamma c^2}\ \tau\ \mathcal{E}_1(\tau)\Big]\mathcal{M}_{fi}(E2,0)\Big\}\end{aligned} \tag{38}$$

where $\mathcal{E}_3(\tau)$ is the quadrupole electric field of nucleus 1, given by

$$\mathcal{E}_3(\tau) = \frac{Z_1 e}{b^3\ [1+\tau^2]^{5/2}}. \tag{39}$$

The fields $\mathcal{E}_i(\tau)$ peak around $\tau = 0$, and decrease rapidly within an interval $\Delta\tau \simeq 1$. This corresponds to a collisional time $\Delta t \simeq b/\gamma v$. This means that, numerically one needs to integrate the Coupled-Channels equations (Eq. 3) only in a time interval within a range $n \times \Delta\tau$ around $\tau = 0$, with n equal to a small integer number.

0.3.2 First-order perturbation theory

In most cases, the first-order perturbation theory is a good approximation to calculate the amplitudes for relativistic Coulomb excitation. It amounts to using $a_k = \delta_{k0}$ on the right

hand side of Eq. 3. Using the integrals (K_i = modified Bessel functions)

$$\int_{-\infty}^{\infty} \frac{dt\ e^{i\omega t}}{\left[b^2+\gamma^2 v^2 t^2\right]^{1/2}} = \frac{2}{\gamma v}\ K_0\left(\frac{\omega b}{\gamma v}\right) \tag{40}$$

$$\int_{-\infty}^{\infty} \frac{dt\ e^{i\omega t}}{\left[b^2+\gamma^2 v^2 t^2\right]^{3/2}} = \frac{2}{\gamma v b^2}\ \left(\frac{\omega b}{\gamma v}\right)\ K_1\left(\frac{\omega b}{\gamma v}\right) \tag{41}$$

$$\int_{-\infty}^{\infty} \frac{dt.t.\ e^{i\omega t}}{\left[b^2+\gamma^2 v^2 t^2\right]^{3/2}} = \frac{2i}{\gamma^2 v^2 b}\ \left(\frac{\omega b}{\gamma v}\right)\ K_0\left(\frac{\omega b}{\gamma v}\right) \tag{42}$$

one gets

$$\begin{aligned} a_{1st}^{(E1)} &= -i\sqrt{\frac{8\pi}{3}}\ \frac{Z_1 e}{\hbar v b}\ \xi\ \Bigg\{K_1(\xi)\ \left[\mathcal{M}_{fi}(E1,-1)-\mathcal{M}_{fi}(E1,1)\right] \\ &+ i\frac{\sqrt{2}}{\gamma}\ K_0(\xi)\ \mathcal{M}_{fi}(E1,0)\Bigg\} \end{aligned} \tag{43}$$

where K_1 (K_2) is the modified Bessel function of first (second) degree, and $\xi = \omega b/\gamma v$. For the $E2$ and $M1$ multipolarities, we obtain respectively [4, 5],

$$\begin{aligned} a_{1st}^{(E2)} &= 2i\ \sqrt{\frac{\pi}{30}}\ \frac{Z_1 e}{\gamma\hbar v b^2}\ \xi^2\Bigg\{K_2(\xi)\ \Big[\mathcal{M}_{fi}(E2,2)+\mathcal{M}_{fi}(E2,-2)\Big] \\ &+ i\gamma\ \left(2-\frac{v^2}{c^2}\right)\ K_1(\xi)\ \Big[\mathcal{M}_{fi}(E2,-1)+\mathcal{M}_{fi}(E2,1)\Big] \\ &- \sqrt{6}\ K_0(\xi)\ \mathcal{M}_{fi}(E2,0)\Bigg\}\ , \end{aligned} \tag{44}$$

and

$$a_{1st}^{(M1)} = \sqrt{\frac{8\pi}{3}}\ \frac{Z_1 e}{\hbar c b}\ \xi\ K_1(\xi)\ \left[\mathcal{M}_{fi}(M1,1)-\mathcal{M}_{fi}(M1,-1)\right]\ . \tag{45}$$

The formulas above have been derived under the assumption of the long-wavelength approximation. When this approximation is not valid the matrix elements given by Eqs. 33 and 37 are to be replaced by the full matrix-elements for electromagnetic excitations [1], i.e.,

$$\mathcal{M}(E\lambda,\mu) = \frac{(2\lambda+1)!!}{\kappa^{\lambda+1}c(\lambda+1)}\int \mathbf{J}(\mathbf{r})\cdot\nabla\times\mathbf{L}\left[j_\lambda(\kappa r)Y_{\lambda\mu}(\hat{\mathbf{r}})\right]d^3r\ , \tag{46}$$

$$\mathcal{M}(M\lambda,\mu) = -i\frac{(2\lambda+1)!!}{\kappa^{\lambda}c(\lambda+1)}\int \mathbf{J}(\mathbf{r})\cdot\mathbf{L}\left[j_\lambda(\kappa r)Y_{\lambda\mu}(\hat{\mathbf{r}})\right]d^3r\ , \tag{47}$$

for electric and magnetic excitations ($\kappa = \omega/c$), respectively. However, the other factors do not change (see, e.g., Ref. [3]).

0.3.3 Excitation probabilities and virtual photon numbers

The square modulus of Eqs. 43, 44 and 45 gives the probability of exciting the target nucleus from the initial state $\mid I_i M_i >$ to the final state $\mid I_f M_f >$ in a collision with impact parameter b. If the orientation of the initial state is not specified, the probability for exciting the nuclear state of energy E_f and spin I_f is

$$P_{i\to f} = \frac{1}{2I_i+1} \sum_{M_i,M_f} \mid a_{fi} \mid^2 . \tag{48}$$

Integration of Eq. 48 over all energy transfers $\varepsilon = \hbar\omega$, and summation over all possible final states of the projectile nucleus (making use of the Wigner-Eckart theorem and the orthogonality of the properties of the Clebsch-Gordan coefficients) leads to the Coulomb excitation probability in a collision with impact parameter b:

$$P_C = \sum_f \int P_{i\to f}(b)\ \rho_f(\varepsilon)\ d\epsilon \tag{49}$$

where $\rho_f(\varepsilon)$ is the density of final states of the target with energy $E_f = E_i + \varepsilon$.

Inserting Eqs. 43, 44 and 45 into Eq. 49 one finds

$$P_C(b,\varepsilon) = \sum_{\pi\lambda} P_{\pi\lambda}(b,\varepsilon) = \sum_{\pi\lambda} \int \frac{d\varepsilon}{\varepsilon}\ n_{\pi\lambda}(b,\varepsilon)\ \sigma_\gamma^{\pi\lambda}(\varepsilon), \tag{50}$$

where

$$\sigma_\gamma^{\pi\lambda}(\varepsilon) = \frac{(2\pi)^3(\lambda+1)}{\lambda\left[(2\lambda+1)!!\right]^2} \sum_f \rho_f(\varepsilon)\,\kappa^{2\lambda-1}\ B(\pi\lambda, I_i \to I_f) \tag{51}$$

are the photonuclear absorption cross sections for a given multipolarity $\pi\lambda$. The reduced transition probability $B(\pi\lambda, I_i \to I_f)$ is given by

$$\begin{aligned} B(\pi\lambda; I_i \longrightarrow I_f) &= \frac{1}{2I_i+1} \sum_{M_i M_f} |< I_i M_i | \mathcal{M}(\pi\lambda,\ \mu) | I_f M_f >|^2 \\ &= \frac{1}{2I_i+1}\ |< I_i || \mathcal{M}(\pi\lambda) || I_f >|^2 . \end{aligned} \tag{52}$$

The total photonuclear cross section is a sum of all these multipolarities,

$$\sigma_\gamma = \sum_{\pi\lambda} \sigma_\gamma^{\pi\lambda}(\varepsilon) . \tag{53}$$

The functions $n_{\pi\lambda}(\varepsilon)$ are called the *virtual photon numbers*, and are given by

$$n_{E1}(b,\varepsilon) = \frac{Z_1^2\alpha}{\pi^2}\,\frac{\xi^2}{b^2}\,(\frac{c}{v})^2\,\left\{K_1^2+\frac{1}{\gamma^2}\,K_0^2\right\} \quad (54)$$

$$n_{E2}(b,\varepsilon) = \frac{Z_1^2\alpha}{\pi^2 b^2}\,(\frac{c}{v})^4\,\left\{\frac{4}{\gamma^2}\,\left[K_1^2+\xi K_0K_1+\xi^2K_0^2\right]+\xi^2(2-v^2/c^2)^2K_1^2\right\} \quad (55)$$

$$n_{M1}(b,\varepsilon) = \frac{Z_1^2\alpha}{\pi^2}\,\frac{\xi^2}{b^2}\,K_1^2 \quad (56)$$

where all K_μ's are functions of $\xi(b)=\omega b/\gamma v$.

Since all nuclear excitation dynamics is contained in the photoabsorption cross section, the virtual photon numbers, Eqs. 54, 55 and 56, do not depend on the nuclear structure. They are kinematical factors, depending on the orbital motion. They may be interpreted as the number of equivalent (virtual) photons that hit the target per unit area. These expressions show that Coulomb excitation probabilities are exactly directly proportional to the photonuclear cross sections, although the exchanged photons are off-shell. This arises from the condition that the reaction is peripheral and the nuclear charge distributions of each nuclei do not overlap during the collision. This result can be proved from first principles, and has been shown in some textbooks (see, e.g., Ref. [14]).

The usefulness of Coulomb excitation, even in first order processes, is displayed in Eq. 50. The field of a real photon contains all multipolarities with the same weight and the photonuclear cross section 53 is a mixture of the contributions from all multipolarities, although only a few contribute in most processes. In the case of Coulomb excitation the total cross section is weighted by kinematical factors which are different for each projectile or bombarding energy. This allows one to disentangle the multipolarities when several ones are involved in the excitation process, except for the very high bombarding energies $\gamma \gg 1$ for which all virtual photon numbers can be shown to be the same [8].

0.3.4 Second-order perturbation theory

To second-order, the amplitude for a two-step excitation to a state $|2>$ via intermediate states $|1>$ is given by

$$a_{20}^{2nd} = \sum_1\,\frac{1}{(i\hbar)^2}\,\int_{-\infty}^{\infty} dt\; e^{i\omega_{21}t}\;V_{21}(t)\;\int_{-\infty}^{t}\;dt'\;e^{i\omega_{10}t'}V_{10}(t')\,, \quad (57)$$

where $V_{21}(t)$ is a short notation for the interaction potential inside brackets of the integral of Eq. 57 for the transition $|1>\rightarrow|2>$.

Using the integral representation of the step function

$$\Theta(t-t') = -\lim_{\delta\to 0^+} \frac{1}{2\pi i}\int_{-\infty}^{\infty} \frac{e^{-iq(t-t')}}{q+i\delta} dq = \begin{cases} 1, & if \;\; t > t' \\ 0, & if \;\; t < t' \end{cases} \tag{58}$$

one finds [1]

$$\begin{aligned} a_{20}^{2nd} &= \frac{1}{2}\sum_1 a_{21}^{1st}(\omega_{21})\; a_{10}^{1st}(\omega_{10}) \\ &+ \frac{i}{2\pi}\sum_1 \mathcal{P}\int_{-\infty}^{\infty} \frac{dq}{q}\; a_{21}^{1st}(\omega_{21}-q)\; a_{10}^{1st}(\omega_{10}+q)\;, \end{aligned} \tag{59}$$

where $\mathcal{P}$ stands for the principal value of the integral. For numerical evaluation it is more appropriate to rewrite the principal value integral in Eq. 59 as

$$\begin{aligned} &\mathcal{P}\int_{-\infty}^{\infty} \frac{dq}{q}\; a_{21}^{1st}(\omega_{21}-q)\; a_{10}^{1st}(\omega_{10}+q) = \\ &\int_0^{\infty} \frac{dq}{q}\left[a_{21}^{1st}(\omega_{21}-q)\; a_{10}^{1st}(\omega_{10}+q) - a_{21}^{1st}(\omega_{21}+q)\; a_{10}^{1st}(\omega_{10}-q)\right]. \end{aligned} \tag{60}$$

To calculate $a^{1st}(\omega)$ for negative values of ω, we note that the interaction potential can be written as a sum of an even and an odd part. This implies that $a^{1st}(-\omega) = -\left[a^{1st}(\omega)\right]^*$.

For three-phonon excitation we use the third term of the time-dependent perturbation expansion, and the same procedure as above (Eqs. 58 - 60).

0.3.5 Cross sections and total virtual photon numbers

The cross section is obtained by the impact parameter integral of the excitation probabilities. Eq. 50 shows that we only need to integrate the number of virtual photons over impact parameter. One has to introduce a minimum impact parameter b_0 in the integration. Impact parameters smaller than b_0 are dominated by nuclear fragmentation processes. One finds

$$d\sigma_C = \sum_{\pi\lambda} \sigma_{\pi\lambda} = \sum_{\pi\lambda}\int \frac{d\varepsilon}{\varepsilon}\; N_{\pi\lambda}(\varepsilon)\; \sigma_\gamma^{\pi\lambda}(\varepsilon)\,, \tag{61}$$

where the *total virtual photon numbers* $N_{\pi\lambda}(\varepsilon) = 2\pi \int db\ b\ n(b,\varepsilon)$ are given analytically by

$$N_{E1}(\varepsilon) = \frac{2Z_1^2\alpha}{\pi}(\frac{c}{v})^2 \left[\xi K_0 K_1 - \frac{v^2\xi^2}{2c^2}(K_1^2 - K_0^2)\right] \quad (62)$$

$$N_{E2}(\varepsilon) = \frac{2Z_1^2\alpha}{\pi}(\frac{c}{v})^4 \left[2(1-\frac{v^2}{c^2})K_1^2 + \xi(1-\frac{v^2}{c^2})^2 K_0 K_1 + \frac{\xi^2 v^4}{2c^4}(K_1^2 - K_0^2) + \xi^2(2 - v^2/c^2)^2 K_1^2\right] \quad (63)$$

$$N_{M1}(\varepsilon) = \frac{2Z_1^2\alpha}{\pi}\frac{\xi^2}{b^2}\left[\xi K_0 K_1 - \frac{\xi^2}{2}(K_1^2 - K_0^2)\right] \quad (64)$$

where all K_μ's are now functions of $\xi(b) = \omega b_0/\gamma v$.

Supplement B

0.4 Harmonic oscillator model for surface vibrations

The radial vector for a point on the surface of a slightly deformed nucleus is given by

$$R(\theta) = R_0\left\{1 + \sum_{\lambda\mu}\alpha^*_{\lambda\mu}\,Y_{\lambda\mu}(\theta) + \mathcal{O}(\alpha^2)\right\}. \quad (65)$$

Since $R(\theta)$ is real, one gets

$$\sum_\mu \alpha^*_{\lambda\mu}\,Y_{\lambda\mu} = \sum_\mu \alpha_{\lambda\mu}\,Y^*_{\lambda\mu} = \sum_\mu (-1)^\mu\,\alpha_{\lambda\mu}\,Y_{\lambda,-\mu}. \quad (66)$$

Thus

$$\alpha^*_{\lambda\mu} = (-1)^\mu\ \alpha_{\lambda,-\mu} \quad (67)$$

A Hamiltonian for small amplitude oscillations of the nuclear surface has to be quadratic in both $\alpha_{\lambda\mu}$ and $\dot\alpha_{\lambda\mu}$, scalar and invariant under time reversal. This implies that the Hamiltonian has to be equal to

$$H = \frac{1}{2}\sum_{\lambda\mu}\left[B_\lambda\,|\dot\alpha_{\lambda\mu}|^2 + C_\lambda|\alpha_{\lambda\mu}|^2\right]. \quad (68)$$

The classical solution for this Hamiltonian is given by

$$\omega_\lambda = \left(\frac{C_\lambda}{B_\lambda}\right)^{1/2}$$

$$\alpha_{\lambda\mu} = \epsilon_{\lambda\mu}\,\cos(\omega_\lambda t)$$

$$E = \sum_{\lambda\mu}\frac{1}{2}|\epsilon_{\lambda\mu}|^2\omega_\lambda^2 B_\lambda. \quad (69)$$

We now quantize the Hamiltonian by using the quantization rules

$$\pi_{\lambda\mu} = \frac{\partial H}{\partial \dot{\alpha}_{\lambda\mu}} = B_\lambda \dot{\alpha}^*_{\lambda\mu}, \qquad [\alpha_{\lambda\mu}, \pi_{\lambda\mu}] = i\hbar \tag{70}$$

which implies that

$$\pi_{\lambda\mu} = -i\hbar \frac{\partial}{\partial \alpha_{\lambda\mu}}. \tag{71}$$

If we now introduce the boson operators

$$\begin{aligned} O^+_{\lambda\mu} &= \left(\frac{\omega_\lambda B_\lambda}{2\hbar}\right)^{1/2} \left[\alpha_{\lambda\mu} - \frac{i}{\omega_\lambda B_\lambda}(-1)^\mu \pi_{\lambda,-\mu}\right] \\ O_{\lambda\mu} &= \left(\frac{\omega_\lambda B_\lambda}{2\hbar}\right)^{1/2} \left[(-1)^\mu \alpha_{\lambda,-\mu} + \frac{i}{\omega_\lambda B_\lambda}\pi_{\lambda\mu}\right] \end{aligned} \tag{72}$$

we get the commutation relation

$$\left[O_{\lambda\mu}, O^+_{\lambda\mu}\right] = 1. \tag{73}$$

The Hamiltonian 68 can be rewritten as

$$H = \sum_{\lambda\mu} \hbar\omega_\lambda \left(O^+_{\lambda\mu} O_{\lambda\mu} + \frac{1}{2}\right). \tag{74}$$

The operator $O^+_{\lambda\mu}$ obeys the equations of motion

$$\left[H, O^+_{\lambda\mu}\right] = \hbar\omega_\lambda \, O^+_{\lambda\mu}. \tag{75}$$

The ground-state is defined as

$$O_{\lambda\mu}\phi_0(\alpha) = 0; \qquad \text{all } \lambda\mu, \tag{76}$$

and the number operator as $N_{\lambda\mu} = O^+_{\lambda\mu} O_{\lambda\mu}$. Using these definitions and Eq. 73, the excited states can be found by means of standard techniques for the harmonic oscillator model [9].

0.5 Coulomb excitation at intermediate energies

0.5.1 Classical trajectory: recoil and retardation corrections

The semiclassical theory of Coulomb excitation in low energy collisions accounts for the Rutherford bending of the trajectory, but relativistic retardation effects are neglected [2]. On the other hand, in the theory of relativistic Coulomb excitation [3] recoil effects on

the trajectory are neglected (one assumes straight-line motion) but retardation is handled correctly. In fact, the onset of retardation brings new important effects such as the steady increase of the excitation cross sections with bombarding energy. In a heavy ion collision around 100A MeV the Lorentz factor γ is about 1.1. Since this factor enters the excitation cross sections in many ways, like in the *adiabacity parameter*, $\xi(R) = \omega_{fi}R/\gamma v$, one expects that some sizable modifications in the theory of relativistic Coulomb excitation should occur [10]. Recoil corrections are not negligible either, and the relativistic calculations based on the straight-line parametrization should not be completely appropriate to describe the excitation probabilities and cross sections. The Coulomb recoil in a single collision is of the order of

$$a_0 = \frac{Z_1 Z_2 e^2}{m_0 v^2}, \tag{77}$$

which is *half-distance of closest approach* in a head-on collision, with m_0 equal to the reduced mass of the colliding nuclei. Although this recoil is small for intermediate energy collisions, the excitation probabilities are quite sensitive to it. This is important for example in the excitation of giant resonances because the adiabacity parameter is of the order of one. When $\xi(b) \ll 1$, the excitation probabilities depends on b approximately like $1/b^2$, while when $\xi(b)$ becomes greater than one they decrease approximately as $e^{-2\pi\xi(b)}/b^2$. Therefore, when $\xi \simeq 1$ a slight change of b may vary appreciably the excitation probabilities.

In the semiclassical theory of Coulomb excitation the nuclei are assumed to follow classical trajectories and the excitation probabilities are calculated in time-dependent perturbation theory. At low energies one assumes Rutherford trajectories for the relative motion while at relativistic energies one assumes straight-line motion. In intermediate energy collisions, where one wants to account for recoil and retardation simultaneously, one should solve the general classical problem of the motion of two relativistic charged particles. But, even if radiation is neglected, this problem can only be solved if one particle has infinite mass [11]. This approximation should be sufficient if we take, e.g., the collision ^{16}O + ^{208}Pb as our system. An improved solution may be obtained by use of the reduced mass, as we show next, in a formalism developed by Aleixo and Bertulani [10].

In the classical one-body problem, one starts with the relativistic Lagrangian

$$\mathcal{L} = -m_o c^2 \left\{ 1 - \frac{1}{c^2}\left(\dot{r}^2 + r^2\dot{\phi}^2\right) \right\}^{1/2} - \frac{Z_1 Z_2 e^2}{r} \ , \tag{78}$$

where $\dot{r}$ and $\dot{\phi}$ are the radial and the angular velocity of the particle, respectively (see Fig. 1(b)). Using the Euler-Lagrange equations one finds three kinds of solutions, depending on the sign of the charges and the angular momentum in the collision. In the case of our interest, the appropriate solution relating the collisional angle ϕ and the distance r between the nuclei is [11]

$$\frac{1}{r} = A\left[\epsilon\ \cos(W\phi) - 1\right] \tag{79}$$

where

$$W = \left[1 - (\frac{Z_1 Z_2 e^2}{cL_0})^2\right]^{1/2}, \qquad A = \frac{Z_1 Z_2 e^2 E}{c^2 L_0^2 W^2}, \tag{80}$$

$$\epsilon = \frac{cL_0}{Z_1 Z_2 e^2 E}\left[E^2 - m_0^2 c^4 + (\frac{m_0 c Z_1 Z_2 e^2}{L_0})^2\right]^{1/2}. \tag{81}$$

E is the total bombarding energy in MeV, m_0 is the mass of the particle and L_0 its angular momentum. In terms of the Lorentz factor γ and of the impact parameter b, $E = \gamma m_o c^2$ and $L_0 = \gamma m_0 v b$. The above solution is valid if $L_0 > Z_1 Z_2 e^2/c$. In heavy ion collisions at intermediate energies one has $L_0 \gg Z_1 Z_2 e^2/c$ for impact parameters that do not lead to strong interactions. It is also easy to show that, from the magnitudes of the parameters involved in heavy ion collisions at intermediate energies, the trajectory 79 can be very well described by approximating

$$W = 1, \qquad A = \frac{a_o}{\gamma b^2}, \qquad \epsilon = \sqrt{\frac{b^2\gamma^2}{a_0^2} + 1}, \tag{82}$$

where a_0 is half the distance of closest approach in a head on collision (if the nuclei were pointlike and if non-relativistic kinematics were used), and ϵ is the eccentricity parameter. In the approximation 82 ϵ is related to the deflection angle ϑ by $\epsilon = (a_0/\gamma)\cot\vartheta$.

The time dependence for a particle moving along the trajectory, Eq. 79, may be directly obtained by solving the equation of angular momentum conservation. Introducing the parametrization

$$r(\chi) = \frac{a_0}{\gamma}\left[\epsilon\cosh\chi + 1\right] \tag{83}$$

we find

$$t = \frac{a_0}{\gamma v}\left[\chi + \epsilon\sinh\chi\right]. \tag{84}$$

Using the scattering plane perpendicular to the Z-axis, one finds that the corresponding components of $\mathbf{r}$ may be written as

$$x = a\left[\cosh\chi + \epsilon\right], \tag{85}$$

$$y = a\sqrt{\epsilon^2 - 1}\sinh\chi, \tag{86}$$

$$z = 0, \tag{87}$$

where $a = a_0/\gamma$. This parametrization is of the same form as commonly used in the non-relativistic case [2], except that a_0 replaced by $a_0/\gamma \equiv a$.

In the limit of straight-line motion $\epsilon \simeq b/a \gg 1$, and the equations above reduce to the simple parametrization

$$y = vt, \qquad x = b, \quad \text{and} \quad z = 0. \tag{88}$$

As we quoted before, the classical solution for the relative motion of two relativistic charges interacting electromagnetically can only be solved analytically if one of the particles has infinite mass. Non-relativistically the two-body problem is solvable by introduction of center of mass and relative motion coordinates. Then, the result is equivalent to that of a particle with reduced mass $m_0 = m_P m_T/(m_P + m_T)$ under the action of the same potential. The particle with reduced mass m_0 is lighter than those with mass m_P and m_T, and this accounts for the simultaneous recoil of them. An exact relativistic solution should reproduce this behavior as the relative motion energy is lowered. We shall use the reduced mass definition of m_0 as usual in the parametrization of the classical trajectory of Coulomb excitation in intermediate energy collisions, as outlined above. For a ^{16}O + ^{208}Pb collision this is not a bad approximation. For heavier systems like U+U it would be the simplest way to overcome this difficulty. But, as energy increases, this approximation is again unimportant since the trajectories will be straight-lines parametrized by an impact parameter b. A more exact result was obtained numerically by Aguiar, Aleixo and Bertulani [12] using the Darwin Lagrangian to determine the classical trajectory in collisions at intermediate energies . But, the parametrization of the classical trajectory as given by Eqs. 85, 86 and 87 with a reduced mass particle, besides reproducing both the non-relativistic and the relativistic energies, gives a reasonable solution to the kind of collisions we want to study.

0.5.2 Excitation amplitudes

We first notice that the retarded Green's function, appropriate for Coulomb excitation, i.e., $e^{i\kappa|\mathbf{r}-\mathbf{r}'(t)|}/\mid \mathbf{r}-\mathbf{r}'(t)\mid$ where $\kappa = \omega/c$, has the same Fourier transform as the Liénard-Wiechert potential of Eq. 20. Thus

$$\phi(\omega,\,\mathbf{r}) = Z_1 e \int_{-\infty}^{\infty} e^{i\omega t}\,\frac{e^{i\kappa|\mathbf{r}-\mathbf{r}'(t)|}}{\mid \mathbf{r}-\mathbf{r}'(t)\mid}\,dt \tag{89}$$

$$\mathbf{A}(\omega,\,\mathbf{r}) = \frac{Z_1 e}{c} \int_{-\infty}^{\infty} \mathbf{v}'(t)\,e^{iwt}\,\frac{e^{i\kappa|\mathbf{r}-\mathbf{r}'(t)|}}{\mid \mathbf{r}-\mathbf{r}'(t)\mid}\,dt \tag{90}$$

are the retarded potentials generated by a projectile with charge Z_1 following a Coulomb trajectory. When the magnitude of the excitation amplitudes are small compared to unity, the use of first order perturbation theory is justified.

We now use the expansion

$$\frac{e^{i\kappa|\mathbf{r}-\mathbf{r}'|}}{\mid \mathbf{r}-\mathbf{r}'\mid} = 4\pi\; i\kappa \sum_{\lambda\mu} j_\lambda(\kappa r_<) Y^*_{\lambda\mu}(\hat{\mathbf{r}}_<) h_\lambda(\kappa r_>)\, Y_{\lambda\mu}(\hat{\mathbf{r}}_>)\;, \tag{91}$$

where j_λ (h_λ) denotes the spherical Bessel (Hankel) functions (of first kind), $\mathbf{r}_>$ ($\mathbf{r}_<$) refers to whichever of $\mathbf{r}$ and $\mathbf{r}'$ has the larger (smaller) magnitude. Assuming that the projectile does

not penetrate the target, we use $\mathbf{r}_>$ ($\mathbf{r}_<$) for the projectile (target) coordinates. At collision energies above the Coulomb barrier this assumption only applies for impact parameters larger than a certain minimum, below which the nuclei penetrate each other.

Using the continuity equation, $\nabla \cdot \mathbf{j}_{fi} = -i\omega\rho_{fi}$, for the nuclear transition current, we can show that the expansion 91 can be expressed in terms of spherical tensors (see, e.g., Ref. [14], Vol. II) and Eq. 27 becomes

$$a_{fi} = \frac{Z_1 e}{i\hbar} \sum_{\lambda\mu} \frac{4\pi}{2\lambda+1} (-1)^\mu \left\{ S(E\lambda,\, \mu)\mathcal{M}_{fi}(E\lambda,\, -\mu) + S(M\lambda,\, \mu)\mathcal{M}_{fi}(M\lambda,\, -\mu) \right\} \tag{92}$$

where $\mathcal{M}(\pi\lambda, \mu)$ are the matrix elements for electromagnetic transitions, as defined in Eqs. 46 and 47.

The orbital integrals $S(\pi\lambda, \mu)$ are given by

$$\begin{aligned} S(E\lambda, \mu) &= -\frac{i\kappa^{\lambda+1}}{\lambda(2\lambda-1)!!} \int_{-\infty}^{\infty} \frac{\partial}{\partial r'} \left\{ r'(t) h_\lambda \left[\kappa r'(t)\right] \right\} Y_{\lambda\mu} \left[\theta'(t), \phi'(t)\right] e^{i\omega t}\, dt \\ &- \frac{\kappa^{\lambda+2}}{c\lambda(2\lambda-1)!!} \int_{-\infty}^{\infty} \mathbf{v}'(t) \cdot \mathbf{r}'(t)\, h_\lambda[\kappa r'(t)]\, Y_{\lambda\mu}[\theta'(t), \phi'(t)]\, e^{i\omega t}\, dt \end{aligned} \tag{93}$$

and

$$S(M\lambda, \mu) = -\frac{i}{\gamma m_0 c} \frac{\kappa^{\lambda+1}}{\lambda(2\lambda-1)!!} \mathbf{L}_0 \cdot \int_{-\infty}^{\infty} \nabla' \left\{ h_\lambda[\kappa r'(t)]\, Y_{\lambda\mu}[\theta'(t), \phi'(t)] \right\} e^{i\omega t}\, dt \tag{94}$$

where $\mathbf{L}_0$ is the angular momentum of relative motion, which is constant:

$$L_0 = \gamma a m_0 v \cot \frac{\vartheta}{2} \tag{95}$$

with ϑ equal to the (center-of-mass) scattering angle.

In non-relativistic collisions

$$\kappa r' = \frac{\omega r'}{c} = \frac{v}{c}\frac{\omega r'}{v} < \frac{v}{c} \ll 1 \tag{96}$$

because when the relative distance r' obeys the relations $\omega r'/v \geq 1$ the interaction becomes adiabatic. Then one uses the limiting form of h_λ for small values of its argument [13] to show that

$$S^{NR}(E\lambda, \mu) \simeq \int_{-\infty}^{\infty} r'^{-\lambda-1}(t)\, Y_{\lambda\mu} \left\{ \theta'(t), \phi'(t) \right\} e^{i\omega t}\, dt \tag{97}$$

and

$$S^{NR}(M\lambda,\mu) \simeq -\frac{1}{\lambda m_o c}\,\mathbf{L}_0 \cdot \int_{-\infty}^{\infty} \nabla' \left\{ r'^{-\lambda-1}(t)\, Y_{\lambda\mu}\left[\theta'(t),\phi'(t)\right]\right\} e^{i\omega t}\, dt \tag{98}$$

which are the usual orbital integrals in the non-relativistic Coulomb excitation theory with hyperbolic trajectories (see Eqs. (II.A.43) of Ref. [2]).

In the intermediate energy case the relation 95 is partially relaxed (of course, for relativistic energies, v $\sim$ c, it is not valid) and one has to keep the more complex forms, Eqs. 93 and 94, for the orbital integrals.

For convenience, we define

$$I(E\lambda,\mu) = \frac{v a^\lambda}{\mathcal{C}_{\lambda\mu}}\, S(E_\lambda,\mu) \tag{99}$$

where

$$\mathcal{C}_{\lambda\mu} = \begin{cases} \sqrt{\frac{2\lambda+1}{4\pi}}\,\frac{\sqrt{(\lambda-\mu)!(\lambda+\mu)!}}{(\lambda-\mu)!!(\lambda+\mu)!!}\,(-1)^{(\lambda+\mu)/2}, & \text{for } \lambda+\mu = \text{even}\ , \\ 0, & \text{for } \lambda+\mu = \text{odd}\ , \end{cases} \tag{100}$$

and we translate the path of integration by an amount $i\pi/2$ to avoid strong oscillations of the integral. This yields [10]

$$\begin{aligned} I(E\lambda,\mu) &= -i(\frac{v\eta}{c})^{\lambda+1}\,\frac{1}{\lambda(2\lambda-1)!!}\,e^{-\pi\eta/2}\int_{-\infty}^{\infty} d\chi\; e^{-\eta\epsilon\cosh\chi}\, e^{i\eta\chi} \\ &\times \frac{(\epsilon + i\sinh\chi - \sqrt{\epsilon^2-1}\cosh\chi)^\mu}{(i\epsilon\sinh\chi+1)^{\mu-1}} \\ &\times \left[(\lambda+1)\,h_\lambda - z\,h_{\lambda+1} - (\frac{v}{c})^2\epsilon\,\eta\,\cosh\chi\cdot h_\lambda\right] \end{aligned} \tag{101}$$

where all h_λ's are now functions of

$$z = \frac{v}{c}\,\eta\,(i\epsilon\sinh\chi+1)\,, \qquad \eta = \frac{\omega a}{v} = \frac{\omega a_o}{\gamma v}\,. \tag{102}$$

In the case of magnetic excitations, defining

$$I(M\lambda,\mu) = -\frac{\lambda c a^\lambda S(M\lambda,\mu)}{\mathcal{C}_{\lambda+1,\mu}\,\cot\vartheta/2}\,\left\{[(2\lambda+1)/(2\lambda+3)]\,[(\lambda+1)^2-\mu^2]\right\}^{-1/2} \tag{103}$$

one obtains [10]

$$\begin{aligned} I(M\lambda,\mu) &= \frac{i(v\eta/c)^{\lambda+1}}{(2\lambda-1)!!}\,e^{-\pi\eta/2}\int_{-\infty}^{\infty} d\chi\; h_\lambda(z)\; e^{-\eta\epsilon\,\cosh\chi} \\ &\times e^{i\eta\chi}\,\frac{(\epsilon + i\sinh\chi - \sqrt{\epsilon^2-1}\,\cosh\chi)^\mu}{(i\epsilon\sinh\chi+1)^\mu}\,. \end{aligned} \tag{104}$$

The orbital integrals 101 and 104 can only be solved numerically.

0.5.3 Cross sections and equivalent photon numbers

In the high-energy limit the classical trajectory reduces to a straight-line. One can show that using the approximation $\epsilon = b/a \gg 1$ the orbital integrals, Eqs. 101 and 104, can be expressed in terms of simple analytical functions. However it is instructive and useful to deduce the excitation amplitudes from the first principles again.

The square modulus of Eq. 92 gives the probability of exciting the target nucleus from the initial state $\mid I_i M_i >$ to the final state $\mid I_f M_f >$ in a collision with c.m. scattering angle ϑ. If the orientation of the initial state is not specified, the cross section for exciting the nuclear state of spin I_f is

$$d\sigma_{i\to f} = \frac{a^2\epsilon^4}{4}\,\frac{1}{2I_i+1}\sum_{M_i,M_f}\mid a_{fi}\mid^2\, d\Omega\,, \tag{105}$$

where $a^2\epsilon^4 d\Omega/4$ is the elastic (Rutherford) cross section. Using the Wigner-Eckart theorem and the orthogonality properties of the Clebsch-Gordan coefficients, one can show that

$$\frac{d\sigma_{i\to f}}{d\Omega} = \frac{4\pi^2 Z_1^2 e^2}{\hbar^2}\; a^2\epsilon^4 \sum_{\lambda\mu}\frac{B(\pi\lambda, I_i\to I_f)}{(2\lambda+1)^3}\;\mid S(\pi\lambda,\mu)\mid^2, \tag{106}$$

where $\pi = E$ or M stands for the electric or magnetic multipolarity.

Integration of 106 over all energy transfers $\varepsilon = \hbar\omega$, and summation over all possible final states of the projectile nucleus leads to

$$\frac{d\sigma_C}{d\Omega} = \sum_f \int \frac{d\sigma_{i\to f}}{d\Omega}\;\rho_f(\varepsilon)\; d\epsilon\,, \tag{107}$$

where $\rho_f(\varepsilon)$ is the density of final states of the target with energy $E_f = E_i + \varepsilon$. Inserting Eq. 106 into Eq. 107 one finds

$$\frac{d\sigma_C}{d\Omega} = \sum_{\pi\lambda}\frac{d\sigma_{\pi\lambda}}{d\Omega} = \sum_{\pi\lambda}\int\frac{d\varepsilon}{\varepsilon}\;\frac{dn_{\pi\lambda}}{d\Omega}(\varepsilon)\;\sigma_\gamma^{\pi\lambda}(\varepsilon)\,, \tag{108}$$

where $\sigma_\gamma^{\pi\lambda}$ are the photonuclear absorption cross sections for a given multipolarity $\pi\lambda$. The *virtual photon numbers*, $n_{\pi\lambda}(\varepsilon)$, are given by

$$\frac{dn_{\pi\lambda}}{d\Omega} = \frac{Z_1^2\alpha}{2\pi}\;\frac{\lambda\left[(2\lambda+1)!!\right]^2}{(\lambda+1)(2\lambda+1)^3}\;\frac{c^2a^2\epsilon^4}{\kappa^{2(\lambda-1)}}\sum_\mu\mid S(\pi\lambda,\mu)\mid^2\;. \tag{109}$$

In terms of the orbital integrals $I(E\lambda,\mu)$, given by Eq. 102, and using the Eq. 109, we find for the electric multipolarities

$$\begin{aligned}\frac{dn_{E\lambda}}{d\Omega} &= \frac{Z_1^2\alpha}{8\pi^2}\,(\frac{c}{v})^{2\lambda}\,\frac{\lambda\left[(2\lambda+1)!!\right]^2}{(\lambda+1)(2\lambda+1)^2}\,\epsilon^4\,\eta^{-2\lambda+2} \\ &\times \sum_{\mu\lambda+\mu=even}\frac{(\lambda-\mu)!(\lambda+\mu)!}{\left[(\lambda-\mu)!!(\lambda+\mu)!!\right]^2}\;\mid I(E\lambda,\mu)\mid^2\;. \end{aligned} \tag{110}$$

In the case of magnetic excitations we find

$$\begin{aligned}\frac{dn_{M\lambda}}{d\Omega} &= \frac{Z_1^2\alpha}{8\pi^2}\,(\frac{c}{v})^{2(\lambda-1)}\,\frac{\left[(2\lambda+1)!!\right]^2}{\lambda(\lambda+1)(2\lambda+1)^2}\,\eta^{-2\lambda+2}\,\epsilon^4\,(\epsilon^2-1) \\ &\times \sum_{\mu\lambda+\mu=odd}\frac{\left[(\lambda+1)^2-\mu^2\right]\,(\lambda+1-\mu)!(\lambda+1+\mu)!}{\left[(\lambda+1-\mu)!!(\lambda+1+\mu)!!\right]^2}\;\mid I(M\lambda,\mu)\mid^2\;. \end{aligned} \tag{111}$$

Only for the $E1$ multipolarity the integrals can be performed analytically and we get closed expression

$$\frac{dn_{E1}}{d\Omega} = \frac{Z_1^2\alpha}{4\pi^2}\,\left(\frac{c}{v}\right)^2\,\epsilon^4\,\zeta^2\;\;e^{-\pi\zeta}\,\left\{\frac{1}{\gamma^2}\,\frac{\epsilon^2-1}{\epsilon^2}\,\left[K_{i\zeta}(\epsilon\zeta)\right]^2+\left[K'_{i\zeta}(\epsilon\zeta)\right]^2\right\}, \tag{112}$$

where $\epsilon = 1/\sin(\theta/2)$, $\alpha = 1/137$, $\zeta = \omega a_0/\gamma v$ and $a_0 = Z_1Z_2e^2/2E_{Lab}$. $K_{i\zeta}$ is the modified Bessel function with imaginary index, $K'_{i\zeta}$ is the derivative with respect to its argument.

Since the impact parameter is related to the scattering angle by $b = a\cot\vartheta/2$, we can also write

$$n_{\pi\lambda}(\varepsilon,b) \equiv \frac{dn_{\pi\lambda}}{2\pi b db} = \frac{4}{a^2\epsilon^4}\,\frac{dn_{\pi\lambda}}{d\Omega} \tag{113}$$

which are interpreted as the number of equivalent photons of energy $\varepsilon = \hbar\omega$, incident on the target per unit area, in a collision with impact parameter b.

Again we stress the usefulness of the concept of virtual photon numbers, especially in relativistic collisions. In these collisions the momentum and the energy transfer due to the Coulomb interaction are related by $\Delta p = \Delta E/v \simeq \Delta E/c$. This means that the virtual photons are almost real. One usually explores this fact to extract information about real photon processes from the reactions induced by relativistic charges, and vice-versa. This is the basis of the *Weizsäcker-Williams method*, commonly used to calculate cross sections for Coulomb excitation, particle production, Bremsstrahlung, etc (see, e.g., Ref. [23]). In the case of Coulomb excitation, even at low energies, although the equivalent photon numbers should not be interpreted as (almost) real ones, the cross sections can still be written as a product of them and the cross sections induced by real photons, as we have shown above.

Supplement 6.C

0.6 Electromagnetic transition strengths

The nuclear excitations induced by photons (real and virtual) involve matrix elements of the operator

$$M_{\lambda\mu} = r^{\lambda}\, Y^{*}_{\lambda\mu}(\widehat{\mathbf{r}}). \tag{114}$$

Specifically, the matrix element for an electric multipole transition is given by

$$\mathcal{M}(E\lambda\mu) = \int r^{\lambda}\, Y^{*}_{\lambda\mu}(\theta)\delta\rho^{c}_{\alpha}(\mathbf{r}\,)d^{3}r \tag{115}$$

where $\delta\rho^{C}_{\alpha}$ is the transition density for the nuclear charge. For a collective surface oscillation, as explained in Supplement B, $\delta\rho^{C}_{\alpha}$ will be peaked at the surface. Using Eq. 65 the charge density of the excited nucleus is not spherically symmetric, but is slightly deformed. The equidensity surfaces are given by Eq. 65, i.e.,

$$r_{\theta} = r\left[1 + \sum_{\lambda\mu} \alpha^{*}_{\lambda\mu}\, Y_{\lambda\mu}(\theta)\right] \tag{116}$$

for constant r. In other words,

$$\rho^{C}_{\alpha}(r_{\theta},\theta) = \rho^{C}_{0}(r) \tag{117}$$

where $\rho^{C}_{0}(r)$ is the non-deformed density, or ground state density.

Conversely,

$$\begin{aligned}\rho^{C}_{\alpha}(r,\theta) &= \rho^{C}_{0}\left(\frac{r}{1+\sum_{\lambda\mu}\alpha^{*}_{\lambda\mu}Y_{\lambda\mu}(\theta)}\right)\\ &\cong \rho^{C}_{0}(r) - r\frac{d\rho^{C}_{0}}{dr}(r)\sum_{\lambda\mu}\alpha^{*}_{\lambda\mu}\,Y_{\lambda\mu}(\theta) + \mathcal{O}(\alpha^{2}).\end{aligned} \tag{118}$$

Thus, for small oscillations, the transition density in 115 is given by

$$\delta\rho^{c}_{\alpha}(\mathbf{r}\,) = \rho^{C}_{\alpha}(r,\theta) - \rho^{C}_{0}(r) = -r\,\frac{d\rho^{C}_{0}}{dr}\,(r)\sum_{\lambda\mu}\alpha^{*}_{\lambda\mu}Y_{\lambda\mu}(\theta). \tag{119}$$

The charge density maybe related to the matter density by means of

$$\rho^{C}_{0}(r) = \frac{Ze}{A}\rho_{0}(r). \tag{120}$$

Inserting 119 and 120 into 115 one obtains

$$\begin{aligned}\mathcal{M}(E\lambda\mu) &= -\frac{Ze}{A}\int r^{\lambda}Y^{*}_{\lambda\mu}(\theta)\left\{r\frac{d\rho_0(r)}{dr}\sum_{\ell m}\alpha^{*}_{\ell m}\,Y_{\ell m}(\theta)\right\}d^3r \\ &= -\frac{Ze}{A}\,\alpha^{*}_{\lambda\mu}\int r^{\lambda+3}\,\frac{d\rho_0(r)}{dr}dr \\ &= Ze\,\alpha^{*}_{\lambda\mu}\frac{(\lambda+3)}{4\pi}\left\{\frac{4\pi}{A}\int r^{\lambda+2}\rho_0(r)dr\right\}. \qquad (121)\end{aligned}$$

That is,

$$\mathcal{M}(E\lambda,\mu)=\frac{\lambda+3}{4\pi}Ze\langle r^{\lambda}\rangle_0\alpha^{*}_{\lambda\mu}. \qquad (122)$$

Using the definitions of the creation and annihilation operators given in Eq. 72 we can rewrite Eq. 122 as

$$\mathcal{M}(E\lambda\mu)=\frac{\lambda+3}{4\pi}Ze\langle r^{\lambda}\rangle_0\left(\frac{\hbar}{2\omega_\lambda B_\lambda}\right)^{1/2}\left[O_{\lambda\mu}+(-1)^{\mu}\,O^{+}_{\lambda,-\mu}\right]. \qquad (123)$$

In going from 122 to 123 we have quantized the matrix element $\mathcal{M}(E\lambda\mu)$ in form of an operator. It now connects states through collective vibrations of $\lambda\mu$ multipolarity.

A very common quantity which appears in the calculation of cross sections for electromagnetic processes is the so-called reduced transition probability. The matrix element of the operator 123 for the nuclear transition $|i\rangle\rightarrow|f\rangle$ is given by

$$\langle f|\mathcal{M}(E\lambda\mu)|i\rangle=(J_i\lambda J_f|M_i\;\mu\;M_f)\,\langle f||\mathcal{M}(E\lambda)||i\rangle \qquad (124)$$

where we have used the *Wigner-Eckart theorem* [9]. (J_iM_i) and (J_fM_f) are the initial and final nucleus spins and projection quantum numbers, $(J_i\,\lambda\,J_f\,|M_i\,\mu\,M_f)$ is a Clebsh Gordan coefficient, $\mu=M_f-M_i$, and $\langle f||M(E\lambda\mu)||i\rangle$ is the *reduced matrix element,* which does not depend on the nuclear spin. The matrix element 124 appears in the excitation cross sections. In most cases, the nucleus is initially unpolarized and its final polarization is unobserved. Thus, in the cross sections we must average over initial spins and sum over final spins. Therefore, the reduced transition probability

$$B(E\lambda,J_i\rightarrow J_f)=\frac{1}{2J_i+1}\sum_{M_iM_f}|\langle f|\mathcal{M}(E\lambda\mu)|i\rangle|^2 \qquad (125)$$

appears often in the cross section calculations. Using 124 we get

$$B(E\lambda,J_i\rightarrow J_f)=|\langle f||\mathcal{M}(E\lambda)||i\rangle|^2\frac{1}{2J_{i+1}}\sum_{M_iM_f}\left(J_I\,\lambda\,J_f|M_i,M_f-M_I,M_f\right)^2. \qquad (126)$$

Using the orthogonality properties of the Clebsh-Gordan coefficients [16] we get

$$B(E\lambda; J_i \to J_f) = \frac{2J_f+1}{2J_i+1} \left|\langle f||\mathcal{M}(E\lambda)||i\rangle\right|^2 . \tag{127}$$

The electric multipole operator 123 links states which differ by a unit of phonons. I.e.,

$$\Delta n_{\lambda\mu} = \pm 1. \tag{128}$$

For transitions from the ground state, $|0\rangle \to |\lambda\mu\rangle$, we obtain using 123,

$$\begin{aligned} B(E\lambda, 0 \to \lambda) &= (2\lambda+1) \left|\langle 0||\mathcal{M}(E\lambda)||\lambda\rangle\right|^2 \\ &= (2\lambda+1) \left[\frac{\lambda+3}{4\pi} Ze\langle r^\lambda\rangle_0\right]^2 \frac{\hbar}{2\omega_\lambda B_\lambda}. \end{aligned} \tag{129}$$

For a constant matter distribution with radius R_0

$$\langle r^\lambda\rangle_0 = \frac{3R_0^\lambda}{\lambda+3}, \tag{130}$$

and

$$B(E\lambda, 0 \to \lambda) = (2\lambda+1) \left[\frac{3}{4\pi} Ze\, R_0^\lambda\right]^2 \frac{\hbar}{2\omega_\lambda B_\lambda}. \tag{131}$$

We now define the deformation length

$$\delta_\lambda = \left[(2\lambda+1)\frac{\hbar}{2\omega_\lambda B_\lambda}\right]^{1/2} R_0. \tag{132}$$

It measures the amplitude of the surface oscillations for a given mode λ . In terms of δ_λ

$$B(E\lambda, 0 \to \lambda) = \left[\frac{3}{4\pi} Ze\, R_0^{\lambda-1}\right]^2 \delta_\lambda^2. \tag{133}$$

In this macroscopic model, the magnetic transitions are predicted to be zero since the deformation of a uniformly charged fluid induces no magnetic moment. In fact, $M1$ transitions are inhibited by factors of order $1/100$ for good vibrational nuclei.

In lowest order in $\alpha_{\lambda\mu}$ the transition density conserves particle number. This can be seen from Eq. 118. An integration over volume implies that

$$\int \rho_\alpha^c(r,\theta) d^3r = \int \rho_0^C(r) d^3r. \tag{134}$$

This relationship fails if $\lambda = 0$. The $\lambda = 0$ modes are interesting and correspond to monopole excitations often called by *"breathing" modes*. To conserve particle number we have to add a correction to 118 for the $\lambda = 0$ case. It is easy to check that a transition density given by

$$\delta\rho^C_{\alpha(\lambda=0)}(\mathbf{r}) = -\alpha^*_0 \left[3\rho^C_0(r) + r\frac{d\rho^C_0}{dr}\right] Y_{00}(\hat{\mathbf{r}}) \tag{135}$$

conserves particle number, since

$$\int \delta\rho^C_{\alpha(\lambda=0)}(r) d^3r = 0.$$

For electromagnetic monopole transitions

$$\mathcal{M}(E0) = \frac{Ze}{A}\int r^2 \delta\rho_{\alpha(\lambda=0)}(\mathbf{r})\, Y_{00}(\hat{\mathbf{r}}) d^3r \tag{136}$$

is the matrix element of interest.

Repeating the same procedure as before, we get in terms of α_0,

$$\mathcal{M}(E0) = \frac{\alpha^*_0}{2\pi} Ze\langle r^2\rangle$$

and

$$B(E0) = \left[\frac{Ze\langle r^2\rangle}{2\pi}\right]^2 \frac{\hbar}{2\omega_0 B_0}$$

or, else

$$B(E0) = \left[\frac{3ZeR^2_0}{10\pi}\right]^2 \alpha^2_0. \tag{137}$$

In Supplement D we will show how the sum rules can be used to obtain the values of δ_λ and of α_0.

0.7 Comparison of Coulomb excitation at low energies and at relativistic energies

Inserting the non-relativistic orbital integrals into Eq. 109, we get the following relation for the non-relativistic equivalent photon numbers (NR)

$$\frac{dn^{(NR)}_{\pi\lambda}}{d\Omega} = Z^2_1\alpha \frac{\lambda[(2\lambda+1)!!]^2}{(2\pi)^3(\lambda+1)} \zeta^{-2\lambda+2} (\frac{c}{v})^{2(\lambda+\delta)} \frac{df_{\pi\lambda}}{d\Omega}(\vartheta,\zeta)\,, \tag{138}$$

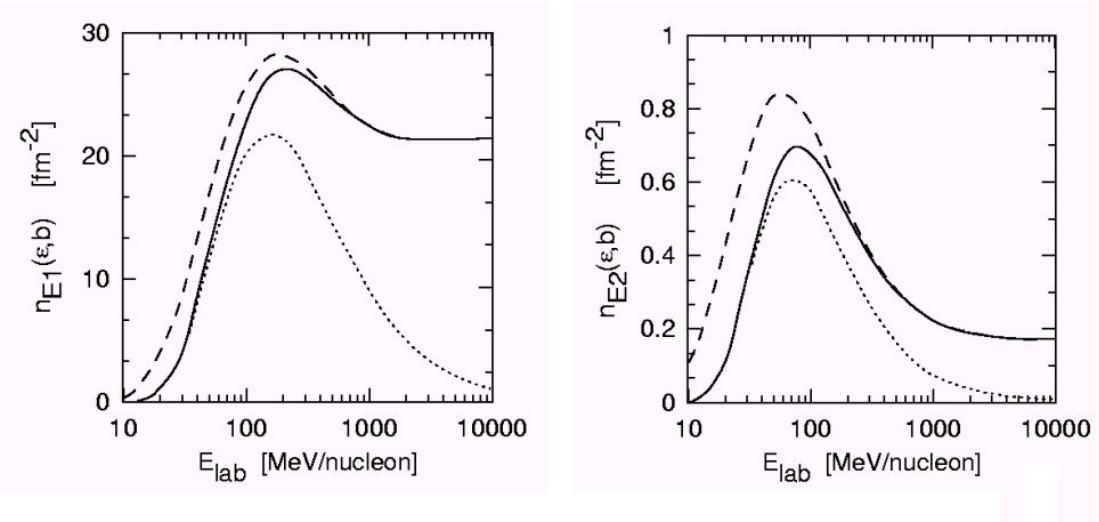

Figure 2: Electric dipole (E1) and quadrupole (E2) number of equivalent photons per unit area $d^2b \equiv 2\pi b\, db$, with energy of 10 MeV, incident on ^{208}Pb in a collision with ^{16}O at impact parameter $b = 15\ fm$, and as a function of the bombarding energy in MeV per nucleon. The dotted line and the dashed line correspond to calculations performed with the non-relativistic and with the relativistic approaches, respectively. The solid line represents a more correct calculation, as described in the text.

where $\delta = 0$ for electric, and $\delta = -1$ for magnetic multipolarities, and $\zeta = \omega a_0/v$. The non-relativistic Coulomb excitation functions $f_{\pi\lambda}(\vartheta, \zeta)$ are very well known and, e.g., are tabulated in Ref. [2], or maybe calculated numerically.

Using the Eqs. 110, 111 and 112, we make an analysis of Coulomb excitation extending from low to high energy collisions. As an example, we study the excitations induced by ^{208}Pb in ^{16}O + ^{208}Pb collisions. Since the expression 109 is quite general, valid for all energies, under the assumption that the nuclei do not overlap, the equivalent photon numbers contain all information about the differences among the low and the high energy scattering. In Figs. 2 and 3(a) we show $dn_{\pi\lambda,\varepsilon}$, for the $E1$, $E2$ and $M1$ multipolarities, and for the collision ^{16}O + ^{208}Pb with an impact parameter $b = 15$ fm. They are the equivalent photon numbers with frequency $\omega = 10$ MeV/$\hbar$ incident on ^{208}Pb. The dotted lines are obtained by using the non-relativistic Eq. (138), while the dashed lines correspond to the relativistic expressions 54, 55 and 56. One observes that the relativistic expressions overestimate the equivalent photon numbers at low energies, while the non-relativistic expressions underestimate them at high energies. The most correct values are given by the solid lines, calculated according to Eqs. 110 and 111. They reproduce the low and the high energy limits, giving an improved

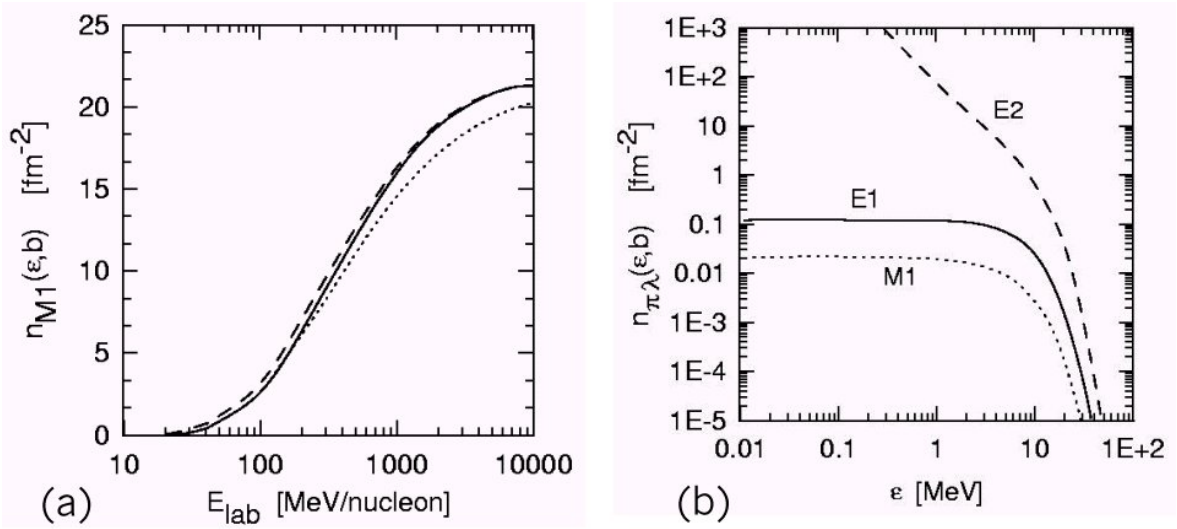

Figure 3: (a) Same as Fig. 2, but for the $M1$ multipolarity. (b) Equivalent photon numbers per unit area incident on ^{208}Pb, in a collision with ^{16}O at 100A MeV and with impact parameter $b = 15$ fm, as a function of the photon energy $\hbar\omega$. The curves for the $E1$, $E2$ and $M1$ multipolarities are shown.

interpolation between these limits at intermediate energies. These discrepancies are more apparent for the $E1$ and the $E2$ multipolarities. In the energy interval around 100A MeV neither the low energy theory nor the high energy one can reproduce well the correct values. This energy interval is indeed very sensitive to the effects of retardation and of Coulomb recoil.

At these bombarding energies, the differences between the magnitude of the non-relativistic and the correct relativistic virtual photon numbers are kept at a constant value, of about 20%, for excitation energies $\varepsilon = \hbar\omega < 10$ MeV. However, they increase sharply when one reaches the excitation energy of $\varepsilon = \hbar\omega > 10$ MeV. The reason is that, for such excitation energies, the adiabacity factor becomes greater than unity ($\xi > 1$). This means that excitation energies of order of 10 MeV (like in the case of giant resonance excitation) are in the transition region from a constant behavior of the equivalent photon numbers to that of an exponential ($\sim e^{-\pi\xi}$) decay. This is more transparent in Fig. 3(b) where we plot the equivalent photon numbers for E_{lab} =100A MeV, $b = 15$ fm, and as a function of $\hbar\omega$. One also observes from this figure that the $E2$ multipolarity component of the electromagnetic field dominates at low frequencies. Nonetheless, over the range of $\hbar\omega$ up to some tens of MeV, the $E2$ matrix elements of excitation are much smaller than the $E1$ elements for most nuclei, and the $E2$ effects become unimportant. However, such effects are relevant for the

excitation of the isoscalar $E2$ giant resonance (GQR_{is}) which have large matrix elements.

We will discuss the differential cross sections as a function of the scattering angle later, when we introduce the effects of strong absorption. To obtain the total cross sections, one has to integrate the equivalent photon numbers in Eqs. 110 and 111 from 0° to a maximum scattering angle θ_{max}, where the nuclear absorption sets in, or equivalently, one can integrate over the impact parameter, from a minimum value b_{mim} up to infinity.

Only for the $E1$ multipolarity the angular integration can be performed analytically. One obtains[1]

$$N_{E1} = \frac{2}{\pi}\, Z_1^2\alpha\, e^{-\pi\zeta}\, (c/v)^2 \left\{ -\xi K_{i\zeta} K'_{i\zeta} - \frac{1}{2}(c/v)^2\xi^2 \right. \tag{139}$$
$$\left. \times \left[(\zeta/\xi)^2 K_{i\zeta}^2 + K_{i\zeta}'^2 - K_{i\zeta}^2 - \frac{i}{\epsilon_0}\left(K_{i\zeta}\left(\frac{\partial K'_\mu}{\partial\mu}\right)_{\mu=i\zeta} - K'_{i\zeta}\left(\frac{\partial K_\mu}{\partial\mu}\right)_{\mu=i\zeta}\right)\right\} ,$$

where

$$\epsilon_0 = \begin{cases} 1, & \text{for } 2a > b_{mim} , \\ R/a - 1, & \text{for } 2a < b_{mim} , \end{cases} \tag{140}$$

and $\xi = \epsilon_0\zeta = \omega b_{mim}/\gamma v$.

It is easy to see that this equation reduces to Eq. 62 in the relativistic limit, when $\zeta \longrightarrow 0$, $\epsilon_0 \longrightarrow \infty$.

The cross sections increase very rapidly to large values, which are already attained at intermediate energies. A salient feature is that the cross section for the excitation of giant quadrupole modes is very large at low and intermediate energies, decreasing in importance (about 10% of the $E1$ cross section) as the energy increases above 1A GeV. This occurs because the equivalent photon number for the $E2$ multipolarity is much larger than that for the $E1$ multipolarity at low collision energies. That is, $n_{E2} \gg n_{E1}$, for $v \ll c$. This has a simple explanation. Pictorially, as seen from an observer at rest, when a charged particle moves at low energies the lines of force of its corresponding electric field are isotropic, diverging from its center in all directions. This means that the field carries a large amount of tidal ($E2$) components. On the other hand, when the particle moves very fast its lines of force appear contracted in the direction perpendicular to its motion due to Lorentz contraction. For the observer this field looks like a pulse of plane waves of light. But plane waves contain all multipolarities with the same weight, and the equivalent photon numbers become all approximately equal, i.e., $n_{E1} \simeq n_{E2} \simeq n_{M1}$, and increase logarithmically with the energy for $\gamma \gg 1$. The difference in the cross sections when $\gamma \gg 1$ are then approximately equal to the difference in the relative strength of the two giant resonances $\sigma_\gamma^{E2}/\sigma_\gamma^{E1} < 0.1$. The excitation of giant magnetic monopole resonances is of less importance, since for low energies

[1]We observe that the original formula for the dipole case appearing in [23] has a misprinted sign in one of its terms.

$n_{M1} \ll n_{E1}$ ($n_{M1} \simeq (v/c)^2 n_{E1}$), whereas for high energies, where $n_{M1} \simeq n_{E1}$, it will be also much smaller than the excitation of electric dipole resonances since their relative strength $\sigma_\gamma^{M1}/\sigma_\gamma^{E1}$ is much smaller than unity.

At very large energies the cross sections for the Coulomb excitation of giant resonances overcome the nuclear geometrical cross sections. Since these resonances decay mostly through particle emission or fission, this indicates that Coulomb excitation of giant resonances is a very important process to be considered in relativistic heavy ion collisions and fragmentation processes, especially in heavy ion colliders. At intermediate energies the cross sections are also large and this offers good possibilities to establish and study the properties of giant resonances.

Supplement D

0.8 Sum rules and $E\lambda$ moments

Sum rules are very useful to calculate the cross sections when the reduced matrix elements $B(E\lambda)$ are not known.

For a system governed by a Hamiltonian H, we can define the sum

$$S(F) = \sum_a (E_a - E_0) \, |\langle a|F|0\rangle|^2 \tag{141}$$

for the excitation $|0\rangle \rightarrow |a\rangle$ induced by the operator F. If F is Hermitian

$$\begin{aligned} S(F) &= \sum_a \langle a|F|0\rangle \, (E_a - E_0) \, \langle 0|F|a\rangle \\ &= \frac{1}{2} \sum_a \langle 0|F|a\rangle \, \{ \langle a|[H,F]|0\rangle - \langle 0|[H,F]|a\rangle \, \} \, \langle a|F|0\rangle \\ &= \frac{1}{2} \, \langle 0 \, |[F,[H,F]]| \, 0\rangle \, . \end{aligned} \tag{142}$$

For a microscopic operator (interaction) acting on each nucleon k, we can write

$$F = \sum_k \, F(\mathbf{r}_k \,) \tag{143}$$

and

$$H = \sum_k \left[-\frac{\hbar^2 \nabla_k^2}{2m_k} + V(\mathbf{r}_k) \right] . \tag{144}$$

Then, Eq. 142 becomes

$$S(F) = \frac{1}{2}\left\langle 0 \left| \sum_k \frac{\hbar^2}{2m_k} \left[F(\mathbf{r}_k), \left[\nabla_k^2, F(\mathbf{r}_k)\right]\right] \right| 0 \right\rangle . \tag{145}$$

Since the expectation value of HF^2 and F^2H are the same, $\langle 0|F^2\nabla^2|0\rangle = \langle 0|(\nabla^2 F)F|0\rangle$, and

$$\begin{aligned} \left\langle 0 \left| \left[F, \left[\nabla^2, F\right]\right] \right| 0 \right\rangle &= \left\langle 0 \left| F\,\nabla^2 F - 2(\nabla^2 F)F + F\nabla^2 F \right| 0 \right\rangle \\ &= \left\langle 0 \left| 2F\nabla^2 F - 2(\nabla^2 F)F \right| 0 \right\rangle . \end{aligned}$$

But

$$\nabla \cdot (F\nabla F) = (\nabla F)^2 + F\nabla^2 F$$

and

$$\left\langle 0 \left| [F, [\nabla^2, F]] \right| 0 \right\rangle = 2 \left\langle 0 \left| (\nabla F)^2 \right| 0 \right\rangle . \tag{146}$$

Thus

$$S(F) = \left\langle 0 | \sum_k \frac{\hbar^2}{2m_k} \left[\nabla_k F(\mathbf{r}_k)\right]^2 | 0 \right\rangle . \tag{147}$$

For nuclear and Coulomb excitation one often encounters operators of the form

$$F \equiv F_{\lambda\mu} = f(r)\, Y_{\lambda\mu}(\hat{\mathbf{r}}). \tag{148}$$

Then, one can show that (see Ref. [17], p. 400-401)

$$\begin{aligned} &\sum_\mu \nabla \left[f(r) Y^*_{\lambda\mu}(\hat{\mathbf{r}})\right] \cdot \nabla \left[f(r) Y_{\lambda\mu}(\hat{\mathbf{r}})\right] \\ &= \frac{2\lambda+1}{4\pi} \left[\left(\frac{df}{dr}\right)^2 + \lambda(\lambda+1) \left(\frac{f}{r}\right)^2 \right] \end{aligned} \tag{149}$$

and

$$\begin{aligned} S(F_\lambda) &\equiv \sum_{\alpha\mu} (E_\alpha - E_0) \left|\langle \alpha | F_{\lambda\mu} | 0 \rangle\right|^2 \\ &= \left\langle 0 \left| \frac{\hbar^2}{2m} \sum_{\mu,k} \left|\nabla_k F_{\lambda\mu}(\mathbf{r}_k)\right|^2 \right| 0 \right\rangle \\ &= \frac{2\lambda+1}{4\pi} \frac{\hbar^2}{2m} A \left\langle 0 \left| \left(\frac{df}{dr}\right)^2 + \lambda(\lambda+1)\left(\frac{f}{r}\right)^2 \right| 0 \right\rangle . \end{aligned} \tag{150}$$

The electric multipole matrix elements are given by

$$\begin{aligned}\mathcal{M}(E\lambda;\mu) &= e\sum_{k=\text{protons}}\left[r^\lambda\, Y_{\lambda\mu}\right]_k \\ &\equiv e\sum_k\left[\left(\frac{1}{2}-\tau_Z\right)r^\lambda Y_{\lambda\mu}\right]_k \end{aligned} \tag{151}$$

where

$$\tau_z\,\psi_{\text{proton}} = -\frac{1}{2}\,\psi_{\text{proton}}, \qquad \tau_z\,\psi_{\text{neutron}} = \frac{1}{2}\,\psi_{\text{neutron}}. \tag{152}$$

It is important to include recoil corrections for $E1$-transitions. The matrix elements in 151 include not only internal displacement of the protons but also contain a spurious displacement of the center of mass.

For $\lambda = 1$, Eq. 151 maybe written as

$$\mathcal{M}(E1,\mu) = \left(\sum_{i=1}^{A} e_i\,\mathbf{r}_i\right)_\mu$$

($e_i = e$ for protons, 0 for neutron). Subtracting the coordinates $\mathbf{r}_i$ from the center of mass $\mathbf{R} = \dfrac{1}{A}\sum_{i=1}^{A}\mathbf{r}_i$, one gets (we drop the index μ for the moment)

$$\begin{aligned}\mathcal{M}(E1) &= \sum_{i=1}^{A} e_i\,(\mathbf{r}_i-\mathbf{R}) = e\sum_{i=1}^{Z}\mathbf{r}_i - \frac{eZ}{A}\sum_{i=1}^{A}\mathbf{r}_i \\ &= e\sum_{i=1}^{Z}\left(1-\frac{Z}{A}\right)\mathbf{r}_i - \frac{eZ}{A}\sum_{i=Z+1}^{A}\mathbf{r}_i = \frac{eN}{A}\sum_{i=1}^{Z}\mathbf{r}_i - \frac{eZ}{A}\sum_{i=Z+1}^{A}\mathbf{r}_i.\end{aligned}$$

This expression shows that the inclusion of the center of mass recoil correction can be accomplished from the beginning by assuming that neutron have an effective charge eN/A and protons an effective charge $(-e\,Z/A)$. It can be shown that in the general case (any λ) (see [14])

$$e_p^{\text{eff}} = e\,\frac{1}{A^\lambda}\left[(A-1)^\lambda + (-1)^\lambda(Z-1)\right] \tag{153}$$

and

$$e_n^{\text{eff}} = e\,Z\left(-\frac{1}{A}\right)^\lambda. \tag{154}$$

For multipoles higher $E1$ the effective charges involve corrections of order of λ/A or smaller. Therefore, they are small for heavy nuclei.

Including recoil correction the $E1$-matrix element is given by

$$\mathcal{M}(E1,\mu) = e\sum_k \left[\left(\frac{N-Z}{2A} - \tau_z\right) r\, Y_{\lambda\mu}\right]_k \tag{155}$$

Using Eq. 150

$$\begin{aligned} S(E1) &= \frac{3}{4\pi}\frac{\hbar^2}{2m}\cdot 3e^2\left\{\left(\frac{N-Z}{2A}-\frac{1}{2}\right)^2 N + \left(\frac{N-Z}{A}+\frac{1}{2}\right)^2 Z\right\} \\ &= \frac{9}{4\pi}\frac{\hbar^2}{2m}\frac{NZ}{A}\,e^2 = 14.8\,\frac{NZ}{A}\,e^2\,\mathrm{fm}^2\,\mathrm{MeV}. \end{aligned} \tag{156}$$

For $\lambda \geq 2$ and isoscalar excitations, using 150,

$$S(E\lambda) = \frac{\lambda(2\lambda+1)^2}{4\pi}\frac{\hbar^2}{2m}\,Z\,e^2\langle r^{2\lambda-2}\rangle_{\mathrm{prot.}} \tag{157}$$

where $\langle r^{2\lambda-2}\rangle_{\mathrm{prot}}$ is defined in terms of the one-particle $|\psi_p|^2$ as

$$\begin{aligned} \langle r^{2\lambda-2}\rangle_{\mathrm{prot}} &= \sum_p \int |\psi_p|^2\, r^{2\lambda-2}\, d^3r \\ &= \frac{Z}{A}\int \rho(r) r^{2\lambda-2}\, d^3r = \frac{Z}{A}\langle r^{2\lambda-2}\rangle \end{aligned} \tag{158}$$

where $\rho(r)$ is the total particle density. Thus,

$$S(E\lambda) = \frac{\lambda(2\lambda+1)^2}{4\pi}\frac{\hbar^2}{2m}\frac{Z^2e^2}{A}\,\langle r^{2\lambda-2}\rangle. \tag{159}$$

For a uniform charge distribution we use 130:

$$\langle r^{2\lambda-2}\rangle = \frac{3}{(2\lambda+1)}\,R^{2\lambda-2} \tag{160}$$

and

$$S(E\lambda) = \lambda(2\lambda+1)\,\frac{\hbar^2}{2m}\,\frac{3Z^2}{4\pi A}\,R^{2\lambda-2}\,e^2. \tag{161}$$

For $(E0)$ monopole transitions

$$\mathcal{M}(E0) = e\sum_k \left[\left(\frac{1}{2}-\tau_Z\right) r^2\right]_k Y_{00} \tag{162}$$

and

$$S(E0) = \frac{\hbar^2}{2\pi\, m}\, Z\, e^2 \langle r^2 \rangle_{\rm prot} = \frac{\hbar^2}{2\pi\, m}\, \frac{Z^2}{A}\, e^2 \langle r^2 \rangle. \tag{163}$$

For a uniform charge distribution

$$S(E0) = \frac{3\hbar^2}{10\pi\, m}\, \frac{Z^2}{A}\, R^2 e^2 \tag{164}$$

Using the sum rules, Eqs. 159, 161 and 164, and the relation between the transition matrix elements and the deformation parameters, Eqs. 133 and 137, we get

$$\delta^2_{\lambda\geq 2} = \frac{4\pi}{3}\, \lambda(2\lambda+1)\, \frac{\hbar^2}{2m}\, \frac{1}{AE_x} \tag{165}$$

and

$$\alpha_0^2 = \frac{10\pi}{3}\, \frac{\hbar^2}{m}\, \frac{1}{AR^2 E_x} \tag{166}$$

where E_x is the energy of a state assuming to exhaust the full sum rule, i.e.,

$$S(E\lambda) \equiv \sum_i E_i\, B(E\lambda, 0 \to \lambda) \cong E_x B(E\lambda, 0 \to \lambda). \tag{167}$$

This approximation is good for giant resonance states, which exhaust most part of the sum rule.

For the $E1$ case, recoil corrections amount in the replacement of Z by NZ/A in Eq. 133. That is,

$$B(E1, 0 \to 1) = \left[\frac{3}{4\pi}\, \frac{NZ}{A} e\right]^2 \delta_1^2. \tag{168}$$

Using Eq. 156 one gets

$$\delta_1^2 = 4\pi\, \frac{\hbar^2}{2m}\, \frac{A}{NZ}\, \frac{1}{E_x}. \tag{169}$$

0.9 Quantum description of Coulomb excitation at high energies

Inelastic scattering of heavy ions at intermediate energy collisions is an important tool to investigate the structure of stable and unstable nuclei. The angular distribution of the inelastically scattered fragments are particularly useful to identify unambiguously the multipolarity of the interaction, and consequently the spin and parities of the excited states. In previous Sections we have shown that recoil and retardation effects, are important at

this energy regime. However, as shown by Bertulani and Nathan [33], in order to describe correctly the angular distribution, absorption and diffraction effects have to be included properly. Next we show how quantum mechanical effects show up in the differential cross sections.

0.9.1 Inelastic amplitudes and virtual photon numbers

Defining $\mathbf{r}$ as the separation between the centers of mass of the two nuclei and $\mathbf{r}'$ to be the intrinsic coordinate of the target nucleus to first-order the inelastic scattering amplitude is given by

$$f(\theta) = \frac{ik}{2\pi\hbar v} \int d^3r \; d^3r' < \Phi^{(-)}_{\mathbf{k}'}(\mathbf{r}) \; \phi_f(\mathbf{r}') \mid V_{int}(\mathbf{r}, \; \mathbf{r}') \mid \Phi^{(+)}_{\mathbf{k}}(\mathbf{r}) \; \phi_i(\mathbf{r}') > , \tag{170}$$

where $\Phi^{(-)}_{\mathbf{k}'}(\mathbf{r})$ and $\Phi^{(+)}_{\mathbf{k}}(\mathbf{r})$ are the incoming and outgoing distorted waves, respectively, for the scattering of the center of mass of the nuclei, and $\phi(\mathbf{r}')$ is the intrinsic nuclear wavefunction of the target nucleus.

At intermediate energies, $\Delta E/E_{lab} \ll 1$, and forward angles, $\theta \ll 1$, we can use eikonal wavefunctions for the distorted waves; i.e.,

$$\Phi^{(-)*}_{\mathbf{k}'}(\mathbf{r}) \; \Phi^{(+)}_{\mathbf{k}}(\mathbf{r}) = \exp\left\{ -i\mathbf{q}.\mathbf{r} + i\chi(b) \right\} , \tag{171}$$

where

$$\chi(b) = \frac{i}{\hbar v} \int_{-\infty}^{\infty} U^{opt}_N(z', \; b) \; dz' + i\psi_C(b) \tag{172}$$

is the eikonal-phase, $\mathbf{q} = \mathbf{k}' - \mathbf{k}$, U^{opt}_N is the nuclear optical potential, and $\psi_C(b)$ is the Coulomb eikonal phase. We have defined the impact parameter $\mathbf{b}$ by $\mathbf{b} = |\mathbf{r} \times \hat{\mathbf{z}}|$.

For high energy collisions, the optical potential $U(r)$ can be constructed by using the t-$\rho\rho$ approximation [32].

In Eq. 170 the interaction potential, assumed to be purely Coulomb, is given by

$$V_{int}(\mathbf{r}, \; \mathbf{r}') = \frac{v^\mu}{c^2} \; j_\mu(\mathbf{r}') \; \frac{e^{i\kappa|\mathbf{r}-\mathbf{r}'|}}{|\mathbf{r}-\mathbf{r}'|} , \tag{173}$$

where $v^\mu = (c, \; \mathbf{v})$, with $\mathbf{v}$ equal to the projectile velocity, $\kappa = \omega/c$, and $j_\mu(\mathbf{r}')$ is the charge four-current for the intrinsic excitation of nucleus 1 by an energy of $\hbar\omega$. Inserting Eqs. 172 and 173 in Eq. 170 one finds [33]

$$\begin{aligned} f(\theta) &= i\frac{Z_1 e k}{\gamma\hbar v} \sum_{\pi\lambda m} i^m \left(\frac{\omega}{c}\right)^\lambda \sqrt{2\lambda+1} \; e^{-im\phi} \\ &\times \; \Omega_m(q) \; G_{\pi\lambda m}\left(\frac{c}{v}\right) < I_f \; M_f \mid \mathcal{M}(\pi\lambda, \; -m) \mid I_i \; M_i > \end{aligned} \tag{174}$$

where $\pi\lambda m$ denotes the multipolarity, $G_{\pi\lambda m}$ are the *Winther-Alder relativistic functions* [3], and $< I_f\ M_f|\mathcal{M}(\pi\lambda,-m)|I_i\ M_i >$ is the matrix element for the electromagnetic transition of multipolarity $\pi\lambda m$ from $|I_i\ M_i >$ to $|I_f\ M_f >$, with $E_f - E_i = \hbar\omega$. The function $\Omega_m(q)$ is given by [33]

$$\Omega_m(q) = \int_0^\infty db\ b\ J_m(qb)\ K_m\left(\frac{\omega b}{\gamma v}\right)\ \exp\{i\chi(b)\}\ , \tag{175}$$

where $q = 2k\sin(\theta/2)$ is the momentum transfer, θ and ϕ are the polar and azimuthal scattering angles, respectively.

For the $E1$, $E2$ and $M1$ multipolarity, the functions $G_{\pi\lambda m}(c/v)$ are given by [3]

$$\begin{aligned}
G_{E11}(x) &= -G_{E1-1}(x) = (1/3)\,x\sqrt{8\pi}; \quad G_{E10}(x) = -i\,(4/3)\,\sqrt{\pi(x^2-1)};\\
G_{M11}(x) &= G_{M1-1}(x) = -i\,(1/3)\,\sqrt{8\pi}; \quad G_{M10}(x) = 0;\\
G_{E22}(x) &= G_{E2-2}(x) = -\,(2/5)\,x\sqrt{\pi(x^2-1)/6};\\
G_{E21}(x) &= -G_{E2-1}(x) = i\,(2/5)\,\sqrt{\pi/6}(2x^2-1);\\
G_{E20}(x) &= (2/5)\,x\sqrt{\pi(x^2-1)}\ .
\end{aligned} \tag{176}$$

Using the Wigner-Eckart theorem, one can calculate the inelastic differential cross section from 174, using techniques similar to those discussed in previous Sections. One obtains

$$\frac{d^2\sigma_C}{d\Omega\,dE_\gamma}\ \left(E_\gamma\right) = \frac{1}{E_\gamma}\ \sum_{\pi\lambda}\frac{dn_{\pi\lambda}}{d\Omega}\ \sigma_\gamma^{\pi\lambda}\ \left(E_\gamma\right) \tag{177}$$

where $\sigma_\gamma^{\pi\lambda}\big(E_\gamma\big)$ is the photonuclear cross section for the absorption of a real photon with energy E_γ by nucleus 2, and $dn_{\pi\lambda}/d\Omega$ is the virtual photon number, which is given by [33]

$$\frac{dn_{\pi\lambda}}{d\Omega} = Z_1^2\alpha\ \left(\frac{\omega k}{\gamma v}\right)^2 \frac{\lambda\big[(2\lambda+1)!!\big]^2}{(2\pi)^3\ (\lambda+1)}\ \sum_m\ |G_{\pi\lambda m}|^2\ |\Omega_m(q)|^2\ , \tag{178}$$

where $\alpha = e^2/\hbar c$.

The total cross section for Coulomb excitation can be obtained from Eqs. 177 and 178, using the approximation $d\Omega \simeq 2\pi q dq/k^2$, valid for small scattering angles and small energy losses. Using the closure relation for the Bessel functions, one obtains

$$\frac{d\sigma_C}{dE_\gamma}\ \left(E_\gamma\right) = \frac{1}{E_\gamma}\ \sum_{\pi\lambda} n_{\pi\lambda}\big(E_\gamma\big)\ \sigma_\gamma^{\pi\lambda}\ \left(E_\gamma\right)\ , \tag{179}$$

where

$$n_{\pi\lambda}(\omega) = Z_1^2\alpha\ \frac{\lambda\big[(2\lambda+1)!!\big]^2}{(2\pi)^3\ (\lambda+1)}\ \sum_m\ |G_{\pi\lambda m}|^2\ g_m(\omega)\ , \tag{180}$$

and

$$g_m(\omega) = 2\pi \left(\frac{\omega}{\gamma v}\right)^2 \int db\ b\ K_m^2\left(\frac{\omega b}{\gamma v}\right)\ \exp\{-2\ \chi_I(b)\}\ , \tag{181}$$

where $\chi_I(b)$ is the imaginary part of $\chi(b)$, which is obtained from Eq. 172 and the imaginary part of the optical potential.

We point out that for very light heavy ion partners, the distortion of the scattering wavefunctions caused by the nuclear field is not important. This distortion is manifested in the diffraction peaks of the angular distributions, characteristic of strong absorption processes. If $Z_1 Z_2 \alpha \gg 1$, one can neglect the diffraction peaks in the inelastic scattering cross sections and a purely Coulomb excitation process emerges. One can gain insight into the excitation mechanism by looking at how the semiclassical limit of the excitation amplitudes emerges from the general result 178. We do this next.

0.9.2 Semiclassical limit of the excitation amplitudes

If we assume that Coulomb scattering is dominant and neglect the nuclear phase in Eq. 172, we get

$$\Omega_m(q) \simeq \int_0^\infty db\ b\ J_m(qb)\ K_m\left(\frac{\omega b}{\gamma v}\right)\ \exp\{i\psi_C(b)\}\ . \tag{182}$$

This integral can be done analytically by rewriting it as

$$\Omega_m(q) = \int_0^\infty db\ b^{1+i2\eta}\ J_m(qb)\ K_m\left(\frac{\omega b}{\gamma v}\right)\ , \tag{183}$$

where we used the simple form $\psi_C(b) = 2\eta\ \ln(kb)$, with $\eta = Z_1 Z_2 e^2/\hbar v$. Using standard techniques found in Ref. [34], we find

$$\begin{aligned}\Omega_m(q) &= 2^{2i\eta}\ \frac{1}{m!}\ \Gamma(1+m+i\eta)\Gamma(1+i\eta) \\ &\times \Lambda^m \left(\frac{\gamma v}{\omega}\right)^{2+2i\eta} F\Big(1+m+i\eta;\ 1+i\eta;\ 1+m;-\Lambda^2\Big)\ ,\end{aligned} \tag{184}$$

where

$$\Lambda = \frac{q\gamma v}{\omega}\ , \tag{185}$$

and F is the hypergeometric function [34].

The connection with the semiclassical results may be obtained by using the low momentum transfer limit

$$\begin{aligned}J_m(qb) &\simeq \sqrt{\frac{2}{\pi qb}}\ \cos\left(qb - \frac{\pi m}{2} - \frac{\pi}{4}\right) \\ &= \frac{1}{\sqrt{2\pi qb}}\left\{e^{iqb}\ e^{-i\pi(m+1/2)/2} + e^{-iqb}\ e^{i\pi(m+1/2)/2}\right\}\ ,\end{aligned} \tag{186}$$

and using the stationary phase method, i.e.,

$$\int G(x)\ e^{i\phi(x)}\ dx \simeq \left(\frac{2\pi i}{\phi''(x_0)}\right)^{1/2} G(x_0)\ e^{i\phi(x_0)}\ , \tag{187}$$

where

$$\frac{d\phi}{dx}(x_0) = 0 \qquad \text{and} \qquad \phi''(x_0) = \frac{d^2\phi}{dx^2}(x_0)\ . \tag{188}$$

This result is valid for a slowly varying function $G(x)$.

Only the second term in brackets of Eq. (186) will have a positive ($b = b_0 > 0$) stationary point, and

$$\Omega_m(q) \simeq \frac{1}{\sqrt{2\pi q}} \left(\frac{2\pi i}{\phi''(b_0)}\right)^{1/2} \sqrt{b_0}\ K_m\!\left(\frac{\omega b_0}{\gamma v}\right)\ \exp\!\left\{i\phi(b_0) + i\frac{\pi(m+1/2)}{2}\right\}, \tag{189}$$

where

$$\phi(b) = -qb + 2\eta\ \ln(kb)\ . \tag{190}$$

The condition $\phi'(b_0) = 0$ implies

$$b_0 = \frac{2\eta}{q} = \frac{a_0}{\sin(\theta/2)}\ , \tag{191}$$

where $a_0 = Z_1 Z_2 e^2/\mu v^2$ is half the distance of closest approach in a classical head-on collision.

We observe that the relation 191 is the same [with $\cot(\theta/2) \sim \sin^{-1}(\theta/2)$] as that between impact parameter and deflection angle of a particle following a classical Rutherford trajectory. Also,

$$\phi''(b_0) = -\frac{2\eta}{b_0^2} = -\frac{q^2}{2\eta}\ , \tag{192}$$

which implies that in the semiclassical limit

$$\begin{aligned} |\Omega_m(q)|^2_{s.c.} &= \frac{4\eta^2}{q^4}\ K_m^2\!\left(\frac{2\omega\eta}{\gamma v q}\right) \\ &= \frac{1}{k^2}\left(\frac{d\sigma}{d\Omega}\right)_{Ruth} K_m^2\!\left(\frac{\omega a_0}{\gamma v \sin(\theta/2)}\right)\ . \end{aligned} \tag{193}$$

Using the above results, Eq. 178 becomes

$$\frac{dn_{\pi\lambda}}{d\Omega} = \left(\frac{d\sigma}{d\Omega}\right)_{Ruth} Z_1^2\alpha \left(\frac{\omega}{\gamma v}\right)^2 \frac{\lambda\big[(2\lambda+1)!!\big]^2}{(2\pi)^3\ (\lambda+1)} \sum_m\ |G_{\pi\lambda m}|^2\ K_m^2\!\left(\frac{\omega a_0}{\gamma v \sin(\theta/2)}\right)\ . \tag{194}$$

If strong absorption is not relevant, the above formula can be used to calculate the equivalent photon numbers. The stationary value given by Eq. 191 means that the important values of b which contribute to $\Omega_m(q)$ are those close to the classical impact parameter. Dropping the index 0 from Eq. 191, we can also rewrite Eq. 194 as

$$\frac{dn_{\pi\lambda}}{2\pi b\ db} = Z_1^2\alpha\ \left(\frac{\omega}{\gamma v}\right)^2 \frac{\lambda\big[(2\lambda+1)!!\big]^2}{(2\pi)^3\ (\lambda+1)}\ \sum_m\ |G_{\pi\lambda m}|^2\ K_m^2\left(\frac{\omega b}{\gamma v}\right)\,, \tag{195}$$

which is equal to the semi-classical expression given in Ref. [10], Eq. (A.2).

For very forward scattering angles, such that $\Lambda << 1$, a further approximation can be made by setting the hypergeometric function in Eq. 184 equal to unity [34], and we obtain

$$\Omega_m(q) = 2^{2i\eta}\ \frac{1}{m!}\ \Gamma(1+m+i\eta)\ \Gamma(1+i\eta)\ \Lambda^m\ \left(\frac{\gamma v}{\omega}\right)^{2+2i\eta}\,. \tag{196}$$

The main value of m in this case will be $m=0$, for which one gets

$$\begin{aligned}\Omega_0(q) &\simeq 2^{2i\eta}\ \Gamma(1+i\eta)\ \Gamma(1+i\eta)\ \left(\frac{\gamma v}{\omega}\right)^{2+2i\eta} \\ &= -\eta^2\ 2^{2i\eta}\ \Gamma(i\eta)\ \Gamma(i\eta)\ \left(\frac{\gamma v}{\omega}\right)^{2+2i\eta}\,,\end{aligned} \tag{197}$$

and

$$|\Omega_0(q)|^2 = \eta^4\ \left(\frac{\gamma v}{\omega}\right)^4\ \frac{\pi^2}{\eta^2\ \sinh^2(\pi\eta)}\,, \tag{198}$$

which, for $\eta \gg 1$, results in

$$|\Omega_0(q)|^2 = 4\pi^2\ \eta^2\ \left(\frac{\gamma v}{\omega}\right)^4\ e^{-2\pi\eta}\,. \tag{199}$$

This result shows that in the absence of strong absorption and for $\eta \gg 1$, Coulomb excitation is strongly suppressed at $\theta = 0$. This also follows from semiclassical arguments, since $\theta \to 0$ means large impact parameters, $b \gg 1$, for which the action of the Coulomb field is weak.

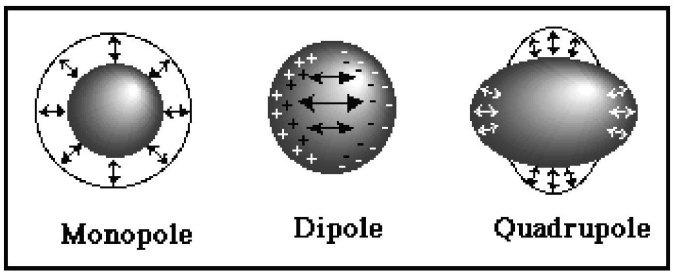

Figure 4: Different kinds of collective vibrations in atomic nuclei.

Supplement E

0.10 Giant resonances

Light, viz. the photon, has played and still does play an important role in the exploration of the microcosmos. In particular the virtual photons exchanged in collisions of electrons with protons probed the by now most elementary building blocks of nature, the partons. As early as 1937 Bothe and Gentner [18] reported an resonance like enhancement of radioactivity irradiating different materials with 17.6 MeV x-rays from the ^{7}Li(p,γ) reaction. They noticed that the cross section for ^{63}Cu was surprisingly high and they suggested that this might be due to a resonance phenomenon. These observations were later confirmed by Baldwin and Klaiber (1947) with photons from a betatron. In 1948 Goldhaber and Teller [19] interpreted these resonances (named by *isovector giant dipole resonances*) with a hydrodynamic model in which rigid proton and neutron fluids vibrate against each other, the restoring force resulting from the surface energy. Steinwendel and Jensen [20] later developed the model, considering compressible neutron and proton fluids vibrating in opposite phase in a common fixed sphere, the restoring force resulting from the volume symmetry energy. The standard microscopic basis for the description of giant resonances is the Random Phase Approximation (RPA) in which giant resonances appear as coherent superpositions of one-particle one-hole ($1p1h$) excitations (see Fig. 5) in closed shell nuclei or two quasi-particle excitations in open shell nuclei (for a review of these techniques, see, e.g., Ref. [21]).

Over the years, these vibrational modes of the nuclei, the *giant resonances*, were investigated in great detail. Much of the information was gained using again virtual or real photons from electron accelerators. But the broad variety of different giant resonance modes could only be discovered using also hadronic probes, such as pions, protons, alpha particles and heavier nuclei.

Giant resonances are classified according to the degree of freedom being involved in the vibration. In general, giant resonances can be understood as small amplitude oscillations of the shape

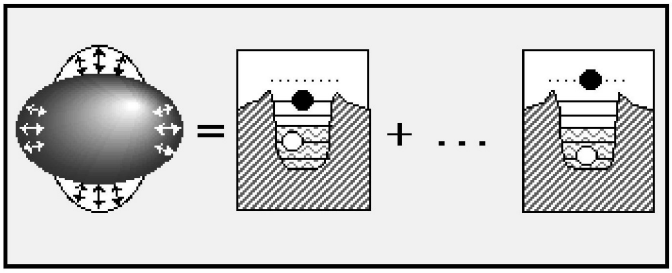

Figure 5: Giant resonances are described in terms of particle-hole excitations in closed shell nuclei or two quasi-particle excitations in open shell nuclei.

and/or density distribution of the nucleus (see Fig. 4). One distinguishes electric vibrations from magnetic vibrations depending on the external field coupling to the charge or spin of the nucleons, respectively. The resonance has *isoscalar* character if proton and neutron are in phase and *isovector* character if not. Depending of the spatial dynamic of the vibration the resonance can be of monopole, dipole or quadrupole type. The *isoscalar quadrupole resonances* were discovered in inelastic electron scattering by Pitthan and Walcher (1971) and in proton scattering by Lewis and Bertrand [22]. *Giant monopole resonances* were found later and their properties are closely related to the compression modulus of nuclear matter. Following these, other resonances of higher multipolarities and giant magnetic resonances were investigated. Typical probes for giant resonance studies are (a) γ's and electrons for the excitation of GDR (isovector giant dipole resonance), (b) α-particles and electrons for the excitation of isoscalar GMR (giant monopole resonance) and GQR (giant quadrupole resonance), and (c) (p, n), or (^{3}He, t), for *Gamow-Teller resonances*, respectively.

The giant vibrational modes are a gross property of all nuclei. The isovector giant dipole resonance, e.g., has been identified in atomic nuclei all along the valley of stable isotopes. The latter appears at excitation energies well approximated by the phenomenological dependence $\hbar\omega = 79A^{-1/3}$ which is equivalent to the picture of standing waves inside the nuclear volume. Giant resonances are broad structures and not necessarily of Breit-Wigner shape. The reasons is a strong damping of the collective motion of nucleons inherent in the giant vibration due to collisions of the nucleons with each other. In addition, they are based on many complex configurations of the nucleons taking part in the oscillation and the strength is not concentrated at one point. Since the amplitudes are small, the restoring force is to a good approximation linear in the amplitude. Hence the giant resonance can be viewed as the excitation of the first phonon of a harmonic oscillator.

Coulomb excitation is a well established tool to unravel interesting aspects of nuclear structure [23]. Examples are the studies of giant resonances in heavy ion accelerators [24, 25, 26, 5]. Important properties of nuclei far from stability [27, 28] have also been studied with this method.

Inelastic scattering studies with heavy ion beams have opened new possibilities in the field (for a review the experimental developments, see Ref. [24]). A striking feature was observed when either

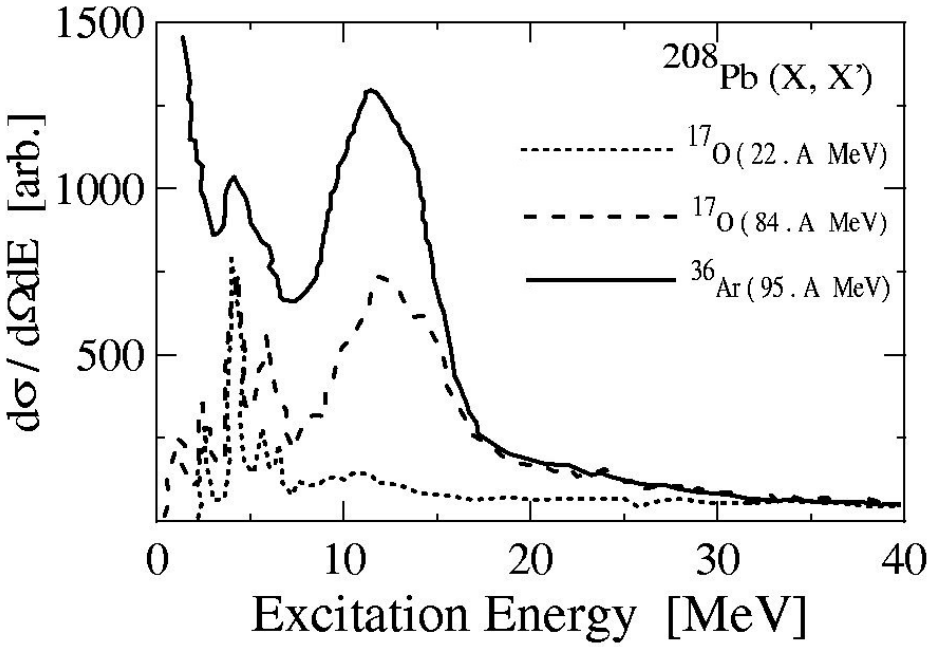

Figure 6: Experimental cross sections (arbitrary units) for the excitation of ^{208}Pb targets by ^{17}O (22A MeV and 84A MeV) and by ^{36}Ar (95A MeV), as a function of the excitation energy.

the beam energy was increased, or heavier projectiles were used, or both [29]. This is displayed in figure 6, where the excitation of the GDR in ^{208}Pb was observed in the inelastic scattering of ^{17}O at 22 MeV/nucleon and 84 MeV/nucleon, respectively, and ^{36}Ar at 95 MeV/nucleon [30, 31]. What one clearly sees is that the "bump" corresponding to the GDR at 13.5 MeV is appreciably enhanced. This feature is solely due to one agent: the electromagnetic interaction between the nuclei. This interaction is more effective at higher energies, and for increasing charge of the projectile.

Baur and Bertulani showed [15] that the excitation probabilities of the GDR in heavy ion collisions approach unity at grazing impact parameters. They also showed that, if double GDR resonance (i.e. a GDR excited on a GDR state) exists then the cross sections for their excitation in heavy ion collisions at relativistic energies are of order of hundreds of millibarns. These calculations motivated experimentalists [24] [30, 31] to look for the signatures of the DGDR in the laboratory. This has by now become a very active field in nuclear physics with a great theoretical and experimental interest [24, 26, 25, 5].

First evidence for the excitation of the two-phonon isovector giant dipole resonance (ivDGDR) came from double charge exchange reactions of pions on different targets. The signal emerges as a broad ridge in the missing energy spectrum of the scattered pion at about twice the energy of the one-phonon giant dipole resonance (ivGDR), which is dominated by a smooth background from

noncoherent excitations. At that time it was argued by Baur and Bertulani [15] that electromagnetic excitation bombarding targets with heavy ion beams at relativistic energies should be an outstanding probe to investigate multiphonon excitations of the giant resonance. Their basic idea was to assume a two-step excitation process, where an oscillator phonon is excited ensuing from the absorption of a virtual phonon, and consequently, if the flux of virtual photons is high enough, a second photon of appropriate energy can be absorbed before the first phonon had time to decay. Indeed, already in 1955, D. Brink [35] has argued that due to the internal structure of such giant resonances they can be build not only on the ground state but on any excited states as well yet also on a giant resonance itself.

This process to take place requires light of special quality. When the two ions are passing by each other, the collision partners recognize, pictorially spoken, flash-lights of very short duration. In the language of Fermi, Weizsäcker and Williams [36], a shower of virtual photons impinges onto the ions. The maximum energy of these photons, their hardness so to say, is determined from adiabacity and can be controlled experimentally by a proper choice of the beam momentum. The intensity of the photon flux is steered by the charge of the collision partners, which is the dominant parameter compared to a relativistic enhancement of the field stemming from retardation. Indeed the electromagnetic field acting in such peripheral collisions of heavy ions, where the minimal distance between the collision partners or impact is as large that strong interaction is impossible, can be hard enough to allow production of Higgs particles through photon-photon fusion in case of the Large Hadron Collider (LHC) currently set into operation at CERN (for a popular review, see Ref. [37]).

0.11 Singles spectra in Coulomb excitation of GDR

In this Section, we apply the formalism developed in previous Sections in the analysis of the data of Ref. [38], in which a projectile of ^{17}O with an energy of $E_{lab} = 84$A MeV excites the target nucleus ^{208}Pb to the GDR. We first seek parameters of the optical potential which fits the elastic scattering data. The optical potential has a standard Woods-Saxon form with parameters

$$\begin{aligned} V_0 &= 50\,\text{MeV}\,, \quad W_0 = 58\,\text{MeV}\,, \quad R_V = R_W = 8.5\,\text{fm} \quad \text{and} \\ a_V &= a_W = 0.85\,\text{fm}\,. \end{aligned} \tag{200}$$

In order to calculate the inelastic cross section for the excitation of the GDR, we use a Lorentzian parameterization for the photoabsorption cross section of ^{208}Pb [39], assumed to be all $E1$, with $E_{\rm GDR} = 13.5\,$MeV and $\Gamma = 4.0\,$MeV. Inserting this form into Eq. 179 and doing the calculations implicit in Eq. 178 for $dn_{E1}/d\Omega$, one can calculate the angular distribution and compare it with the data in Fig. 7 (left). The agreement with the data is excellent, provided we adjust the overall normalization to a value corresponding to 93 % of the energy weighted sum rule (EWSR) in the energy interval $7 - 18.9$ MeV. Taking into account the $\pm 10\%$ uncertainty in the absolute cross sections quoted in Ref. [29], this is consistent with photoabsorption cross section in that energy range, for which approximately 110 % of the EWSR is exhausted.

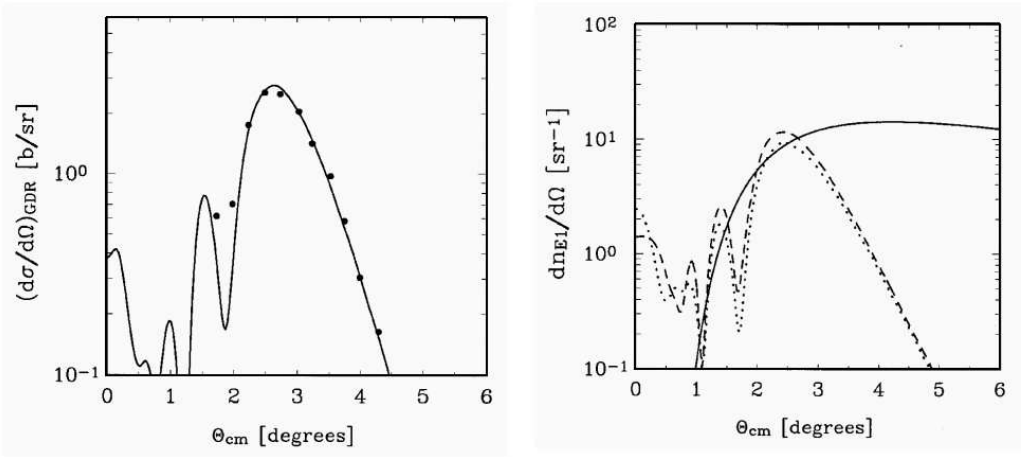

Figure 7: *Left figure:* Ratio to the Rutherford cross section of the elastic cross section for the ^{17}O+^{208}Pb reaction at 84A MeV, as a function of the center-of-mass scattering angle. Data are from Ref. [29]. *Right figure:* Virtual photon numbers for the electric dipole multipolarity generated by 84A MeV ^{17}O projectiles incident on ^{208}Pb, as a function of the center-of-mass scattering angle. The solid curve is a semiclassical calculation. The dashed and dotted curves are eikonal calculations with and without relativistic corrections, respectively.

To unravel the effects of relativistic corrections, one can repeat the previous calculations unplugging the factor $\gamma = (1 - v^2/c^2)^{-1}$ which appears in the expressions 180 and 181 and using the non-relativistic limit of the functions G_{E1m}, as given in Eq. 176. These modifications eliminate the relativistic corrections on the interaction potential. The result of this calculation is shown in Fig. 7 (dotted curve). For comparison, we also show the result of a full calculation, keeping the relativistic corrections (dashed curve). One observes that the two results have approximately the same pattern, except that the non-relativistic result is slightly smaller than the relativistic one. In fact, if one repeats the calculation for the excitation of GDR$_{iv}$ using the non-relativistic limit of Eqs. 180 and 181, one finds that the best fit to the data is obtained by exhausting 113 % of the EWSR. This value is very close to the 110 % obtained by Barrette et al [29].

In Fig. 7 (right) we also show the result of a semiclassical calculation (solid curve) for the GDR$_{iv}$ excitation in lead, using Eq. 194 for the virtual photon numbers. One observes that the semiclassical curve is not able to fit the experimental data. This is mainly because diffraction effects and strong absorption are not included. But the semiclassical calculation displays the region of relevance for Coulomb excitation. At small angles the scattering is dominated by large impact parameters, for which the Coulomb field is weak. Therefore the Coulomb excitation is small and the semiclassical approximation fails. It also fails in describing the large angle data (dark-side of the rainbow angle), since absorption is not treated properly. One sees that there is a "window" in the inelastic scattering data near $\theta = 2 - 3^\circ$ in which the semiclassical and full calculations give approximately the same cross section.

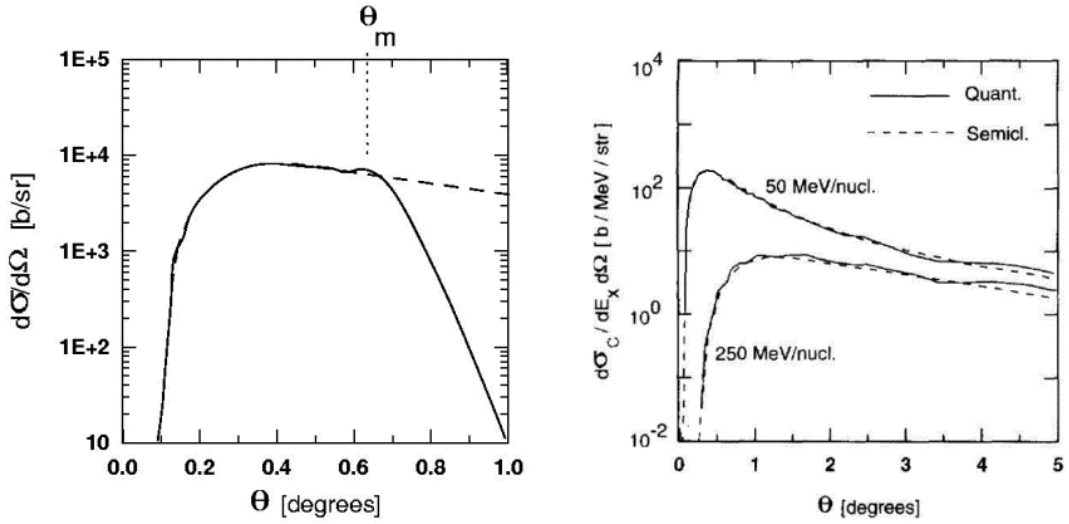

Figure 8: Left side: differential cross section for the excitation of a giant dipole resonance in $Pb + Pb$ collisions at 640 MeV/nucleon, as a function of the center of mass scattering angle. Right side: differential cross sections for the excitation of 350 keV continuun states in ^8B projectiles incident on Pb targets at 50 and 250 MeV/nucleon, respectively.

In Fig. 8 (left) we show a similar calculation, but for the excitation of the GDR in Pb for the collision ^{208}Pb + ^{208}Pb at 640A MeV. The dashed line is the result of a semiclassical calculation. Here we see that a purely semiclassical calculation, using Eq. 112 is able to reproduce the quantum results up to a maximum scattering angle θ_m, at which strong absorption sets in. This justifies the use of semiclassical calculations for heavy systems, even to calculate angular distributions. The cross sections increase rapidly with increasing scattering angle, up to an approximately constant value as the maximum Coulomb scattering angle is neared. This is explained as follows. Very forward angles correspond to large impact parameter collisions in which case $\omega b/\gamma v > 1$ and the excitation of giant resonances in the nuclei is not achieved. As the impact parameter decreases, increasing the scattering angle, this adiabacity condition is fulfilled and excitation occurs. In Fig. 8 (right side) we plot the differential cross sections for the excitation of 350 keV continuum states in ^8B projectiles incident on Pb targets at 50 and 250 MeV/nucleon, respectively. Again, the dashed lines are semiclassical calculations, based on Eq. 112.

As discussed above, the semiclassical result works for large Z nuclei and for relativistic energies where the approximation of Eq. 182 is justified. However, angular distributions are not useful at relativistic energies since the scattering is concentrated at extremely forward angles. The quantity of interest in this case is the total inelastic cross section. If we use a *sharp-cutoff model (or black-sphere model)* for the strong absorption, so that $\chi_I(b) = \infty$ for $b < b_{min}$ and 0 otherwise, then Eqs. 180 and 181 yield the same result as an integration of the semiclassical expression, Eq. 195, from

b_{min} to ∞, as shown in Ref. [23].

Supplement F

0.12 Coulomb excitation of a harmonic oscillator

Let us consider the Coulomb excitation of a linear harmonic oscillator. For dipole excitations the interaction Hamiltonian has the form (see Eq. 32)

$$\mathcal{H}_{int}^{E1}(t) = xf(t) + zg(t) \ , \tag{201}$$

where $f(t)$ and $g(t)$ are time-dependent functions and x and z are the intrinsic nuclear coordinates perpendicular and parallel to the beam, respectively. This field induces oscillations in the perpendicular and parallel directions, and are therefore independent.

Introducing the occupation numbers $n_x \equiv n_1 = 0,\ 1,\ 2,\ \cdots$ and $n_z \equiv n_0 = 0,\ 1,\ 2,\ \cdots$ the total number of occupied states is

$$N = n_x + n_z. \tag{202}$$

Considering only the oscillations along one of the directions, e.g., along the x-direction, the full Hamiltonian is

$$\mathcal{H} = \mathcal{H}_0 - xf(t) \ , \tag{203}$$

where the minus sign is arbitrary and was introduced to simplify further the equations.

The solutions for the intrinsic Hamiltonian, $H_0 = m\omega^2 x^2/2$, are obtained in terms of the Hermite polynomials (here, $n = n_x$)

$$\psi(x) = \left(\frac{m\omega}{\pi\hbar}\right)^{1/4} (2^n n!)^{-1/2} \, H_n\left(\sqrt{\frac{m\omega}{\hbar}}x\right) \exp\left(-\frac{m\omega x^2}{2\hbar}\right). \tag{204}$$

Since this forms a complete basis, the wavefunction at time t can be written as

$$\psi(x,t) = \sum_{n=0}^{\infty} \exp\left[-i\omega\,(n+1/2)\,t\right]\ a_n(t)\ \psi_n(x) \tag{205}$$

with the condition $a_n(0) = \delta_{n,0}$. Inserting this expansion into the time-dependent Schrödinger equation

$$i\hbar\frac{\partial}{\partial t}\psi(x,t) = \left[-\frac{\hbar^2}{2m}\frac{\partial^2}{\partial x^2} + \frac{1}{2}m\omega^2x^2 + xf(t)\right]\psi(x,t) \tag{206}$$

and using the identity (which can be derived from $H_{n+1}(x) = 2xH_n(x) - 2nH_{n-1}(x)$)

$$x\psi_n(x) = \left(\frac{\hbar}{2m\omega}\right)^{1/2} \left[\sqrt{n}\psi_{n-1}(x) + \sqrt{n+1}\psi_{n+1}(x)\right] \tag{207}$$

we get

$$i\hbar\sum_{n=0}^{\infty}\exp\left[-i\omega\left(n+1/2\right)t\right]\ \frac{da_n}{dt}(t)\ \psi_n(x) =$$
$$-\left(\frac{\hbar}{2m\omega}\right)^{1/2} f(t)\sum_{n=0}^{\infty}\exp\left[-i\omega\left(n+1/2\right)t\right]\ a_n(t)$$
$$\times\left[\sqrt{n}\psi_{n-1}(x)+\sqrt{n+1}\psi_{n+1}(x)\right]. \tag{208}$$

Using the orthogonality conditions of ψ_n one obtains

$$\frac{da_n}{dt}(t) = if_0(t)\left[\mathrm{e}^{-i\omega t}\sqrt{n+1}a_{n+1}(t)+\mathrm{e}^{-i\omega t}\sqrt{n}a_{n-1}(t)\right]\ , \tag{209}$$

where

$$f_0(t) = \left(2m\hbar\omega\right)^{-1/2} f(t). \tag{210}$$

The above equation allows to obtain $a_n(t)$ by interaction, starting with $n = 0$. The solution is

$$a_n(t) = i^n\frac{\chi^n(t)}{\sqrt{n!}}\exp\left[-\int_0^t dt' f_0(t')\mathrm{e}^{-i\omega t'}\chi(t')\right] \tag{211}$$

where

$$\chi(t) = \int_0^t dt' f_0(t')e^{-i\omega t'}\chi(t')\ . \tag{212}$$

But,

$$\int_0^t dt' f_0(t')\mathrm{e}^{-i\omega t'}\chi(t') = \int_0^t dt'\frac{d\chi^*}{dt'}(t')\ \chi(t') = \frac{1}{2}\left|\chi(t)\right|^2 \tag{213}$$

and the probability to excite the nth state is

$$P_n(t) = \frac{\left|\chi(t)\right|^{2n}}{n!}\exp\left[-\left|\chi(t)\right|^2\right]. \tag{214}$$

For a nucleus, n can also be considered as the number of phonons for the vibration along the x-direction. The probability to put n_0 vibrations along the z-direction and n_1 vibrations along the x-direction is

$$P_{n_0,n_1}(t) = \frac{\left|\chi_0(t)\right|^{2n_0}\left|\chi_1(t)\right|^{2n_1}}{n_0!n_1!}\exp\left[-\left|\chi_0(t)\right|^2-\left|\chi_1(t)\right|^2\right]. \tag{215}$$

The probability that N-phonons will be excited is

$$\begin{aligned} P_N &= \sum_{n_0,\ n_1(N=n_0+n_1)} P_{n_0,n_1} = \sum_{n_0=0}^{N} P_{n_0,N-n_0} \\ &= \sum_{n_0=0}^{N}\frac{\left|\chi_0(t)\right|^{2n_0}\left|\chi_1(t)\right|^{2(N-n_0)}}{n_0!\left(N-n_0\right)!}\exp\left[-\left|\chi_0(t)\right|^2-\left|\chi_1(t)\right|^2\right] \\ &= \frac{1}{N!}\exp\left[-\left|\chi_0(t)\right|^2-\left|\chi_1(t)\right|^2\right]\sum_{n_0=0}^{N}\frac{N!\left|\chi_0(t)\right|^{2n_0}\left|\chi_1(t)\right|^{2(N-n_0)}}{n_0!\left(N-n_0\right)!}\ . \end{aligned} \tag{216}$$

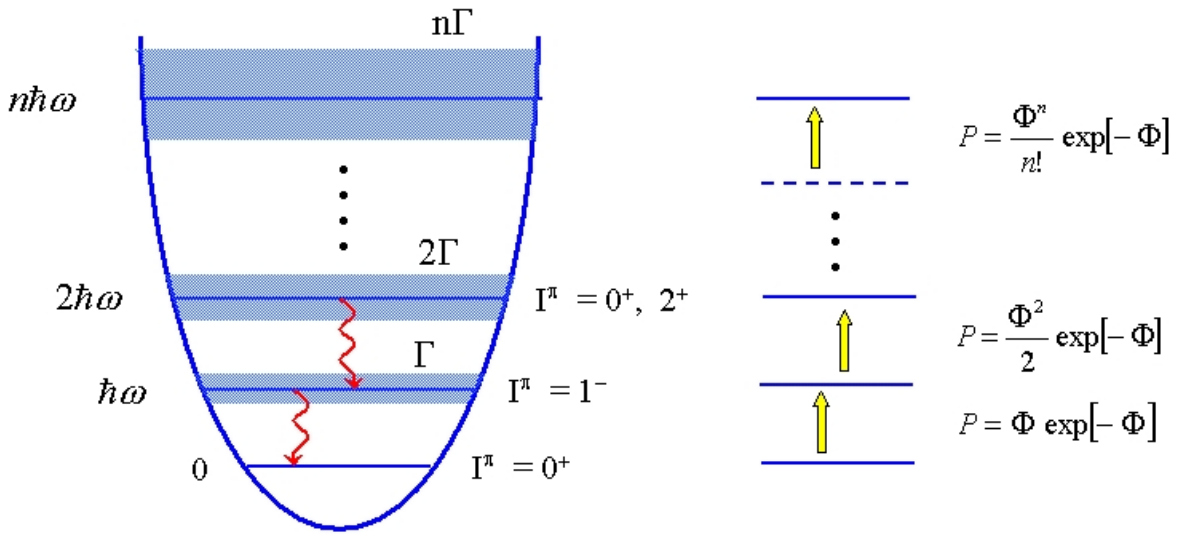

Figure 9: The harmonic oscillator model for the excitation of collective states in nuclei.

The last sum yields $|\phi(t)|^{2N}$, where

$$|\phi(t)|^2 \equiv |\chi_0(t)|^2 + |\chi_1(t)|^2 \,. \tag{217}$$

Thus, one gets the Poisson formula

$$P_N = \frac{1}{N!}\ |\phi(t)|^{2N}\ \exp\left[-|\phi(t)|^2\right] . \tag{218}$$

for dipole excitations of a harmonic oscillator. In Ref. [1, 2] it was shown that the same result can be obtained for quadrupole excitations. Thus, the above result is very general (see Figure 9).

The Poisson equation is very useful one. It shows that all one needs to obtain the probability to excite the nth state is to calculate the probability to excite the $N = 1$ state with first-order perturbation, $P_{0\to 1}^{first} = |\phi(t)|^2$, and use it in the Poisson formula. Although this only holds for a harmonic oscillator system, it has been largely used in many theoretical considerations of more complicated systems. The factor $\exp\left[-|\phi(t)|^2\right]$ accounts for the loss of occupation probability due to the excitation to all states from a given one. It also is responsible for conservation of unitarity, so that $\sum_{N=0}^{\infty} P_N = 1$.

0.13 Excitation and photon decay of the GDR and double-GDR

We now consider the excitation of the target nucleus to the giant dipole resonance and the subsequent photon decay of that excited nucleus, leaving the target in the ground state. Experimentally, one detects the inelastically scattered projectile in coincidence with the decay photon and demands that the energy lost by the projectile is equal to the energy of the detected photon. To the extent that the excitation mechanism is dominated by Coulomb excitation, with the exchange of a single virtual photon, this reaction is very similar to the photon scattering reaction, except that in the present case the incident photon is virtual rather than real. In this Section, we investigate whether the connection between these two reactions can be formalized.

We have seen that, under the conditions $\Delta E/E \ll 1$, the cross section for excitation of the target nucleus partitions into the following expression (we assume that the contribution of the $E1$-multipolarity is dominant):

$$\frac{d^2\sigma_C}{d\Omega dE_\gamma}\ (E_\gamma) = \frac{1}{E_\gamma}\ \frac{dn_\gamma}{d\Omega}\ (E_\gamma)\ \sigma_\gamma\ (E_\gamma)\,, \tag{219}$$

where $\sigma_\gamma\big(E_\gamma\big)$ is the photonuclear cross section for the absorption of a real photon with energy $E_\gamma = \Delta E$ by the target nucleus, and the remaining terms on the right-hand-side are collectively the number of virtual photons per unit energy with energy E_γ. This latter quantity depends on the kinematics of the scattered heavy ion and on the optical potential but is otherwise independent of the target degrees of freedom. This partitioning allows one to relate the excitation cross section to the photoabsorption cross section.

Now, the usual way to write the cross section $d^2\sigma_{C\gamma}/d\Omega dE_\gamma$ for the excitation of the target followed by photon decay to the ground state is simply to multiply the above expression by a branching ratio R_γ, which represents the probability that the nucleus excited to an energy E_γ will emit a photon leaving it in the ground state [30]:

$$\frac{d^2\sigma_{C\gamma}}{d\Omega dE_\gamma}\ (E_\gamma) = \frac{1}{E_\gamma}\ \frac{dn_\gamma}{d\Omega}\ (E_\gamma)\ \sigma_\gamma\ (E_\gamma)\ R_\gamma\ (E_\gamma)\,. \tag{220}$$

Instead, we propose the following expression, in complete analogy with Eq. 219:

$$\frac{d^2\sigma_{C\gamma}}{d\Omega dE_\gamma}\ (E_\gamma) = \frac{1}{E_\gamma}\ \frac{dn_\gamma}{d\Omega}\ (E_\gamma)\ \sigma_{\gamma\gamma}\ (E_\gamma)\,, \tag{221}$$

where $\sigma_{\gamma\gamma}\,(E_\gamma)$ is the cross section for the elastic scattering of photons with energy E_γ. Formally, these expressions are equivalent in that they simply define the quantity R_γ. However, if one treats R_γ literally as a branching ratio, then these expressions are equivalent only if it were true that the photon scattering cross section is just product of the photoabsorption cross section and the branching ratio. In fact, it is well-known from the theory of photon scattering that the relationship between the photoabsorption cross section and the photon scattering cross section is more complicated [41]. In particular, it is not correct to think of photon scattering as a two-step process

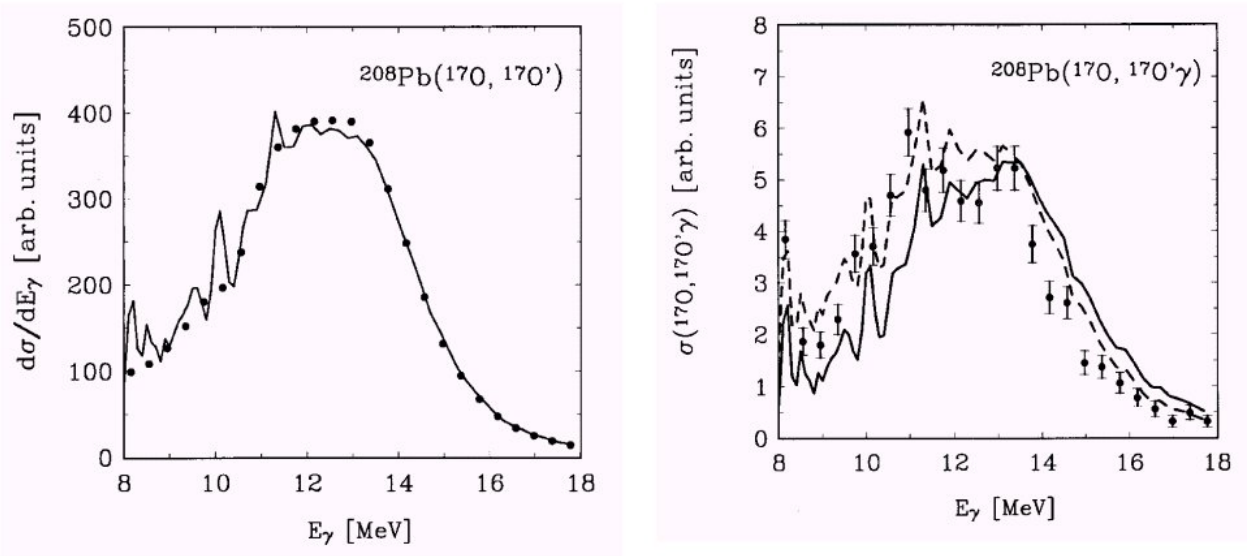

Figure 10: *Left side:* cross section for the excitation of the GDR without the detection of the decay photon. Data are from Ref. [30]. *Right side:* Cross section for excitation followed by γ-decay of ^{208}Pb by ^{17}O projectiles at 84A MeV. The solid (dashed) line includes (excludes) the Thomsom scattering amplitude. Data are from Ref. [30].

consisting of absorption, in which the target nucleus is excited to an intermediate state of energy E_γ, followed by emission, in which the emitted photon has the same energy E_γ. Since the intermediate state is not observable, one must sum over all possible intermediate states and not just those allowed by conservation of energy. Now, if the energy E_γ happens to coincide with a narrow level, then that level will completely dominate in the sum over intermediate states. In that case, it is proper to regard the scattering as a two-step process in the manner described above, and the two expressions for the cross section will be equal. However, for E_γ in the nuclear continuum region (e.g., in the region of the GDR), this will not be the case, as demonstrated in the following discussion.

We again consider the inelastic scattering of ^{17}O projectiles of energy $E_{lab} = 84$ MeV/nucleon from a ^{208}Pb nucleus at an angle of 2.5°. We use Eq. (178) to calculate the $E1$ virtual photon number and we use a Lorentzian parameterization of the GDR of ^{208}Pb. We calculate R_γ and $\sigma_{\gamma\gamma}$ according to the prescriptions of Ref. [30] and Ref. [41], respectively; in both cases we neglect the statistical contribution to the photon decay. The results are compared in Fig. 10 (left), where is very evident that they make very different predictions for the cross section, especially in the wings of the GDR.

We next use these expressions to compare directly with the data of Ref. [30]. For this purpose, we again calculate $\sigma_{\gamma\gamma}$ using the formalism of Ref. [41], which relates $\sigma_{\gamma\gamma}$ to the total photoabsorption. For the latter, we use the numerically-defined data set of Ref. [39] rather than a Lorentzian

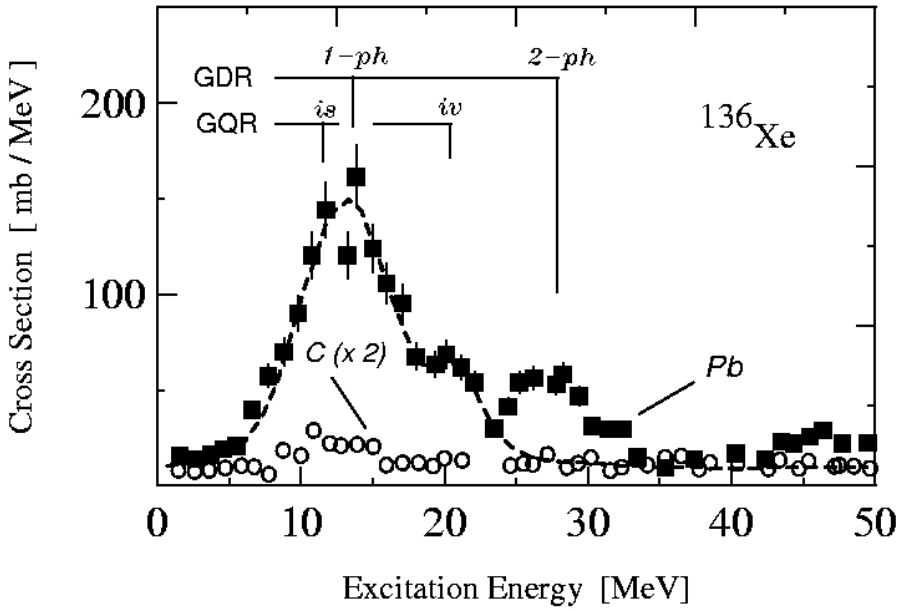

Figure 11: Experimental results for ^{136}Xe projectile excitation (at 690A MeV) on a Pb target (squares) and a C target (circles). The spectrum for the C target is multiplied by a factor 2 for better presentation. The resonance energies for one- and two-phonon giant resonances are indicated. The dashed curve reflects the results of a first-order calculation for the Pb target. The figure is taken from Ref. [43].

parameterization. The effect of the underlying compound nuclear levels (i.e., the statistical contribution to the photon scattering) is also included. The calculation is compared to the data in Fig. 10. The left part shows the cross section for the excitation of the GDR without the detection of the decay photon. The agreement with the data is excellent, giving us confidence that this calculation of the virtual photon number as a function of E_γ is correct. The right part of Fig. 10 shows the cross section for the excitation-decay process as a function of E_γ. Although the qualitative trend of the data are well described, the calculation systematically overpredicts the cross section on the high-energy side of the GDR (solid curve). If the Thompson amplitude is not included in $\sigma_{\gamma\gamma}$, the calculation is in significantly better agreement with the data (dashed curve).

The first Coulomb excitation experiments for the excitation of the DGDR were presented in Refs. [42, 43]. In Fig. 11 we show the result of one of these experiments, which looked for the neutron decay channels of giant resonances excited in relativistic projectiles. The excitation spectrum of relativistic ^{136}Xe projectiles incident on Pb are compared with the spectrum obtained in C targets. A comparison of the two spectra immediately proofs that nuclear contribution to the excitation is very small. Another experiment [42] dealt with the photon decay of the double giant

resonance. A clear bump in the spectra of coincident photon pairs was observed around the energy of two times the GDR centroid energy in ^{208}Pb targets excited with relativistic ^{209}Bi projectiles. The theory of Coulomb excitation in the harmonic picture seems to describe reasonably well the cross sections for these processes.

Coulomb excitation of exotic nuclei

0.14 Introduction

Coulomb excitation is a well established experimental probe in nuclear physics [44, 45, 46]. Traditionally, stable targets of the nuclei to be studied are prepared and then bombarded with heavy-ion beams at beam energies of a few million electron-volts per nucleon, well bellow the Coulomb barrier. When extended to radioactive beams this technique gives rise to some experimental challenges [47]. One of these is that the radioactive beams are several orders of magnitude less intense than stable beams. The other is that the beams prepared in-flight separation have energies of 30-1000 MeV/nucleon. One of the experimental ideas is to scatter exotic beam particles off a stable heavy target and to detect them in coincidence with γ-rays, indicating an inelastic scattering process. The large secondary beam energies allow the use of very thick targets, partially offsetting the low beam intensities.

In Figure 12 we show the energy dependence of the Coulomb excitation cross section for a ^{40}Sn beam incident onto a gold target. We see that the cross section is dominated by giant resonance excitation (GDR and GQR) at large beam energies. We have discussed the topic of excitation of Coulomb excitation of giant resonances. The excitation of a particular low-lying state in the nucleus is a very important tool for the nuclear spectroscopy of unstable nuclei. However, the physics to pursue is clear. These states are well defined in excitation energy and have small widths. Thus, the spin and parities of these states are obtained from a detailed study of the angular distribution of the γ-rays. The excitation cross section carries the information on the reduced transition strengths, $B(\pi\lambda; I_i \longrightarrow I_f)$ for the excitation. A great deal of nuclear structure information has been obtained with this experimental method over the years .

We will investigate the Coulomb excitation to the continuum states of exotic nuclei. Since most of the rare isotope nuclei are weakly-bound, the Coulomb excitation usually leads to their breakup. This situation is similar to what happened with the Comet P/Shoemaker-Levy in 1994 which crashed on the surface of Jupiter. Approximately 1.5 to 2.2 hours after closest approach, the comet (which was presumably a single body at the time) was broken apart by tidal forces into at least 21 pieces. The pieces continued to orbit Jupiter with a period of approximately 2 years. Due to gravitational forces from the Sun which changed the orbits slightly, on the next approach to Jupiter the pieces impacted the planet. The pieces were spread out in a string, with the discernible pieces. The first piece which impacted Jupiter on July 16, 1994 and the last on July 22, 1994.

There are many aspects of the excitation to the continuum which have not been considered yet. In first order perturbation theory the Coulomb excitation cross sections are directly related to the

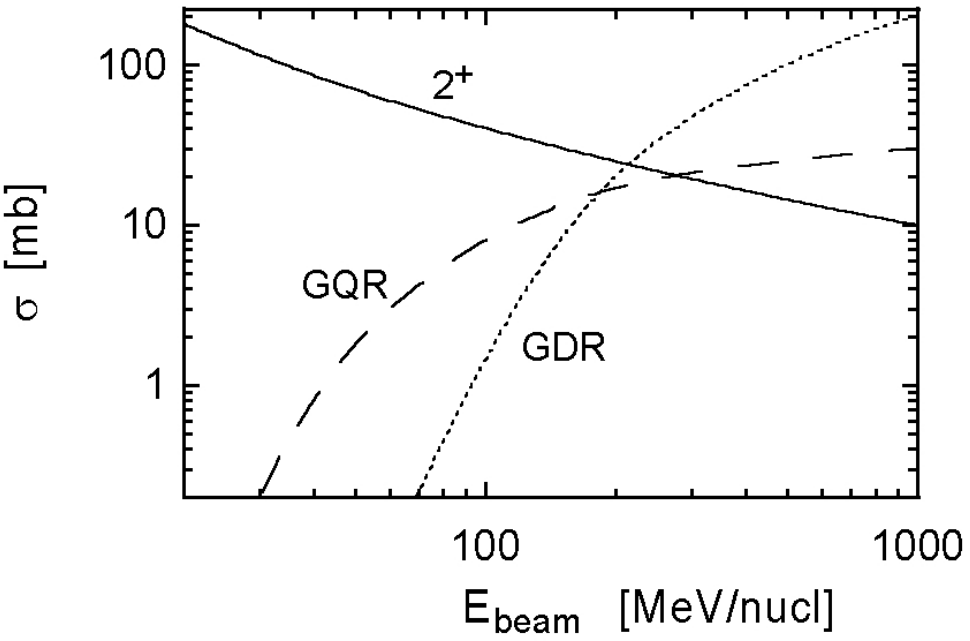

Figure 12: Cross sections for Coulomb excitation of the first excited state (2^+), the giant dipole resonance (GDR), and the giant quadrupole resonance (GQR) for a 40Sn beam incident on a gold target, versus the beam energy. The calculation assumes a minimum impact parameter of 16 fm.

photonuclear cross sections by means of the equation [48]

$$\frac{d\sigma_C\left(E_x\right)}{dE_x} = \sum_{E\lambda} \frac{n_{E\lambda}\left(E_x\right)}{E_x} \sigma^{\gamma}_{E\lambda}\left(E_x\right) + \sum_{M\lambda} \frac{n_{M\lambda}\left(E_x\right)}{E_x} \sigma^{\gamma}_{M\lambda}\left(E_x\right) \ , \tag{222}$$

where $\sigma^{\gamma}_{\pi\lambda}\left(E_x\right)$ are the photonuclear cross sections for the multipolarity $\pi\lambda$ ($\pi = E$ or M, electric or magnetic) and E_x is the excitation energy.

The photo-nuclear cross sections are related to the reduced matrix elements, for the excitation energy E_x, through the relation [49]

$$\frac{d\sigma_C\left(E_x\right)}{dE_x} = \frac{(2\pi)^3(\lambda+1)}{\lambda\left[(2\lambda+1)!!\right]^2} \left(\frac{E_x}{\hbar c}\right)^{2\lambda-1} \frac{dB}{dE_x}\left(\pi\lambda, 0 \rightarrow \lambda, E_x\right) \tag{223}$$

where dB/dE_x, are the reduced matrix elements, or *response functions*.

For differential cross sections one can write

$$\frac{d\sigma(E_x)}{d\Omega} = \frac{1}{E_x} \sum_{\pi\lambda} \frac{dn_{\pi\lambda}}{d\Omega}(E_x, \theta) \sigma^{\pi\lambda}_{\gamma}(E_x). \tag{224}$$

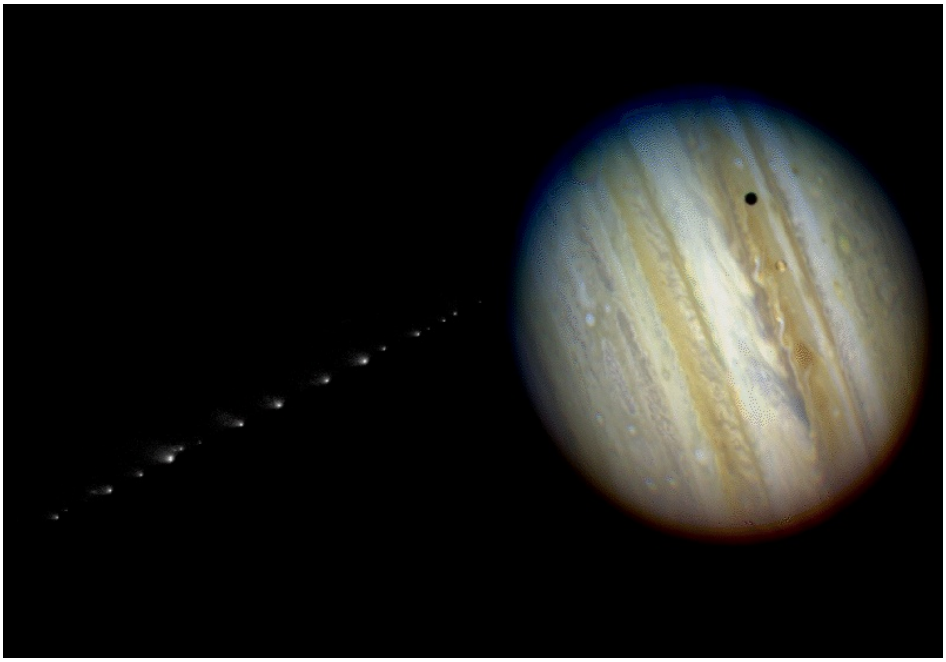

Figure 13: This is a photo of Jupiter and comet Shoemaker-Levy 9, as imaged by the Hubble Space Telescope (HST), on May 18, 1994, when the giant planet was at a distance of 420 million miles (670 million km) from Earth. The gravitational interaction of Jupiter with the comet has broken it up into many pieces, as can be seen in the left part of the figure.

It is important to account for the strong absorption properly. As stated previously, the total cross section for Coulomb excitation in high energy collisions is well described semiclassically or quantum-mechanically. Semiclassically one uses a minimum impact parameter. For stable nuclei this quantity is easily defined. But, for halo nuclei with a diffuse matter distribution, it is not. Moreover, since the Coulomb excitation cross sections are large, an ill-defined minimum impact parameter can lead to a large error in the magnitude of the total Coulomb excitation cross section. A better choice is to use the eikonal approach of Ref. [50].

Assuming that the virtual photon numbers can be well calculated, one needs the photonuclear cross sections $\sigma_\gamma^{\pi\lambda}(E_x)$, or equivalently, $dB(\pi\lambda, J_i \rightarrow J_f, E_x)/dE_x \equiv B(\pi\lambda, J_i \rightarrow J_f, E_x)$. Several nuclear models were developed to obtain the response functions $dB(\pi\lambda, J_i \rightarrow J_f, E_x)/dE_x$ for halo nuclei.

Fortunately, nuclear physics allows us to use simple models as inputs to the Coulomb breakup mechanism. Also, since the nuclear fragments are charged, interesting post-fragmentation phenomena arise. In the next Sections we will describe some commonly used models. Some of them are very crude, but enable to obtain the most relevant features of the fragmentation process.

Supplement G

0.15 Dominance of a state in the continuum

It often occurs that the Coulomb excitation mechanism is dominated by transitions between the ground state and a continuum resonant state. In this case, it was shown by Canto et al. [51] that this part of the excitation mechanism can be described exactly in a coupled-channels approach, while the other excitations can be described perturbatively. The method allows the inclusion of the width of the states in a very simple and straightforward way. Fig. 14 represents the procedure. One resonance is coupled to the ground state while the remaining resonances are fed by these two states according to first order perturbation theory. The coupling matrix elements involves the ground state and a set of doorway states $|D^{(n)}_{\lambda\mu}>$, where n specifies the kind of resonance and $\lambda\mu$ are angular momentum quantum numbers. The amplitudes of these resonances in real continuum states are

$$\alpha^{(n)}(\epsilon) =< \phi(\epsilon)|\mathcal{D}^{(n)}_{\lambda\mu} >, \tag{225}$$

where $\phi(\epsilon)$ denotes the wavefunction of one of the numerous states which are responsible for the broad structure of the resonance. In this equation $\epsilon = E_x - E_n$, where E_x is the excitation energy and E_n is the centroid of the resonance considered.

Let us assume for simplicity that the dominant resonant state has spin and parity $J^P = 1^-$. However, the following results can be easily generalized to all spin-parity types. As we have stated above, in this approach we use the Coupled-Channels equations for the coupling between the ground state and the dominant resonance. This results in the following Coupled-Channels equations [51]:

$$\begin{aligned} i\hbar\frac{da_0}{dt}(t) &= \sum_\mu \int d\epsilon < \phi(\epsilon)|\mathcal{D}^{(1)}_{1\mu} >< \mathcal{D}^{(1)}_{1\mu}|V_{E1,\mu}(t)|0 > \exp\left\{-\frac{i}{\hbar}(E_1+\epsilon)t\right\} a^{(1)}_{\epsilon,1\mu}(t) \\ &= \sum_\mu \int d\epsilon\ \alpha^{(1)}(\epsilon)\ V^{(01)}_\mu(t)\ \exp\left\{-\frac{i}{\hbar}(E+\epsilon)t\right\}\ a^{(1)}_{\epsilon,1\mu}(t), \end{aligned} \tag{226}$$

and

$$i\hbar\ \frac{da^{(1)}_{\epsilon,1\mu}}{dt}(t) = \left[(\alpha^{(1)}(\epsilon)\ V^{(01)}_\mu(t)\right]^*\ \exp\{i(E_1+\epsilon)t/\hbar\}\ a_0(t). \tag{227}$$

Above, $(n = 1)$ stands for the dominant resonance, a_0 denotes the occupation amplitude of the ground state and $a^{(1)}_{\epsilon,1\mu}$ the occupation amplitude of a state located at an energy ϵ away from the centroid of the resonance, and with magnetic quantum number μ ($\mu = -1, 0, 1$). We used the short hand notation $V^{(01)}_\mu(t) =< D^{(1)}_{1\mu}|V_{E1,\mu}(t)|0 >$.

Integrating Eq. 227 and inserting the result in Eq. 226, we get the integro-differential equation

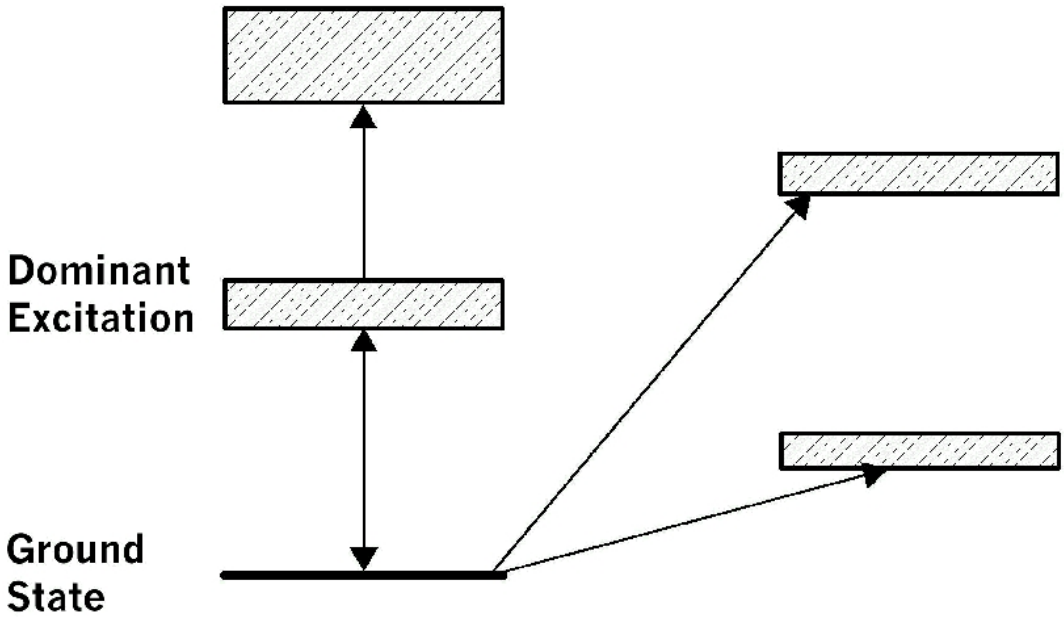

Figure 14: Schematic representation of Coulomb excitation of a dominant resonant state and other states weakly-coupled to the ground state.

for the ground state occupation amplitude

$$\begin{aligned}\frac{d^2a_0}{dt^2}(t) &= -\frac{1}{\hbar^2}\sum_\mu V_\mu^{(01)}(t)\int d\epsilon\ |\alpha^{(1)}(\epsilon)|^2 \\ &\times \int_{-\infty}^{t} dt'\ \left[V_\mu^{(01)}(t')\right]^*\ \exp\left\{-i(E_1+\epsilon)(t-t')/\hbar\right\}\ a_0(t'),\end{aligned} \tag{228}$$

where we used that $a^{(1)}_{\epsilon,1\mu}(t=-\infty)=0$. To carry out the integration over ϵ, we should use an appropriate parametrization for the doorway amplitude $\alpha^{(1)}(\epsilon)$. A convenient choice is the Breit-Wigner (BW) form which yields the square amplitude

$$|\alpha^{(1)}(\epsilon)|^2 = \frac{1}{2\pi}\ \left[\frac{\Gamma_1}{\epsilon^2+\Gamma_1^2/4}\right], \tag{229}$$

where Γ_1 is chosen to fit the experimental width. In this case, this integral will be the simple exponential

$$\int d\epsilon\ |\alpha^{(1)}(\epsilon)|^2\ \exp\left\{-i\frac{(E_1+\epsilon)t}{\hbar}\right\} = \exp\left\{-i\frac{(E_1-i\Gamma_1/2)t}{\hbar}\right\}. \tag{230}$$

A better agreement with the experimental line shapes of the giant resonances is obtained by using a Lorentzian (L) parametrization for $|\alpha^{(1)}(\epsilon)|^2$, i.e.,

$$|\alpha^{(1)}(\epsilon)|^2 = \frac{2}{\pi} \left[\frac{\Gamma_1 E_x^2}{(E_x^2 - E_1^2)^2 + \Gamma_1^2 E_x^2}\right], \tag{231}$$

where $E_x = E_1 + \epsilon$. The energy integral can still be performed exactly [52] but now it leads to the more complicated result [51]

$$\begin{aligned} \int d\epsilon \ |\alpha^{(1)}(\epsilon)|^2 \ \exp\left\{-i\frac{(E_1+\epsilon)t}{\hbar}\right\} &= \left(1 - i\frac{\Gamma_1}{2E_1}\right) \exp\left\{-i\frac{(E_1 - i\Gamma_1/2)t}{\hbar}\right\} \\ &+ \Delta C(t) \ , \end{aligned} \tag{232}$$

where $\Delta C(t)$ is a non-exponential correction to the decay. For the energies and widths involved in the excitation of giant resonances, this correction can be shown numerically to be negligible. It will therefore be ignored. After integration over ϵ, Eq. 228 reduces to

$$\frac{d^2 a_0}{dt^2}(t) = -\mathcal{S}_1 \sum_\mu V_\mu^{(01)}(t) \int_{-\infty}^{t} dt' \left[V_\mu^{(01)}(t')\right]^* \exp\left\{-i\frac{(E_1 - i\Gamma_1/2)(t-t')}{\hbar}\right\} a_0(t') \tag{233}$$

where the factor S_1 is $S_1 = 1$ for BW-shape and $S_1 = 1 - i\Gamma_1/2E_1$ for L-shape.

We can take advantage of the exponential time-dependence in the integral of the above equation, to reduce it to a set of second order differential equations. Introducing the auxiliary amplitudes $A_\mu(t)$, given by the relation

$$a_0(t) = 1 \ + \ \sum_\mu A_\mu(t), \tag{234}$$

with initial conditions $A_\mu(t = -\infty) = 0$, and taking the derivative of Eq. (234), one obtains

$$\ddot{A}_\mu(t) - \left[\frac{\dot{V}_\mu^{(01)}(t)}{V_\mu^{(01)}(t)} \ - \ \frac{i}{\hbar}\left(E_1 - i\frac{\Gamma_1}{2}\right)\right] \dot{A}_\mu(t) \ + \ \mathcal{S}_1 \ \frac{|V_\mu^{(01)}(t)|^2}{\hbar^2} \left[1 + \sum_{\mu'} A_{\mu'}(t)\right] = 0. \tag{235}$$

Solving the above equation, we get $a_0(t)$. Using this amplitude and integrating Eq. (227), one can evaluate $a_{\epsilon,1\mu}^{(1)}(t)$. The probability density for the population of a dominant continuum state with energy E_x in a collision with impact parameter b, $P_1(b, E_x)$, is obtained trough the summation over the asymptotic ($t \to \infty$) contribution from each magnetic substate. This yields

$$P_1(b, \ E_x) = |\alpha^{(1)}(E_x - E_1)|^2 \ \sum_\mu \left| \int_{-\infty}^{\infty} dt' \ \exp\left\{iE_x t'\right\} \ \left[V_\mu^{(01)}(t')\right]^* \ a_0(t') \right|^2, \tag{236}$$

where $|\alpha^{(1)}(E_x - E_1)|^2$ is given by Eq. 229 or by Eq. 231, depending on the choice of the resonance shape.

To first order, the contribution to the excitation of another resonance (the one on the top of Fig. 14) from the dominant one is given by

$$P_2(b,E_x) = |\alpha^{(2)}(E_x-E_2)|^2\,\mathcal{S}_1 \sum_\nu \left| \int_{-\infty}^{\infty} dt'\ \exp\left\{iE_x t'\right\}\ \sum_\mu\ \left[V_{\nu\mu}^{(12)}(t')\right]^* \right.$$
$$\left. \times \int_{-\infty}^{t'} dt'' V_\mu^{(01)}(t'') \exp\left\{-i\frac{(E_1-i\Gamma_1/2)(t-t')}{\hbar}\right\}\ a_0(t'') \right|^2 . \quad (237)$$

We should point out that Eq. 237 is not equivalent to second-order perturbation theory. This would be true only in the limit $a_0(t) \longrightarrow 1$. In this approach, $a_0(t) \neq 1$, since it is modified by the time-dependent coupling to the dominant state. This coupling is treated exactly by means of the Coupled-Channels equations. This approach is justified due to the (assumed) small excitation amplitude for the transition $1 \longrightarrow 2$, since $a_1(t) \ll a_0(t)$.

Equations similar to (236) can also be used to calculate the excitation probabilities directly from the ground-state, with the proper choice of energies, widths, and transition potentials.

0.16 Cluster model

The cluster model [49] assumes a two-body description of one-body halos, e.g., ^{11}Be (^{10}Be + n), ^{8}B(^{7}Be + p), and of three-body halos, e.g., ^{11}Li(^{9}Li + 2n), ^{6}He(^{4}He + n), etc. One can obtain numerically the wave-functions of the $(a = b + c)$-system, given a potential V_{bc} (e.g., Woods-Saxon + spin - orbit + Coulomb, etc). However, as we have seen before, due to the small binding energy of the halo systems the most important part of the wavefunction is beyond the range of the potential V_{bc}. This part of the wavefunction is well described by an Yukawa of the form

$$\psi_{bc}(\mathbf{r}) = N_0\sqrt{\frac{\eta}{2\pi}}\frac{e^{-\eta r}}{r} \quad (238)$$

where $\eta = \sqrt{2\mu_{bc}Q/\hbar}$, μ_{bc} is the reduced mass of $(b + c)$, Q is the separation energy, and $N_0 = e^{\eta r_0}/\sqrt{1+\eta r_0}$ is a normalization factor which corrects the wavefunction to account for the finite range, r_0, of the $(b + c)$ potential. There is no resonance structure in the $b + c$ continuum. This is clearly a good assumption for the deuteron and also for other neutron halo systems.

If we further assume that the final state is a plane-wave state (i.e., we neglect final state interactions) $\psi_f \equiv \langle \mathbf{q}|\mathbf{r}\rangle = e^{i\mathbf{q}.\mathbf{r}}$. The response functions for electric multipole transitions[2]

$$\frac{dB}{dE_x}(E\lambda, E_x) = S\sum_\mu \left|\left\langle \mathbf{q}\left|\hat{O}(E\lambda\mu)\right|\psi_{bc}(\mathbf{r})\right\rangle\right|^2 \frac{d^3q}{(2\pi)^3} \quad (239)$$

where S is a spectroscopic factor (i.e., probability to find the system in the state $(b+c)$). $\hat{O}(E\lambda)$ is the electric multipole operator (see Supplement D) corrected to exclude c.m. motion, i.e.,

[2]Magnetic multiple transtions will be strongly suppressed and will not be considered here.

$$\hat{O}(E\lambda\mu) \;=\; e\sum_{i=p}\left[\left(1-\frac{1}{A}\right)^{\lambda}+(-1)^{\lambda}\frac{(Z-1)}{A^{\lambda}}\right]\; r_i^{\lambda}\,Y_{\lambda\mu} \;+\; e\sum_{i=n} Z\left(-\frac{1}{A^{\lambda}}\right) r_i^{\lambda}Y_{\lambda\mu} \qquad (240)$$

where the sum runs over all protons (p) and neutrons (n) in the nucleus.

For a cluster-system the sum runs over the (effective) charges of the clusters. For example,

$$\begin{aligned}\hat{O}(E1,\mu) &= e\left(\frac{Z_bA_c-Z_cA_b}{A_a}\right) r_{bc}Y_{1\mu}(\widehat{\mathbf{r}}_{bc})\\ \hat{O}(E2_{,\mu}) &= e\left(\frac{Z_bA_c^2+Z_cA_b^2}{A_a^2}\right) r_{bc}Y_{2\mu}(\widehat{\mathbf{r}}_{bc})\end{aligned} \qquad (241)$$

where $\widehat{\mathbf{r}}_{bc}$ is the relative position of $b-c$. Using $d^3q = q^2dqd\Omega_q = \sqrt{2E_x}(\mu_{bc}/\hbar^2)^{3/2}dE\; d\Omega_q$ in Eq. 239 and integrating over Ω, one finds [54]

$$\frac{dB(E\lambda;E_x)}{dE_x} = \frac{2^{\lambda-1}}{\pi^2}(\lambda!)^2(2\lambda+1)\;SN_0^2\left[O(\lambda)\right]^2\left(\frac{\hbar^2}{\mu_{bc}}\right)^{\lambda}\frac{\sqrt{Q}(E_x-Q)^{\lambda+1/2}}{E_x^{2\lambda+2}} \qquad (242)$$

where

$$O(\lambda) = \frac{Z_bA_c^{\lambda}-(-1)^{\lambda}Z_cA_b^{\lambda}}{A_a^{\lambda}}\;e. \qquad (243)$$

The maximum of this function occurs at

$$E_{\lambda} = \frac{2\lambda+2}{\lambda+3/2}\;Q. \qquad (244)$$

In Figure 15(a) we show the photonuclear cross sections obtained by using Eq. 242 in the definition 223. The $E2$ and $E3$ photonuclear cross sections are smaller than the $E1$ by factors of order of 10^5 and 10^9, respectively[3]. The have a longer tail than the $E1$ photonuclear cross section due to the factor $E_x^{2\lambda-1}$ in Eq. 223. These results show that a cluster-like correlation between the valence neutrons is not so effective in producing an enhancement of the low energy part of the photonuclear cross sections for higher multipolarities, as it does for the dipole case.

While the cluster model is questionable for ^{11}Li it is quite reasonable for ^{11}Be. ^{11}Be may be described, in a good approximation, as a neutron bound to a ^{10}Be core. The $1/2^+$ spin-parity of Be^{11} may be reproduced by adjusting the ^{10}Be + n potential so as to yield a ground state for the $2s_{1/2}$ orbit at 505 keV. For example, if one uses a simple Woods-Saxon potential of the form $V = V_0/\left\{1+\exp\left[(r-R)/a\right]\right\} + V_C^{p-Be}(r)$ the parameters $V_0 = -51.55$ MeV, $R = 3$ fm and $a = 0.505$ fm will do the job, assuming that $V_C^{p-Be}(r)$ is the Coulomb potential between a uniform charged sphere, with $Z = 4$, $R_C = R$, and the proton. The response function may be obtained by using this wave function for $\psi_{bc}(\mathbf{r})$ in Eq. 239 and the continuum wave-function calculated for the same potential.

[3]The spectroscopic factor and the normalization constant (S, and N_o, in eq. 242 were set to unity, for simplicity.

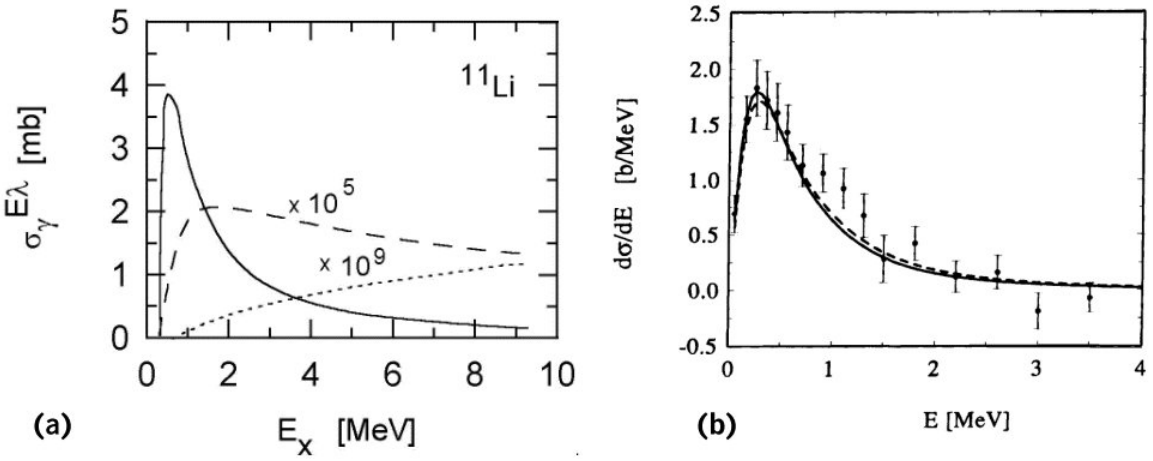

Figure 15: (a) Photo absorption cross section of ^{11}Li in the cluster model. The solid (dashed) [dotted] curve corresponds to dipole (quadrupole) [octupole] multipolarity. The quadrupole (octupole) values were multiplied by a factor of 10^5 (10^9) [54]. (b) Coulomb dissociation cross section ^{11}Be + Pb $\rightarrow$ n + ^{10}Be, at 70 MeV/nucleon, compared to a calculation based on the cluster model. The dashed curve includes a reacceleration effect of the ^{10}Be fragment.

However, the response function will be dominated by the tail of the ground state wave-function. Thus, we can use the analytical formulas deduced above. For the Be^{11} case ($Z = 4$, $A = 11$) and dipole excitations we get [55]

$$\frac{dB(E1)}{dEx} = S_1 \frac{e^{2\eta r_0}}{1+\eta r_0} \frac{3\hbar^2}{\pi^2 \mu} e^2 \left(\frac{Z}{A}\right)^2 \sqrt{Q} \frac{(E_x - Q)^{3/2}}{E_x^4}. \tag{245}$$

The Coulomb dissociation cross section obtained by using this response function is compared to experiment by T. Nakamura et. al.[56]. In Figure 15(b) we show $d\sigma/dE_x$ (solid line), using the cluster model, with $S_1 = 1$, $r_0 = 4$ fm is compared to the experimental data. We remark that the spectroscopic factor $S_1 = 1$ is not very far from the reported value of 0.77 [57] deduced from the ^{11}Be reaction. Thus, in view of the simplicity, we consider the cluster model to work very well in this case. The dashed curve in Fig. 15(b) considers the effect of post-acceleration (or reacceleration) which we shall discuss later.

Supplement B

0.17 The random phase approximation (RPA)

The RPA model is a useful tool to describe the nuclear response function in terms of microscopic

degrees of freedom. There are many ways to derive the RPA. We will adopt the space (or coordinate) representation, following the work of Bertsch and Shlomo [58, 59]. Let us assume that we know the solutions of

$$H\phi_i = e_i\phi_i. \tag{246}$$

The formal solution to $(H + V_x)\Psi = E\Psi$ is

$$\Psi = \phi - \frac{V_x}{H - E}\Psi. \tag{247}$$

If V_1 is a weak perturbation a state ϕ_i will change to a state ϕ_i'. Using $\phi \equiv \phi_i$ and $\Psi \cong \phi_i$ in the above equation

$$\phi_i' \cong \phi_i - \frac{V_x}{H - E}\,\phi_i \tag{248}$$

Using the completeness relation, $\sum_i \mid \phi_i >< \phi_i \mid = 1$, the second term above can be rewritten, as

$$\phi_i' \cong \phi_i + \sum_j \frac{< i \mid V_x \mid j >}{e_i - e_j}\phi_j \tag{249}$$

in an obvious notation.

If a weak time-dependent field $V_x(r)\cos(\omega t)$ is turned on slowly at $t = -\infty$, the perturbed wave functions are found to be

$$\phi_i'(t) = \phi_i + \frac{1}{2}\sum_j \langle\, i|\, V_x \mid j\rangle \,\left\{\frac{e^{-i\omega t}}{e_i - e_j - \omega} + \frac{e^{i\omega t}}{e_i - e_j + \omega}\right\}\phi_j(t) \tag{250}$$

which is a first-order solution of the time dependent Schrödinger equation

$$\frac{i}{\hbar}\frac{\partial\phi_i}{\partial t} = \left[H + V_x\left(\mathbf{r}\right)\cos\omega t\right]\phi_i \;\equiv \frac{\hbar^2}{2m}\nabla^2\phi_i + V\phi_i + V_x\left(\mathbf{r},t\right)\phi_i. \tag{251}$$

The time-dependent density, counting all occupied orbitals, is

$$n\left(\mathbf{r},t\right) = \sum_i^{occ} \left|\phi_i'(t)\right|^2 = \; n_0\left(\mathbf{r}\right) + \cos\omega t \;\; \delta n\left(\mathbf{r}\right) \tag{252}$$

where $n_0\left(\mathbf{r}\right)$ is the initial density (unperturbed), and

$$\delta n\left(\mathbf{r}\right) = \sum_i^{occ}\sum_j \langle\, j|\, V_x \mid i\rangle \;\langle\, i|\, \widehat{n}\left(\mathbf{r}\right) \mid j\rangle \;\left\{\frac{1}{e_i - e_j - \omega} + \frac{1}{e_i - e_j + \omega}\right\}. \tag{253}$$

In this formula $\widehat{n}\left(\mathbf{r}\right)$ means the density operator, and

$$\langle\, i|\, \widehat{n}\left(\mathbf{r}\right) \mid j\rangle \;\; = \sum_k \;\int \phi_i^*\left(\mathbf{r}_1 \ldots \mathbf{r}_n\right)\phi_j\left(\mathbf{r}_1 \ldots \mathbf{r}_n\right)\prod_{\ell\neq k}^{n-1} dr_\ell. \tag{254}$$

The time-dependent current is

$$\mathbf{j}(\mathbf{r},\mathbf{t}) = \sin\omega t \ \sum_{i}^{occ}\sum_{j} \langle\, j|\, V_x \,|\, i\rangle \ \langle\, i|\, \mathbf{j} \,|\, j\rangle \ \left[\frac{1}{e_i - e_j - \omega} - \frac{1}{e_i - e_j + \omega}\right] \tag{255}$$

where

$$\langle\, i|\, \mathbf{j} \,|\, j\rangle \ = \frac{\hbar}{2im} \ \sum_{k} \ \int \left[-\left(\nabla\phi_i^*\right)\phi_j + \phi_i^*\left(\nabla\phi_j\right)\right] \prod_{\ell\neq k}^{n-1} dr_\ell. \tag{256}$$

We now define a response function for the density change at $\mathbf{r}$ inducing by a potential field at $\mathbf{r}'$, leaving out the explicit time dependence:

$$\pi^0\left(\mathbf{r},\mathbf{r}',\omega\right) = \sum_{i}^{occ} \ \sum_{j} \ \langle\, i|\, n\left(\mathbf{r}\right) |\, j\rangle\, \langle\, j|\, n\left(\mathbf{r}'\right) |\, i\rangle \left[\frac{1}{e_i - e_j - \omega} + \frac{1}{e_i - e_j + \omega}\right]. \tag{257}$$

Then the response to an arbitrary external field can be calculated from the integral

$$\delta n_{ip} = \int \pi^0\left(\mathbf{r},\mathbf{r}'\right) V_x\left(\mathbf{r}'\right) d^3r' \tag{258}$$

which is the independent particle response.

But, besides the external field, the induced density oscillation will cause the self-consistent field to oscillate at the same frequency as well. The time-varying mean field is given by

$$\delta V\left(\mathbf{r}\right) = \int d^3r' \ \frac{\delta V\left(\mathbf{r}\right)}{\delta n\left(\mathbf{r}'\right)} \ \delta n\left(\mathbf{r}'\right). \tag{259}$$

Adding this potential to the external field, we obtain an implicit equation for the self-consistent density,

$$\delta n_{RPA}\left(\mathbf{r}\right) = \int \pi^0\left(\mathbf{r},\ \mathbf{r}_2\right) \left[V_x\left(\mathbf{r}_2\right) + \int d^3r' \ \frac{\delta V_x\left(\mathbf{r}_2\right)}{\delta\eta\left(\mathbf{r}'\right)} \ \delta n_{RPA}\left(\mathbf{r}'\right)\right] \ d^3r_2. \tag{260}$$

Defining the RPA response function

$$\delta n_{RPA} = \int \pi^{RPA}\left(\mathbf{r},\mathbf{r}'\right) \ V_x(\mathbf{r}')d^3r' \tag{261}$$

the previous equation is satisfied for any V_x if π^{RPA} satisfies the implicit equation

$$\pi^{RPA}\left(\mathbf{r},\mathbf{r}'\right) = \pi^0\left(\mathbf{r},\mathbf{r}'\right) + \int d^3r_2 d^3r_3 \ \pi^0\left(\mathbf{r},\mathbf{r}_2\right) \frac{\delta V_x\left(\mathbf{r}_2\right)}{\delta n\left(\mathbf{r}_3\right)} \pi^{RPA}\left(\mathbf{r}_3,\mathbf{r}'\right). \tag{262}$$

Compactly, in operator form,

$$\pi^{RPA} = \pi^0 + \pi^0 \frac{\delta V}{\delta n} \ \pi^{RPA} \tag{263}$$

which has the formal solution

$$\pi^{RPA}=\left[1-\pi^0\frac{\delta V}{\delta n}\right]^{-1}\pi^0. \tag{264}$$

In practical terms, the equation is often replaced by a matrix equation, representing $\pi\left(\mathbf{r},\mathbf{r}'\right)$ on a spatial mesh [58]. Then the solution is obtained by inverting the matrix representing $\left(1-\pi^0\delta V/\delta n\right)$.

Of importance to calculate the Coulomb excitation cross sections is the so-called *strength function*, or *response function*, defined as

$$S\left(V_x,\omega\right)=\sum_f\ |<i\left|V_x\right|\ f>|^2\ \delta\left(\omega-E_i-E_f\right). \tag{265}$$

Giving $\pi\left(\mathbf{r},\mathbf{r}',\omega\right)$ a small imaginary part and using $Im\left[1/\left(x+i\eta\right)\right]=\pi\delta\left(x\right)$, one can show that

$$S\left(V_x,\omega\right)=\frac{1}{\pi}\int d^3rd^3r'\ V_x\left(\mathbf{r}\right)V_x\left(\mathbf{r}'\right)Im\pi\left(\mathbf{r},\mathbf{r}'\right). \tag{266}$$

The above formalism is especially useful if one has a separable interaction for $\delta V/\delta n$ in Eq. 264, i.e., if

$$v\left(\mathbf{r},\mathbf{r}'\right)=kf\left(\mathbf{r}\right)f\left(\mathbf{r}'\right)\equiv\delta V/\delta n \tag{267}$$

then

$$\pi^{RPA}\left(\mathbf{r},\mathbf{r}'\right)=\left[1-k\int d^3rd^3r'f\left(\mathbf{r}\right)f\left(\mathbf{r}'\right)\pi^0\left(\mathbf{r},\mathbf{r}'\right)\right]^{-1}\pi^0. \tag{268}$$

The resonances of the RPA theory are found at the singularities of the above function, i.e.,

$$1+k\int d^3rd^3r'f\left(\mathbf{r}\right)f\left(\mathbf{r}'\right)\pi^0\left(\mathbf{r},\mathbf{r}'\right)=0. \tag{269}$$

This is called the RPA dispersion relation. Using Eq. 257 we can rewrite it as

$$\sum_{ph}|<p\mid f\mid h>|^2\left[\frac{1}{e_p-e_h-\omega}+\frac{1}{e_p-e_h+\omega}\right]=-\frac{1}{k}. \tag{270}$$

The qualitative behavior of the RPA resonances may be seen from a graphical solution of 270. (Note that in 270, p denotes particle, or occupied, states and h are hole, or unoccupied, states). The solid lines on Fig. 16 are the left-hand-side of Eq. 270. The function has poles at energies ϵ_i corresponding to particle-hole excitations, e_p-e_h. The solutions to the equation are the frequencies where the functions equals $-1/k$.

For a repulsive interaction ($k>0$) there is a solution at an energy higher than all the particle-hole energy differences. This is the collective vibration; it will have a large transition strength for the field f. There are also other solutions to the dispersion relation located near the unperturbed particle-hole energies, indicated by small dots. When the interaction is attractive, there will be a resonance lower in energy than the lowest particle-hole state (large circles).

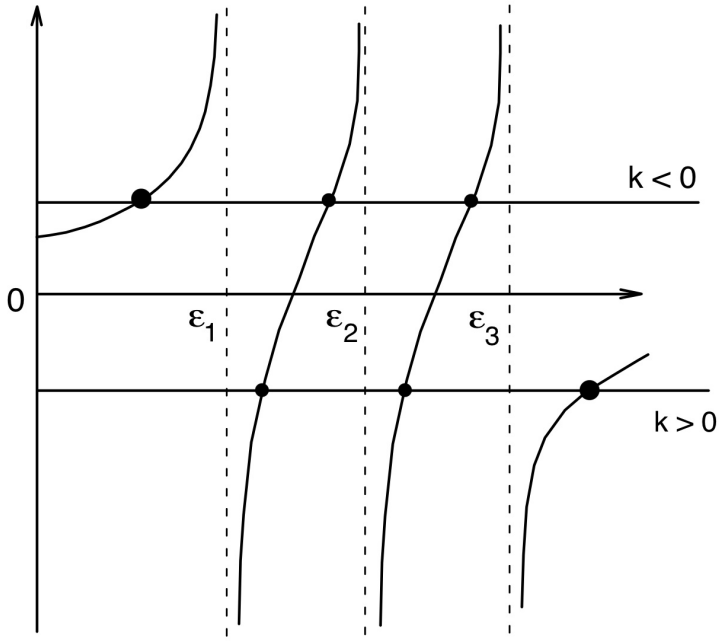

Figure 16: Graphical solution of RPA equations.

In the limit when all particle-hole energies are degenerated in energy, i.e., $e_p - e_h = e$, the dispersion relation 270 has a simple solution given by

$$\omega_c^2 = e^2 + 2ek \sum_{ph} |< p \mid f \mid h >|^2 . \tag{271}$$

Thus, the sign of v determines the direction of the energy shift with respect to the particle-hole state; an attractive v lowers ω while a repulsive interaction raises it.

The above formalism has been used, e.g., in Ref. [58] and RPA computer program along this approach is given in Ref. [59]. But, this formalism depends on the separability of the residual interaction. Since the exchange interaction is non-local, a separable interaction is not always convenient. To treat the non-local interactions properly a matrix formulation of RPA is more appropriate. In orbital representation

$$\pi^0 \left(\mathbf{r}, \mathbf{r}'\right) = \sum_{i,j,k,l} < i \mid \widehat{n}\left(\mathbf{r}\right) \mid j > \pi^0 \left(ij, kl\right) < k \mid \widehat{n}\left(\mathbf{r}'\right) \mid l > \tag{272}$$

where

$$\pi^0(ij, kl) = \delta_{ik}\delta_{jl} \, \frac{n_i - n_j}{e_i - e_j - \omega} \tag{273}$$

with $n_i = 0$ (1) for empty (occupied) states.

It is easy to see that this definition is equivalent to 257. Inserting 272 in 273 we get

$$\begin{aligned}
\pi^0 &= \sum_{i,j,k,l} < i \mid \widehat{n}(\mathbf{r}) \mid j > \delta_{ik}\delta_{jl} \frac{n_i - n_j}{e_i - e_j - \omega} < k \mid \widehat{n}(\mathbf{r}') \mid l > \\
&= \sum_{i,j,k,l} \Big\{ < i_{empty} \mid \widehat{n}(\mathbf{r}) \mid l > \frac{(-n_j)\,\delta_{j_\ell}}{e_i - e_j - \omega} < i_{empty} \mid \widehat{n}(\mathbf{r}') \mid l > \\
&\quad + < i_{occ} \mid \widehat{n}(\mathbf{r}) \mid l > \frac{(1 - n_j)\,\delta_{jl}}{e_i - e_j - \omega} < i_{occ} \mid \widehat{n}(\mathbf{r}') \mid l > \Big\} \\
&= \sum_{ij} \Big\{ < i_{empty} \mid \widehat{n}(\mathbf{r}) \mid j_{occ} > \frac{(-1)}{e_i - e_j - \omega} < i_{empty} \mid \widehat{n}(\mathbf{r}') \mid j_{occ} > \\
&\quad + < i_{occ} \mid \widehat{n}(\mathbf{r}) \mid j_{empty} > \frac{1}{e_i - e_j - \omega} < i_{occ} \mid \widehat{n}(\mathbf{r}') \mid j_{empty} > \Big\}. \qquad (274)
\end{aligned}$$

Exchanging the indices i and j of the first term, the Eq. 257 is obtained.
The residual interaction is represented by

$$< ij \mid v \mid k\ell > = \int d^3r d^3r' \phi_i^*(\mathbf{r})\,\phi_j(\mathbf{r}) \frac{\delta V(\mathbf{r})}{\delta n(\mathbf{r}')} \phi_\ell(\mathbf{r}')\,\phi_k(\mathbf{r}'). \qquad (275)$$

It is often convenient to express the RPA configurational response in a diagonal form. To accomplish this, we define the amplitudes for the orbital pairs (ij) as $x_\alpha(i,j)$, where the α labels the eigenvectors. In this representation the response function is

$$\pi^{RPA}(ij,k\ell) = \sum_\alpha \frac{2\omega_\alpha x_\alpha(ij)\,x_\alpha(k\ell)}{\omega^2 - \omega_\alpha^2}. \qquad (276)$$

The eigenvalue equation is simply

$$(e_i - e_j - \omega_\alpha)\,x(ij) + (n_i - n_j) \sum_{k\ell} < ij \mid v \mid k\ell > x(k\ell) = 0. \qquad (277)$$

The normalization of an $x(i,j)$ vector is

$$\sum_{ij} (n_i - n_j)\,x_\alpha^2(ij) = 1. \qquad (278)$$

It is common to use a notation with particle-hole amplitudes $(n_i - n_j) = +1$ denoted by $X_{ij} = X_{ph}$ and hole-particle amplitudes $(n_j - n_i = +1)$ by Y_{ph}. The matrix eigenvalue equation is written

$$\begin{pmatrix} A & B \\ -B & -A \end{pmatrix} \begin{pmatrix} X \\ Y \end{pmatrix} = \omega \begin{pmatrix} X \\ Y \end{pmatrix} \qquad (279)$$

with

$$A_{ph,p'h'} = (e_p - e_h)\,\delta_{p,p'}\delta_{h,h'} + < ph \mid v \mid p'h' > \qquad (280)$$

and

$$B_{ph,p'h'} =< hp \mid v \mid p'h' > . \tag{281}$$

The corresponding normalization equation is

$$\sum_{ph} \left(X_{ph}^2 - Y_{ph}^2 \right) = 1. \tag{282}$$

In terms of the eigenvector amplitudes, the transition density for the vibration α is given by

$$\delta n \left(\mathbf{r} \right) = \sum_{ij} \left\langle i \right| \widehat{n} \left(\mathbf{r} \right) \left| j \right\rangle x_\alpha \left(ij \right) = \sum_{ph} \left\langle p \right| \widehat{n} \left(\mathbf{r} \right) \left| h \right\rangle X_{ph} + \left\langle h \right| \widehat{n} \left(\mathbf{r} \right) \left| p \right\rangle Y_{ph}. \tag{283}$$

The transition potential of the vibration maybe defined similarly, using

$$\delta V = \int d^3 r' \delta n \left(\mathbf{r}' \right) v \left(\mathbf{r} - \mathbf{r}' \right) \tag{284}$$

where $v \left(\mathbf{r} - \mathbf{r}' \right)$ is the two-particle interaction. Given the transition potential of the vibration, the X and Y amplitudes may be recovered from

$$X_{\alpha,ph} = \frac{< p \mid \delta V \mid h >}{e_p - e_h - \omega_\alpha}, \qquad Y_{\alpha,ph} = \frac{< h \mid \delta V \mid p >}{e_p - e_h + \omega_\alpha} \tag{285}$$

For the simple case that there is only one particle-hole configuration, $\left\langle hp \right| v \left| ph \right\rangle = \left\langle ph \right| v \left| hp \right\rangle = V$. Then, V, X and Y are numbers rather than matrices or vectors and the eigenvalue equation reads (abbreviating $e_p - e_h \equiv e$)

$$eX + V \left(X + Y \right) = \omega X, \qquad -eY - V \left(X + Y \right) = \omega Y$$

or

$$\left(e + 2V \right) \left(X + Y \right) = \omega \left(X - Y \right), \qquad e \left(X - Y \right) = \omega \left(X + Y \right). \tag{286}$$

The $X + Y$ term is proportional to a density and the $X - Y$ term is proportional to a current. The 1st equation behaves like Newton's equation, relating the time derivative of the current to forces which depend linearly on a density distribution. The second equation is a consequence of the continuity condition which relates a time rate of change of density to the current. The two equations can only be satisfied simultaneously if the frequency ω obeys the relation,

$$\omega^2 = e^2 + 2Ve$$

which is the same as Eq. 271.

If V is weak the change in ω is small and $\omega \approx e + V$, what is expected for a small perturbation.

Using 285 and 282 we find

$$X = \sqrt{\frac{e}{\omega}} \frac{V}{e - \omega} \ , \qquad Y = \frac{V}{e + \omega}. \tag{287}$$

Suppose we have an operator M with the particle-hole matrix element $m = \langle p| M |h\rangle = \langle h| M |p\rangle$. Then from Eq. 265 one gets the collective state transition strength

$$[\langle 0| M |RPA\rangle]^2 = m^2 (X+Y)^2 = m^2 \frac{e}{\omega}. \tag{288}$$

Thus excitations which are shifted to lower energy by the interaction have a larger transition strength. But, the oscillator strength (sum rule) associated with the transition is proportional to $288 \times \omega$, and is thus independent of the residual interaction.

0.18 Collective response in halo nuclei

For isovector excitations, i.e., $E1$-excitations, the residual nucleon-nucleon interaction (see Supplement B) can be chosen as a density dependent contact interaction.

$$v = \sum_{i<j} (\tau_i \cdot \tau_j) v_\tau \delta (\mathbf{r}_i - \mathbf{r}_j) \tag{289}$$

with $v_\tau = 350$ MeV fm^3 [58]. The interaction strength v_τ is chosen as a compromise between a value that fits the symmetry energy of nuclear matter and a value that fits the giant dipole in ^{16}O.

The first RPA calculation for ^{11}Li was performed by Bertsch and Foxwell [60]. They have chosen a mean-field Woods-Saxon potential which yields an occupied $p_{1/2}$ neutron orbital bound by 0.2 MeV. Fig. 17(a) shows the results of their calculations for the dipole response of ^{11}Li. The "free response" is what is obtained by switching-off the residual interaction (see Supplement B). This has a broad peak around 15 MeV associated with $1\hbar\omega$ transitions, and a low continuum starting at the neutron threshold. The RPA response has the strength shifted upward, with about half of the energy-weighted sum in a peak at 22 MeV. There is much less collectivity here than for $N = Z$ nuclei.

One sees that the usual RPA fails to yield enough strength at low energies. In fact, the total electromagnetic dissociation cross section that one obtains by using the response presented in Fig.. 17(a) is ≤ 0.28 b for ^{11}Li + Pb at 800 MeV/nucleon. Moreover, an artificial energy for the $p_{1/2}$ orbit (~ 0.2 MeV) is used. The experimentally known value of the one-neutron separation energy is about 1 MeV and for such a value of $\varepsilon_{p_{1/2}}$ a too small cross section is obtained ($\simeq 0.19$ b versus the experimental value of 0.9 b).

To mock-up cluster-like correlations within the RPA, an RPA-cluster model was developed by Teruya et al. [62] with an enlarged $p-h$ configuration space to accommodate the dineutron-dineutron hole excitations. One ends up treating ^{11}Li as composed of three species of particles: protons, neutrons and dineutrons (the dineutron is treated as structureless). In this approach there is no problem in fixing the $p_{1/2}$ energy as 1.0 MeV and the correct dineutron separation energy of $\varepsilon = 0.3$ MeV, since the Woods-Saxon potentials for the nucleons and dineutrons are different. The results of this calculation [62] is presented in the Figure 17(b). Also shown is the dipole response calculated by using the cluster model (dashed line) using $S_1 = 1,\ N_0 = 1$ in Eq. 245. Besides the

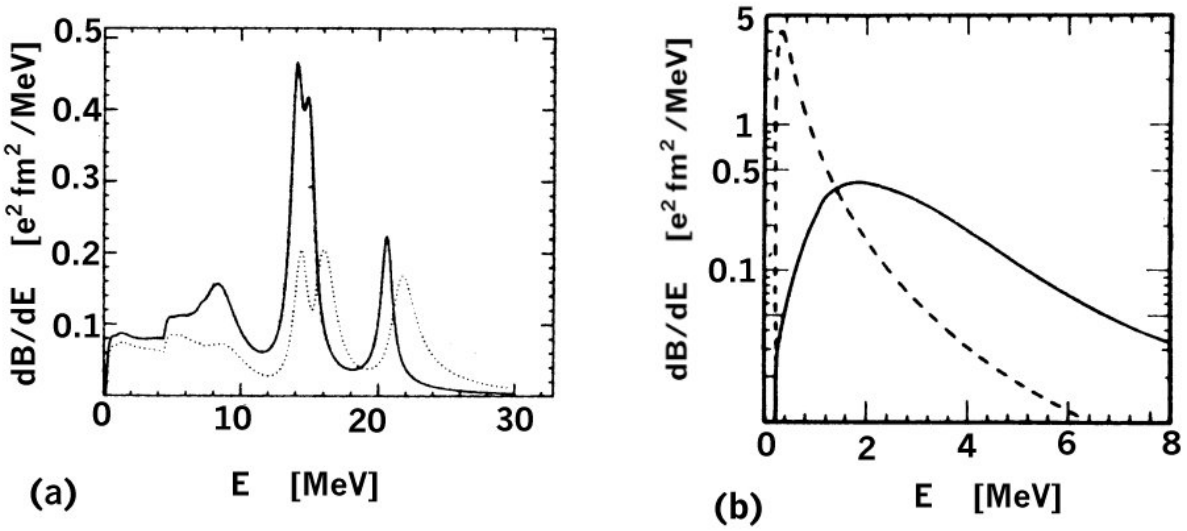

Figure 17: (a) ^{11}Li dipole response. Solid line is the free response. Dashed line is the RPA response. (b) Cluster model reponse (dashed curve) compared with the RPA-cluster model response [62] (solid curve).

usual GDR (Giant Dipole Resonance) at $E \simeq 16$ MeV, not shown in the Figure, one finds a strong peak at 1.81 MeV. The $B(E1)$ value under this peak is found to be 2.38 e^2 fm^2 which corresponds to $\simeq 85\%$ of the dipole cluster sum-rule and 8% of the usual energy weighted sum-rule [63]. Other RPA studies for the electromagnetic response of halo nuclei have been performed, e.g., by Fayans [64] and Bertulani and Sustich [54]. The low energy peak of the E1-response, as observed in Fig. 17(b) is called by *soft dipole mode (*or *Pigmy resonance).*

Some authros interpret the soft dipole mode in halo nuclei as a collective vibration of the core against the valence neutrons. Its strength is located at much loer energies than the usual giant dipole resonances, and they are located at much lower energies. Because of that hey are also known as pigmy resonances (see Fig. 18).

As shown in Ref. [54] the electric dipole interaction is the most relevant for the Coulomb break-up (see Figure 19(a)). This is because the effective multipole charge (Eq. 242) is small for ^{11}Li for higher multipolarities. However, for other systems, like $^8\mathrm{B} \rightarrow \mathrm{p} +^7$ Be, other multipolarities are equally important.

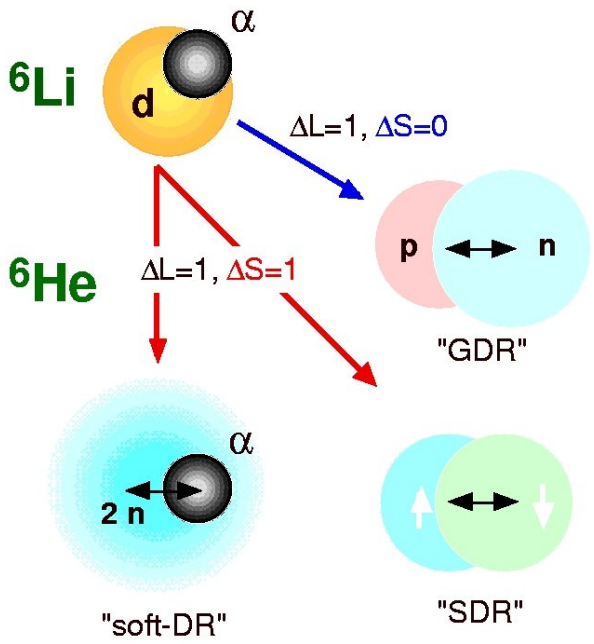

Figure 18: Schematic view of GDR and pigmy resonances (soft dipole resonances) in ^{6}He and ^{6}Li (by Shintaro Nakayama [61]).

0.19 Single-particle model with nucleon-nucleon correlations

To gain insight on the relevance of n-n correlations on the response function of ^{11}Li we take again only two models: (a) the Green's function method of Esbensen and Bertsch [65] and the (b) three-body model of Chulkov, Jonson and Zhukov [66].

The Green's function method is a single-particle + (n-n) correlations. In such a model the dipole strength distributions can be expressed in terms of the two-particle Green function for $J = 1$ final states [65],

$$\begin{aligned} \frac{dB(E1)}{dE} &= \frac{1}{\pi} Im \sum_{\mu} \int d^3r_1 d^3r_2 d^3r_1' d^3r_2' \\ &\times \Psi^*_{g.s.}(\mathbf{r}_1, \mathbf{r}_2) D^*_{\mu}(\mathbf{r}_1, \mathbf{r}_2) G(E, \mathbf{r}_1, \mathbf{r}_2, \mathbf{r}_1', \mathbf{r}_2') D_{\mu}(\mathbf{r}_1', \mathbf{r}_2') \Psi_{g.s.}(\mathbf{r}_1', \mathbf{r}_2') \end{aligned} \tag{290}$$

where $\Psi_{g.s.}\left(\mathbf{r}_1', \mathbf{r}_2'\right)$ is the correlated ground state of the two valence neutrons (see Ref. [65]), and

$$D_{\mu}\left(\mathbf{r}_1, \mathbf{r}_2\right) = -\frac{Ze}{A}\left[r_1 Y_{1\mu}(\widehat{\mathbf{r}}_1) + r_2 Y_{1\mu}(\widehat{\mathbf{r}}_2)\right] \tag{291}$$

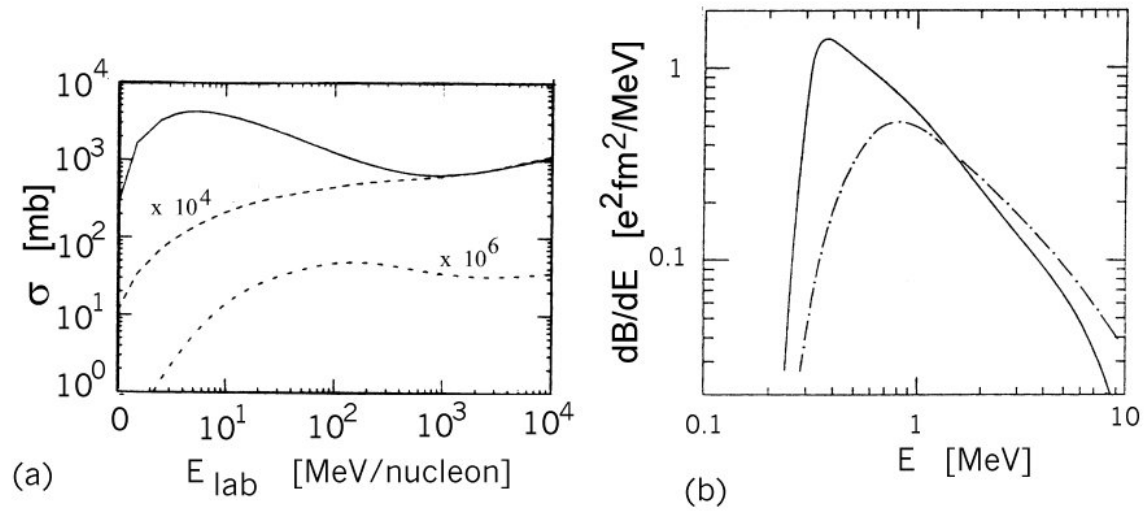

Figure 19: (a) Total Coulomb excitation cross section of ^{11}Li projectiles incident on a lead target as a functiuon of the beam energy. The solid (dashed) line represents the contribution of isovector dipole (effective-charge-corrected quadrupole) excitations. The dash-dotted line represents the contribution of effective-charge-corrected octupole excitations. The quadrupole and the octupole results have been multiplied by 10^4 and 10^6, respectively. (b) Correlated dipole response of ^{11}Li is shown in the figure by a solid line. The dot-dashed curve shows the response neglecting the effect of pair-interaction in the final state.

is the effective dipole operator.

The Green's function G includes the continuum-continuum interactions between the neutrons. In the *Tamm-Dancoff approximation* (TDA) it is given by

$$\begin{aligned} G(E) &= [1 + G_0(E)v]^{-1} G_0(E) \\ &= G_0(E) - G_0(E)v\,[1 + G_0(E)v]^{-1} G_0(E) \end{aligned} \tag{292}$$

where

$$G_0(E) = \sum_{\mu,f} \frac{|(j_1 j_2)_{1\mu}\rangle \langle (j_1 j_2)_{1\mu}|}{e_1 + e_2 - E - i\eta} \tag{293}$$

is the non-interacting two-particle Green's function and the sum over final states (f) includes all independent two-particle states. The second equality in Eq. 292 shows that the TDA response can be written as an uncorrelated response minus a correction term.

The correlated dipole response is shown in Figure 19(b) by a solid line. The dot-dashed curve shows the response neglecting the effect of pair-interaction in the final state. It predicts more

strength at higher energies; the effect of the final state interactions is to shift the maximum in the strength much closer to the threshold.

In a three-body approach, based on hyperspherical harmonics the differential cross section for the ^{11}Li break-up to a final excitation energy of E, and scattering angle θ [66] is given by

$$\frac{d^2\sigma}{dEd\theta} \sim N_{E1}(E)E^2(\sin\theta)^2(\cos\theta)^2 \sum_{KK'\ell_1\ell_2} B_{KK'\ell_1\ell_2}(E)\Psi_K^{\ell_1\ell_2}(\theta)\left[\Psi_{K'}^{\ell_1\ell_2}(\theta)\right]^* \qquad ((2.14))$$

where the coefficients $B_{KK^1\ell_1\ell_2}$ are components of the response function of the operator $\widehat{\mathcal{O}}(E_1)$, $N_{E1}(E)$ is the $E1$-virtual photon number, and $\Psi_K^{\ell_1\ell_2}$. Explicitly,

$$\begin{aligned} B_{KK^1\ell_1\ell_2}(E) &= \sum_{m_1m_2} \left\langle \phi_0 \left| \widehat{\mathcal{O}}(E_1) \right| \frac{i^K}{(q\rho)^2} J_{K+2}\left(\frac{\sqrt{2}}{\hbar}\rho q\right) \left[\mathcal{Y}_{Km_1m_2}^{\ell_1\ell_2}(\Omega_5^\rho)\right]^* \right\rangle \\ &\times \left\langle \phi_0 \left| \widehat{\mathcal{O}}(E_1) \right| \frac{i^K}{(q\rho)^2} J_{K'+2}\left(\frac{\sqrt{2}}{\hbar}\rho q\right) \left[\Psi_{K'm_1m_2}^{\ell_1\ell_2}(\Omega_5^\rho)\right]^* \right\rangle^* \end{aligned} \qquad (294)$$

where J_i are Bessel functions, q is the momentum transfer, Ω_5^ρ is the hyperangle and ρ the hyperradius.

Chulkov et al. [66] have used this approach, and an schematic treatment of the final state interactions, to compare with the experimental data. They found that their calculated curve has the maximum shifted as compared to the experimental data. This might be an indication of Coulomb reacceleration effects which we will discuss later.

In Ref. [68] the experimental data for $d\sigma/dE$ have been compared with some theoretical models. This is shown in Fig. 20 and explained in its caption. The best fit was obtained with a phenomenological Breit-Wigner fit. However, it is questionable if these data can be directly compared with the theoretical response functions, due to reacceleration effects.

0.20 Coulomb reacceleration effect

Breakup processes in nucleus-nucleus collisions are complicated, in whatever way they are treated. They constitute at least a three-body problem, which is further complicated due to the long range Coulomb force. Exact treatments (like the Fadeev-approach) are therefore prohibitively cumbersome. On the other hand, many approximate schemes have been developed in the field of direct nuclear reactions, and these approaches have been used with considerable success [67].

Effects of Coulomb reacceleration were first observed in the experiment of Ieki et al. [68]. In Fig. 21 we see that the velocity of ^{9}Li fragments are faster, in average, than those of the two detached neutrons in a Coulomb break-up of 28 MeV/nucleon ^{11}Li incident on lead targets.

This effect can, in principle (we will discuss this later again), be understood qualitatively as follows. The ^{11}Li is deccelerated up to a point where it dissociates. This occurs around the distance of closest approach. Afterwards the ^{9}Li fragments is accelerated, whereas the neutrons are not.

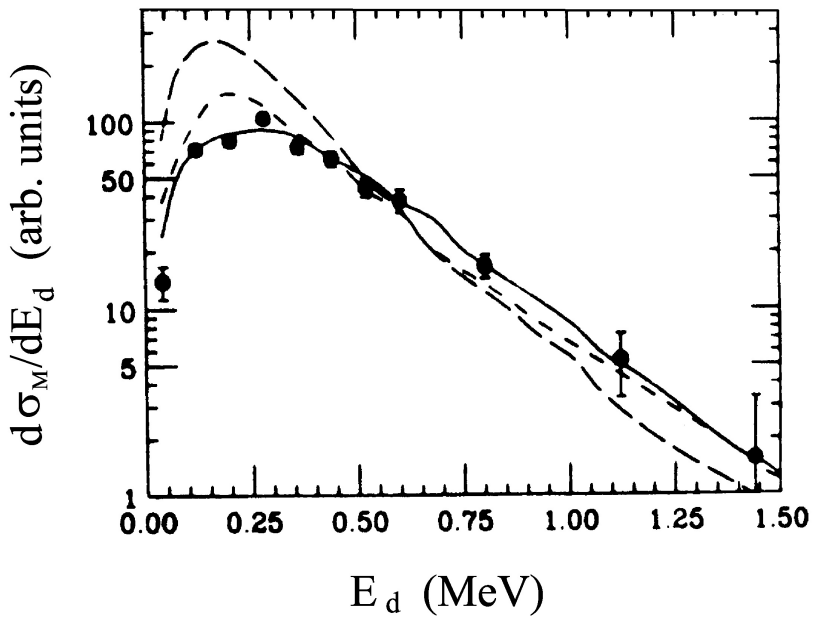

Figure 20: The measured decay energy spectrum $d\sigma_M/dE_d$ for ^{11}Li $\rightarrow$ ^{9}Li +n+n. The curves are results of Monte Carlo simulations for Breit-Wigner-type photonuclear cross sections (solid, $E_0 = 0.70$ MeV, $\Gamma_0 = 0.80$ MeV), a correlated-state model [65] (dashed), and a dineutron-cluster model [55] (long dashed).

Since ^{9}Li is lighter than ^{11}Li its final velocity is greater than the incoming beam velocity. The neutrons are consequently slower.

Baur, Bertulani and Kalassa [69] developed a semiclassical model to obtain quantitatively the extra-amount of energy gained (lost) by ^{9}Li (2n). The model averages the reacceleration energies along the trajectory with the probability that the break-up occurs at time t. For a given impact parameter b the extra-energy gained by reacceleration of ^{9}Li (or the energy lost by the neutrons) is given by

$$\triangle E_9(b) = -\frac{9}{11} < E_x > + \frac{\pi}{22}\frac{Z_T Z_a e^2}{b} \quad (295)$$

$$\Delta E_{2n}(b) = -\frac{2}{11} < E_x > - \frac{\pi}{22}\frac{Z_T Z_a e^2}{b} \quad (296)$$

where Z_T is the target charge, $Z_a = 3$ is the charge number of ^{11}Li, and $< E_x >$ is the average energy transferred by the Coulomb interaction to the break-up of ^{11}Li. The simplest way to calculate $< E_x >$ is by means of the cluster model.

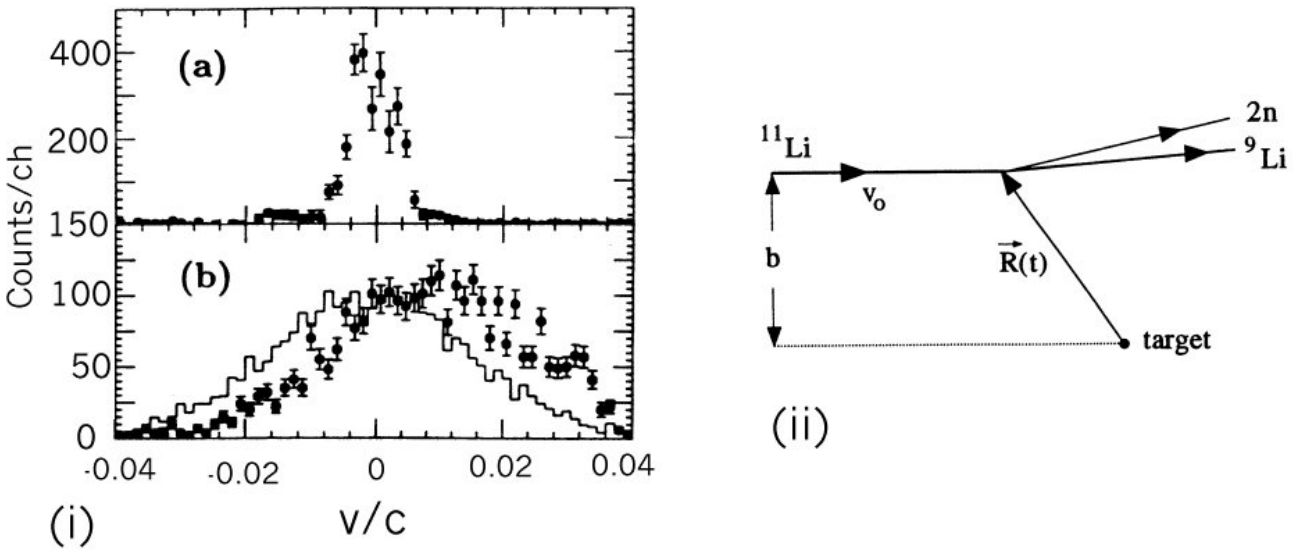

Figure 21: (i) (a) Spectrum of the longitudinal component of the center-of-mass velocity of ^{9}Li and two neutrons in the frame of the incident ^{11}Li. (b) Spectrum of the longitudinal component of the relative velocity V_9 - V_{2n}. The histogram shows the result of a Monte Carlo simulation assuming no Coulomb acceleration effects. (ii) Schematic representation of the breakup of ^{11}Li projectiles.

One has

$$< E_x > (b) = \frac{\int_{S_{2n}}^{\infty} dE_x \; E_x \; dP/dE_x}{\int_{S_{2n}}^{\infty} dE_x \; dP/dE_x} \tag{297}$$

$$\frac{dP}{dE_x} = \frac{N_{E_1}(E_x, b)}{E_x} \sigma_\gamma(E_x) \tag{298}$$

For small impact parameters such that $E_x b/\gamma\hbar v << 1$,

$$n_{E1}(E_x, b) = \frac{Z_T^2 \alpha}{\pi^2} (\frac{E_x}{\gamma\hbar v})^2 (\frac{c}{v})^2 \left[K_1^2(x) + \frac{1}{\gamma^2} K_0^2(x) \right] \tag{299}$$

$$\cong \frac{Z_{\tau^2}^2 \alpha}{\pi^2} \frac{1}{b^2} (\frac{c}{v})^2$$

is roughly independent of E_x, so that

$$< E_x > \cong \frac{\int_{S_{2n}}^{\infty} dE_x \; \sigma_\gamma(E_x)}{\int_{S_{2n}}^{\infty} dE_x \; \sigma_\gamma(E_x)/E_x}. \tag{300}$$

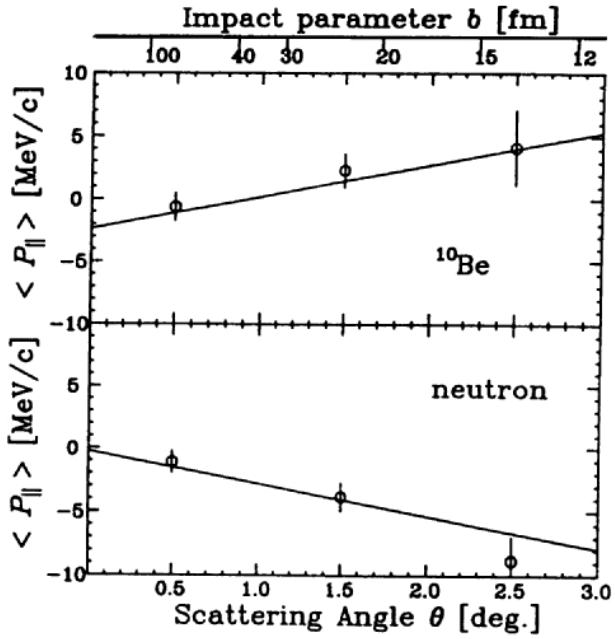

Figure 22: Coulomb reacceleration of ^{10}Be fragments originated from the break-up of 72 MeV/nucleon ^{11}Be projectiles on lead. Data are from [56].The longitudinal momentum $\Delta p_{//}$ is plotted against the scattering angle $\theta(b \sim c_1 + c_2/\theta)$. The theory [69] is shown by curves.

Using Eq. 300 and the definitions of $\sigma_\gamma(E_x)$ given by Eq. 223 we find that

$$\begin{aligned} < E_x > &\cong \frac{\int_{2n}^{\infty} dE_x (E_x - S_{2n})^{3/2}/E_x^3}{\int_{2n}^{\infty} dE_x (E_x - S_{2n})^{3/2}/E_x^4} \\ &= 6S_{2n} \cong 1.8 \text{ MeV}. \end{aligned} \tag{301}$$

At large impact parameters $< E_x >$ will be smaller than this value, monotonically decreasing.

This model has been used by Nakamura et al. [56] in the analysis of the Coulomb reacceleration of ^{10}Be fragments originated from the break-up of 72 MeV/nucleon ^{11}Be projectiles on lead. In this case, the quantities derived above where rewritten in terms of the longitudinal momentum $\Delta p_{//}$ and scattering angle $\theta(b \sim c_1 + c_2/\theta)$. A comparison with his data is given in Fig. 22.

The agreement with the theory of Ref. [69] is good, despite its simplicity.

Another interesting point is to know if the reacceleration effect would influence the decay spectrum. If we rely on Eqs. 295 and 296 and neglect the first terms of both equations we obtain that the relative energy between the fragments is distorted by the reacceleration effect by an amount given by $(a = b + c)$

$$\Delta E_{rel} = \frac{1}{2}\mu_{bc}(v_b - v_c)^2 \cong \frac{1}{4}\frac{m_a}{\mu_{bc}}\frac{(\Delta E)^2}{E_{lab}}. \tag{302}$$

This yields a distortion of order of 100 keV in the spectrum of the relative energy of the fragments, at small impact parameters. Averaging over impact parameters this distortion is of order of 20 keV, which is quite small. Thus, while the spectrum might be distorted, the average relative energy is not much affected.

0.21 Dynamical breakup model in a coupled-channels approach

One should expect that perturbation theory fails in describing the breakup process when the cross sections attain very high values. In fact, as we show later in this Section, the break-up Coulomb probability of weakly-bound nuclei calculated with first-order perturbation theory is close to unity. This can be understood with use of simple arguments. The energy transferred by the Coulomb field to the excitation of a projectile nucleus, with N neutrons and Z protons, incident with velocity v on a target nucleus with charge eZ_T at an impact parameter b is approximately given by [49, 73, 55] $E^* = 2(NZ/A)(Z_T e^2)^2/m_N b^2 v^2$, where m_N is the nucleon mass. For ^{11}Be projectiles ($N = 7,\ Z = 4$) incident on lead at $b = 15$ fm and $v \approx 0.5c$, one gets $E^* \approx 1$ MeV. This energy is more than sufficient to break ^{11}Be apart, since the separation energy a neutron from this nucleus is about 0.5 MeV. This means that, at small impact parameters the break-up probability is of order of unity and a non-perturbative treatment of the break-up process should be carried out.

0.21.1 Coulomb break-up of loosely-bound clusters

Let us consider a projectile nucleus composed of two clusters with charges eZ_b and eZ_c, and masses m_b and m_c, respectively, incident on a target with charge eZ_T. We assume that the projectile follows a straight-line trajectory with velocity v and impact parameter b. In the dipole approximation, the interaction potential (neglecting magnetic interactions and nuclear forces) responsible for the break-up of the projectile, is given by

$$\begin{aligned} V &= \frac{\gamma Z_T e^2}{(b^2+\gamma^2 v^2 t^2)^{3/2}} \sum_{k=b,c} Z_k (b y_k + \gamma v t z_k) = \sqrt{\frac{2\pi}{3}}\, \frac{\gamma Z_T e^2}{(b^2+\gamma^2 v^2 t^2)^{3/2}} \\ &\quad (Z_b \frac{m_c}{m_a} - Z_c \frac{m_b}{m_a}) r \, \left\{ i b \left[Y_{11}(\hat{\mathbf{r}}) + Y_{1-1}(\hat{\mathbf{r}}) \right] + \sqrt{2}\, \gamma\, v\, t\, Y_{10}(\hat{\mathbf{r}}) \right\}, \end{aligned} \tag{303}$$

where $\gamma = (1 - v^2/c^2)^{-1/2}$, and y_k, z_k represent the transverse and longitudinal coordinates of the particles, respectively. $\mathbf{r}$ is the vector from b to c and $m_a = m_b + m_c$. The first (second) term inside the curly brackets represents the transverse (longitudinal) part of the interaction. It is important to notice that the longitudinal part of the interaction has been modified to account for the current-interaction which is very important at relativistic energies. The modification amounts in replacing γ^2 by γ in the term proportional to vt in Eq. 303. This mocks up the effect of the current-interaction and reproduces the correct expression for the $E1$ excitation amplitude to first-order.

In first-order time-dependent perturbation theory, the probability amplitude for the projectile break-up, i.e., the transition from the ground state $\mid 0 >$ to a state $\mid \mathbf{q} >$ in the continuum is given by

$$a^{(1)}_{(\mathbf{q})} = \frac{1}{i\hbar} \int_{-\infty}^{t} e^{-iE_0 - E_q)t'/\hbar} < \mathbf{q}|V(t')|0 > \, dt'. \tag{304}$$

For loosely-bound projectiles the ground state can be represented by an Yukawa wavefunction given by Eq. 238. Neglecting final state interactions, the states $|\mathbf{q} >$ are given by $\phi_{\mathbf{q}}(\mathbf{r}) =< \mathbf{r}|\mathbf{q} >= e^{i\mathbf{q}.\mathbf{r}} + e^{iqr}/r(\eta + iq)$, where the wave number q is related to the energy E_q as $E_q = \hbar^2 q^2/2\mu_{bc}$. The second term of $< \mathbf{r}|\mathbf{q} >$ guarantees the orthogonality and completeness of the initial and final states.

The dipole matrix elements are given by [49]

$$< \mathbf{q}|rY_{1m}(\hat{\mathbf{r}})|0 >= i\ 4\ N_0\sqrt{2\pi\eta}\ \frac{q}{(q^2+\eta^2)^2}\ Y_{1m}(\mathbf{q}). \tag{305}$$

To first order, the breakup probability is obtained by integrating the square modulus of 304 over the density of final states, i.e.,

$$P^{(1)}(b,t) = 2P^{(1)}_{m=1} + P^{(1)}_{m=0} = \int |a^{(1)}_{(\mathbf{q})}|^2\ \frac{d^3q}{(2\pi)^3}, \tag{306}$$

summed over the beam-axis components of the angular momentum carried by the Coulomb field, $m = 0,\ \pm 1$. The integral over q is easily accomplished if one uses the sudden approximation, which is valid for

$$\frac{b}{\gamma v}\ (E_q + B) \ll 1. \tag{307}$$

For weakly-bound nuclei, as ^{11}Be, $E_q + B \approx 1$ MeV, and at bombarding energies $E_{Lab} \sim 1$ GeV, the above relation shows that the sudden approximation is valid for impact parameters $b < 300$ fm.

Within the sudden approximation we can omit the exponential factor in 304 and the integrals can be evaluated analytically as (α is the fine structure constant)

$$\begin{aligned} P^{(1)}(b,\ t) \ &= \ \frac{1}{6}\ \left(\frac{Z_T\alpha c}{\eta b v}\right)^2\ \left(Z_b\ \frac{m_c}{m_a} - Z_c\ \frac{m_b}{m_a}\right)^2 N_0^2 \\ &\times \left\{ \left[1 + \frac{\gamma v t/b}{\sqrt{1+(\gamma v t/b)^2}}\right]^2 + \frac{1}{1+(\gamma v t/b)^2} \right\}. \end{aligned} \tag{308}$$

The first (second) term inside the curly brackets arises from the transverse (longitudinal) part of the interaction potential 303. It is clear that only the transverse contribution survives at $t = \infty$. The longitudinal contribution cancels since the component of the electric field along the beam axis is an odd function of time. The breakup probability at $t = \infty$ is given by

$$P^{(1)}(b,\ \infty) = \frac{2}{3}\ \left(\frac{Z_T\alpha c}{\eta\, b\, v}\right)^2\ \left(Z_b\ \frac{m_c}{m_a} - Z_c\ \frac{m_b}{m_a}\right)^2\ N_0^2. \tag{309}$$

For grazing collisions with heavy targets at high energies the breakup probabilities of Eq. 309 are close to (or even exceeds) unity for halo nuclei incident on heavy targets. Therefore, first-order perturbation theory cannot be used. However, if the sudden approximation holds a non-perturbative closed expression can still be derived to all orders. The amplitude can then be written as [neglecting the longitudinal component of the interaction potential, Eq. 303]

$$a_{(\mathbf{q})}^{(S)} =< \mathbf{q}| \exp\left\{\frac{1}{i\hbar}\int_{-\infty}^{\infty} V(t)dt\right\}|0> =< \mathbf{q}| \exp\left\{-i\mathcal{C}r\sin\theta\sin\phi\right\}|0> , \tag{310}$$

where

$$\mathcal{C} = \frac{2Z_T\alpha c}{bv}\left(Z_b\,\frac{m_c}{m_a} - Z_c\,\frac{m_b}{m_a}\right). \tag{311}$$

Using the completeness relation

$$\phi_0(\mathbf{r})\;\phi_0^*(\mathbf{r}') + \frac{1}{(2\pi)^3}\int \phi_{\mathbf{q}}^*(\mathbf{r})\;\phi_{\mathbf{q}}(\mathbf{r}')\,d^3q = \delta(\mathbf{r}-\mathbf{r}') \tag{312}$$

one finds

$$P^{(S)}(b) = \int |a_{(\mathbf{q})}^{(S)}|^2\;\frac{d^3q}{(2\pi)^3} = 1 - \frac{\eta^2N_0^2}{4\pi^2}\left|\int d^3r\frac{e^{-2\eta r}}{r^2}\;e^{-i\mathcal{C}r\sin\theta\sin\phi}\right|^2. \tag{313}$$

The above integral can be easily evaluated and the result is

$$P^{(S)}(b) = 1 - \frac{4\eta^2N_0^2}{\mathcal{C}^2}\;\left[\arctan(\frac{\mathcal{C}}{2\eta})\right]^2. \tag{314}$$

When $\mathcal{C}/2\eta \ll 1$ (large impact parameters) the above relation reproduces the first-order result 309. If on the other hand $\mathcal{C}/\eta$ is large one gets, to lowest order in $\eta/\mathcal{C}$,

$$P^{(S)}(b) = 1 - \frac{\pi^2\eta^2N_0^2}{\mathcal{C}^2}. \tag{315}$$

For the reaction $^{11}\mathrm{Li} + \mathrm{Pb} \longrightarrow {}^{9}\mathrm{Li} + 2\mathrm{n} + \mathrm{Pb}$ at 100 MeV/nucleon, with an impact parameter of 13 fm, the sudden approximation yields $P^{(S)}(b) \simeq 0.4$, while in first-order perturbation theory we get $P^{(1)}(b,\ \infty) \simeq 0.7$. Thus, first-order approximation fails at small impact parameters.

The results of Eqs. 308, 309 and 314 were obtained on the basis of the sudden approximation. In the example considered, the ^{11}Li break-up probability is appreciable even for large relative energies in the projectile frame ($E_q \sim 2$ MeV), where the sudden approximation starts to break-down. In addition, the treatment of this Section cannot account for the energy distribution of the break-up cross section. A more powerful coupled-channels treatment is therefore desirable. However, one faces the difficulty that the final states are in the continuum (one would have to consider a continuous channel label) and the coupling matrix elements present divergency problems, caused by the non-localized behavior of the continuum wavefunctions. This difficulty is avoided by a discretization of the continuum along the lines proposed by Bär and Soff [76] in their non-perturbative calculations of atomic ionization by heavy ions. In the next Section we use a similar treatment of the continuum developed by Bertulani and Canto [74]. The method is a useful starting point to understand the main features of a coupled-channels calculation with states in the continuum.

0.21.2 Discretization of the continuum and semiclassical treatment of the coupled-channels problem

Our basis of time-dependent discrete states are defined as

$$|\phi_0\rangle = e^{-iE_0 t/\hbar}\,|0\rangle\,, \quad \text{with } E_0 = -B \quad \text{and} \quad |\phi_{j\ell m}\rangle = e^{-iE_j t/\hbar}\int \Gamma_j(E)\ |E,\ell m\rangle \tag{316}$$

where $|E,\ell m>$ are continuum wavefunctions of the projectile fragments (without the interaction with the target), with good energy and angular momentum quantum numbers E, ℓ, m. The functions $\Gamma_j(E)$ are assumed to be strongly peaked around an energy E_j in the continuum. Therefore, the discrete character of the states $|\phi_{j\ell m}>$ (together with $|\phi_0>$) allows an easy implementation of the coupled-states calculations. We assume that the projectile has no bound excited states. This assumption is often the rule for very loosely-bound systems. The orthogonality of the discrete states 316 is guaranteed if

$$\int dE\ \Gamma_i(E)\ \Gamma_j(E) = \delta_{ij}. \tag{317}$$

For the continuum set $|E\ell m>$ we use, for the sake of simplicity, the plane wave basis

$$<\mathbf{r}|E\ell m> = u_{\ell,\,E}(r)\,Y_{\ell m}(\mathbf{r}) = \left(\frac{2\mu}{\hbar^2}\right)^{3/4}\ \frac{E^{1/4}}{\sqrt{\pi}}\ j_\ell(qr)\ Y_{\ell m}(\hat{\mathbf{r}}) \tag{318}$$

which obey the normalization condition ($E = \hbar^2 q^2/2\mu$)

$$<E\ell m|E'\ell' m'> = \delta_{\ell\ell'}\delta_{mm'}\delta(E-E'). \tag{319}$$

These states arise from the partial wave expansion of the plane wave $\exp(i\mathbf{q}.\mathbf{r})$. Writing the time-dependent Schrödinger equation for $\Psi(t) = \sum_{j\ell m} a_{j\ell m}\,\phi_{j\ell m}$, taking the scalar product with the basis states and using orthonormality relations, we get the equations

$$i\hbar\frac{da_{j\ell m}}{dt} = \sum_{j'\ell' m'} V_{j\ell m;j'\ell' m'}\ a_{j'\ell' m'}\ e^{-i(E'_j-E_j)t/\hbar}. \tag{320}$$

We use the index $j=0$ for the ground state $|0>$ and $j=1,2,\ldots$ for the discrete continuum states. $V_{j\ell m;j'\ell' m'}$ are the matrix elements $<\phi_{j\ell m}|V|\phi_{j'\ell' m'}>$.

For $\Gamma_j(E)$ we consider two different sets of functions. Firstly the set $\Gamma_1(E),\ldots\ ,\Gamma_N(E)$;

$$\Gamma_j(E) = \frac{1}{\sqrt{\sigma}}\,, \quad \text{for } (j-1)\sigma < E < j\sigma, \text{ and } \quad \Gamma_j(E) = 0\,, \qquad \text{otherwise.} \tag{321}$$

This set corresponds to histograms of constant height $1/\sqrt{\sigma}$ and width σ. The states $\Gamma_j(E)$ trivially satisfy the orthonormalization condition of Eq. 317. They present the advantage of leading to simple analytical expressions for the coupling matrix elements. On the other hand they have discontinuities at the edges, which lead to numerical difficulties. The second set consists of the functions

$$\chi_j(E) = N_{n_j}\ \left(\frac{E}{\sigma}\right)^{n_j^2}\ e^{-n_j(E/\sigma)}. \tag{322}$$

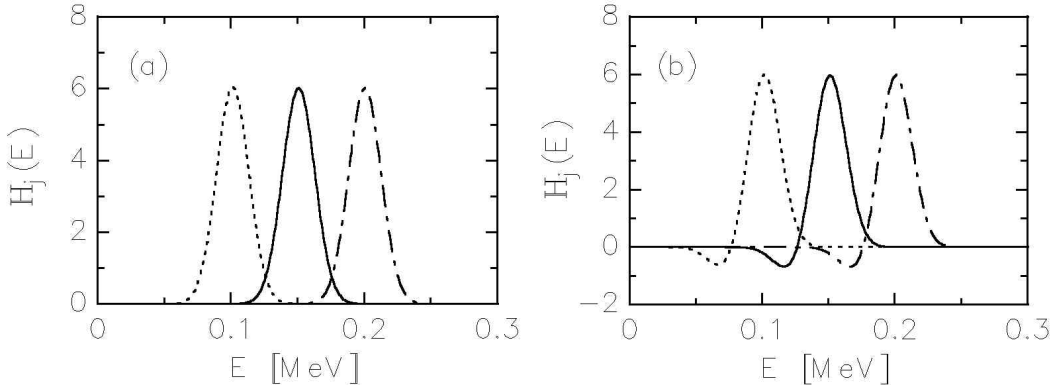

Figure 23: A set of functions given by the expression 322 of text, before (a) and after (b) orthogonalization.

The normalization constant

$$N_{n_j} = \frac{1}{\sqrt{\sigma}} \left[\frac{(2n_j)^{2n_j^2+1}}{(2n_j^2)!} \right]^{1/2}, \tag{323}$$

guarantees that $\int \chi_j(E)\,\chi_j(E)\,dE = 1$. The functions χ_j are peaked at $E = n_j\,\sigma$ and have width $\approx \sigma$. The integer $n_j = K.j$ is proportional to the index-j and the proportionality constant, a small integer K, is a parameter of the set which determines the overlap of two consecutive functions χ_j and χ_{j+1}. Three consecutive functions χ_4, χ_5 and χ_6 are shown in Fig. 23(a) for $K = 3$ and $\sigma = 40/3$ keV. With this choice χ_5 is peaked at the maximum of the experimental break-up cross-section ($E \approx 250$ keV) of ^{11}Li projectiles. However, this set fails to satisfy the orthogonality condition of Eq. 320. This shortcoming can be fixed by the definition of a new set $\Gamma_j(E)$ of linear combinations

$$\Gamma_j(E) = \sum_{k=1}^{N} C_{jk}\,\chi_k(E), \tag{324}$$

with the coefficients C_{ij} determined so that the resulting combinations be orthogonal. These coefficients can be found by means of an orthogonalization procedure as, e.g., the *Gram-Schmidt method* [75]. The result of the application of this method to the functions of Fig. 23(a) is shown in Fig. 23(b). The set of Eq. 324 has the advantages of being continuously derivable and of leading to reasonably simple coupling matrix elements.

A comparison between basis states $\phi_{j\ell m}(r)$ generated with each of these sets [through Eq. 316] is made in Figs. 24(a) and 24(b). We chose for convenience the parameters $\sigma = 40$ keV, $j = 5$ for the first set (Eq. 321) and $K = 3$, $j = 5$, $\sigma = 13.3$ keV for the second set (Eq. 322). With this choice one of the E_j is equal to 200 keV for both sets. We take $\ell = 1$, $m = 1$, as example. One observes that the discrete wavefunctions $\phi_{j\ell m}$ decrease rapidly enough with r, so that the matrix elements $< \phi_{j\ell m}|rY_{1\mu}|\phi_{j'\ell'm'} >$ are finite. The use of the histograms 321 for $\Gamma_j(E)$ leads to beats in $\phi_{j\ell m}$ as displayed in Fig. 24(a). These beats are the result of the discontinuous nature of $\Gamma_j(E)$ and

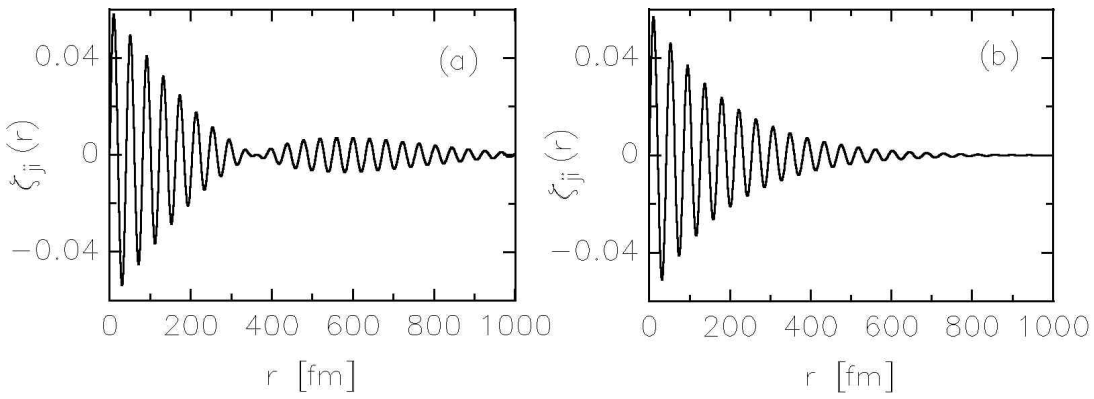

Figure 24: Radial wave functions for the discretized continuum using the histogram set (a) and the continuous set (b). We used $E_j = 200\ keV$, and $\ell = 1$.

arise from the interference from the borders of the histograms. Due to this behavior, the numerical evaluation of $< \phi_{j\ell m}|rY_{1\mu}|\phi_{j'\ell'm'} >$ is more involved than with the second set of Γ_j-functions, 324. Indeed, as we see from Fig. 24(b) the beats disappear with the use of the basis set 324. Although the use of plane-wave basis allows the derivation of simple results with both sets, this fact is of relevance for improved coupled-channels calculations in the continuum.

Using 316 and the properties of the spherical harmonics one finds

$$V_{j\ell m;j'\ell'm'} = \frac{(-1)^m}{\sqrt{2}}\gamma Z_T e^2 \left(Z_c\,\frac{m_b}{m_a} - Z_b\,\frac{m_c}{m_a}\right) \frac{\sqrt{(2\ell+1)(2\ell'+1)}}{(b^2+\gamma^2v^2t^2)^{3/2}} \begin{pmatrix} \\ \ell 0\,1\,0\,\ell' 0 \end{pmatrix}$$
$$\times \quad \left\{ ib\left[\begin{pmatrix} \\ \ell -m\,1\,1\,\ell' m' \end{pmatrix} + \begin{pmatrix} \\ \ell -m\,1 -1\,\ell' m' \end{pmatrix}\right] + \sqrt{2}\,\gamma vt \begin{pmatrix} \\ \ell -m\,1\,0\,\ell' m' \end{pmatrix}\right\} I_{j\ell;j'\ell'} \quad (325)$$

where

$$I_{j\ell;j'\ell'} = \int r^3 dr \int dE\ \Gamma_j(E) \int dE'\ \Gamma_{j'}(E')\ u^*_{\ell,\,E}(r) u_{\ell',\,E'}(r). \quad (326)$$

From 325 one deduces that the interaction potential is different from zero only if $|\ell - \ell'| = 1$, as expected.

The use of the plane wave basis is especially useful because, exploiting the recursion and closure relations of the spherical Bessel functions, one obtains the general result

$$I_{j\ell;j'\ell'} = \frac{\hbar^2}{\mu}\ \left\{ \frac{\ell+\ell'+2}{2}\ F_{jj'} + \delta_{\ell,\ell'+1}\,G_{j,j'} + \delta_{\ell+1,\ell'}\,G_{j'j} \right\}, \quad (327)$$

where

$$F_{jj'} = \int dq\ \Gamma_j(E)\ \Gamma_{j'}(E) \qquad G_{jj'} = \int dq\ q\ \Gamma_j(E)\ \frac{d}{dq}\Gamma_{j'}(E) \quad (328)$$

with $E = \hbar^2 q^2/2\mu$. Explicit forms can be found for each basis set:

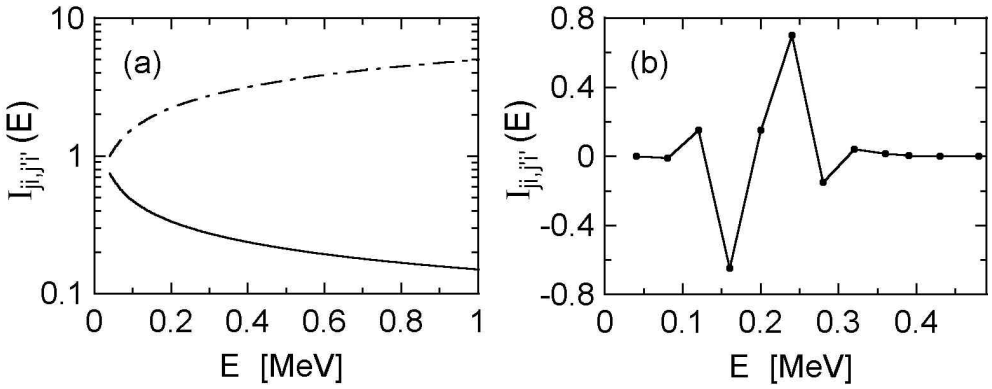

Figure 25: (a) Radial matrix elements, Eqs. 325 and 326 for the transition $j \to j+1$ (dashed-line), and for the $j \to j$ one (solid line). We used $\ell = 0$ and $\ell' = 1$. (b) Radial matrix elements for the transition $j \to j'$, keeping $E_j = 200$ keV and varying $E_{j'}$.

(a) Histogram - Applying this relation to the histogram set 321, one can show that for $j,\ j' \neq 0$

$$I_{j\ell;j'\ell'} = \hbar\sqrt{\frac{2}{\mu\sigma}} \begin{cases} \frac{\ell+\ell'+1}{2}\ \left[\sqrt{j}-\sqrt{j-1}\right] & \text{if} \quad j = j' \\ -(-1)^{(j+\ell-j'-\ell')/2}\sqrt{\frac{j+j'-1}{2}} & \text{if} \quad |j-j'| = 1 \\ 0 \quad \text{otherwise.} \end{cases} \tag{329}$$

For $j = 0$ or $j' = 0$, only the integral with ℓ, or $\ell' = 1$ is necessary, and the result is

$$I_{00;\,j1} = I_{j1;\,00} = \frac{\sqrt{2\eta\sigma}}{\pi}\ \frac{E_j^{3/4}}{(E_0+E_j)^2}\ \left(\frac{\hbar^2}{2\mu}\right)^{3/4} \tag{330}$$

where $E_j = (j-1/2)\,\sigma$.

(b) Continuous basis - For the set of continuous energy functions 324 one finds, for $j,\ j' \neq 0$

$$\left\{ \begin{array}{c} F_{jj'} \\ G_{jj'} \end{array} \right\} = \sqrt{\frac{\mu\sigma}{2\hbar^2}} \sum_{n,n'} C_{jn}\, C_{j'n'} N_n\, N_{n'} \frac{\Gamma(n^2+n'^2+1/2)}{(n+n')^{n^2+n'^2+1/2}} \left\{ \begin{array}{c} 1 \\ 2n'^2 - \frac{n'(2n^2+2n'^2+1)}{n+n'} \end{array} \right\} \tag{331}$$

where $\Gamma(z)$ is the gamma-function and we simplified the notation using $n \equiv n_j$. For $j = 0$, or $j' = 0$, one finds

$$I_{00;\,j1} = I_{j1;\,00} = \frac{\sqrt{2\eta\sigma}}{\pi}\ \frac{E_j^{3/4}}{(E_0+E_j)^2}\ \left(\frac{\hbar^2}{2\mu}\right)^{3/4} \sum_n \frac{n^2!}{n^{n^2+1}} \sqrt{\frac{(2n)^{2n^2+1}}{(2n^2)!}}\, C_{jn}\,. \tag{332}$$

As we have seen above, the use of the plane wave basis 318 results in the elegant derivation of $I_{j\ell;\,j'\ell'}$ presented by Eqs. 327 and 328. Nonetheless, the s-wave ($\ell = 0$) state of Eq. 318 is not

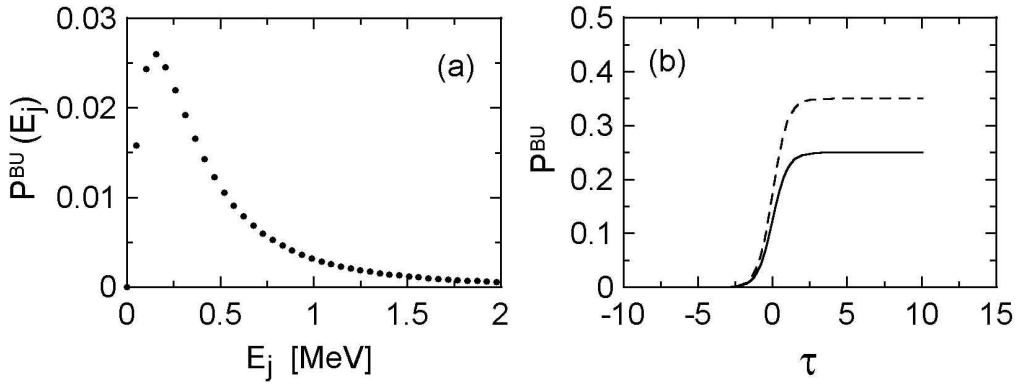

Figure 26: (a) Coulomb break-up probability, per unit energy interval (MeV^{-1}), of ^{11}Li projectiles incident on lead at 100 MeV/nucleon and $b = 15$ fm, as a function of the final total kinetic energy of the fragments. (b) Breakup probability as a function of the time, $\tau = vt/c$.

orthogonal to the bound-state wave function. To restore orthogonality one has to add an extra piece to this function. One expects however that this approximation does not affect the results appreciably since to access this state one needs at least two transitions: the $0 \to j1$ followed by the $j'1 \to j'0$ one. But the later transition competes with the transition to the ground state, $j1 \to 00$, which is the dominant one. A more severe restriction is the use of plane waves to describe the continuum. A realistic calculation would have to use outgoing waves for $u^{(+)}_{\ell,\,E}(r)$ which would carry information about the final state interactions of the $(b + c)$-system.

0.21.3 Application to the breakup of ^{11}Li

Let us consider the break-up of ^{11}Li-projectiles incident on heavy targets at energies around 100 MeV/nucleon. In Figure 25 we show the integrals $I_{jl;j'l'}$ for the continuum-continuum coupling $(j, j' \neq 0)$. In particular we choose $\ell = 0$ and $\ell = 1$. The coupling $j0 \to j' = j, 1$, shown in Fig. 25(a) ($\ell = 0$ to $\ell = 1$ in this case) of the state. In Figure 25(a) we plot $I_{j0;j'1}$ for a transition between states with different energies. In particular we take the transition between neighboring states, with $j' = j + 1$. Using the results obtained with the continuous energy set, Eqs. 331 and 332. One observes that while the integral for the jj-coupling decreases with energy, the one for the $j, j + 1$-coupling increases steadily. These results reproduce the trend shown by Eq. 329. In Figure 25(b) it is shown how $I_{j0;j'1}$ varies as a function of E'_j, for a fixed $E_j = 0.2$ MeV. One observes that it is maximum for neighboring energy states and has an oscillatory behavior. This has as a consequence that the $j, j' \neq j$-coupling will practically not contribute to the total break-up probability, $P^{BU}_{(E)}$, since its contribution will be washed out.

The break-up probability per unit energy interval, $P^{BU}_{(E)}$, is given by

$$P^{BU}_{(E)} = \sum_{ij} \Gamma_i(E)\, \Gamma_j(E)\, Q_{ij} \tag{333}$$

where

$$Q_{ij} = \mathcal{R}e \left[\sum_{\ell m} a^*_{i\ell m}\, a_{j\ell m} \right] . \tag{334}$$

In Figure 26(a) we show the break-up probability per unit energy interval for the reaction ^{11}Li + Pb at 100 MeV/nucleon and $b = 15$ fm, calculated from Eq. 333 by solving the coupled-differential Eqs. 320 for $a_{i\ell m}$. We see that the energy distribution of the fragments is peaked at $E \sim 0.25$ MeV. Therefore, the most relevant momentum transfer to the ^{11}Li nucleus occurs at $q = \sqrt{2\mu_{bc}B}/\hbar \sim 20$ fm^{-1}.

The validity of the dipole approximation for the interaction potential 325 to calculate the continuum-continuum coupling can only be justified for $qr \ll 1$. But, as shown in Fig. 24, the discretized wavefunctions extend up to 400 fm. Thus, unless the matrix elements for the continuum-continuum coupling, Eq. 326, have its main contribution from $r \ll 20$fm, the dipole approximation is not valid. The jj-coupling do satisfy this requirement. In this case the wave functions have equal energies, but different angular momenta. This causes an asymptotically ($r \gg 1/q$) constant phase difference between the wave functions entering in $I_{jl;jl'}$. This leads to cancellations in the integrand of Eq. 326 for large r. The situation is different for the $(j, j' \neq j)$-coupling. In this case the integrand has contributions from larger values of r and these contributions increase with the energy. With a correct treatment of the multipole expansion of the interaction potential 303 the integrals $I_{j\ell;j'\neq j,\ell'}$ would decrease with E. We expect that the transitions between $00 \to j', \ell = 1$ and $j', \ell = 1 \to 00$ dominate the excitation process, so that the matrix elements between states with $j \neq j' \neq 0$ do not play an important role. Also, to minimize the consequence of the breaking down the dipole approximation in the continuum-continuum coupling at $j \neq j'$, one can use a large parameter K (e.g., here $K = 4$ was used). This leads to small $I_{j\neq j'}$.

In Figure 26(b) the solid line represents P^{BU}, the total breakup probability [Eq. 333 integrated over energy], as a function of the adimensional parameter $\tau = vt/b$, for $b = 15$ fm. This is obtained by solving the coupled-channels Eqs. 320 for a time t and calculating the sum $P^{BU}(t) = \sum_{j\ell m} |a_{j\ell m}|^2$. The dashed-line corresponds to the neglect of all transitions, except for the $0 \to j\ell$ ones. In the low energy limit, Eq. 307, this gives the same result as Eq. 307. The solid-line includes all possible transitions. The break-up probability occurs in a time scale of $\Delta t \sim b/v$. As $t \to \infty$ the break-up probability is 40% smaller than that calculated by first order perturbation theory.

Improvements of the model described in this Section have been done in Refs. [77, 78].

0.21.4 Dynamical breakup model in space-time lattice

In order to obtain the spectrum of relative energy of the fragments, a non-perturbative solution of the Schrödinger equation is necessary. Such a solution would include the effects of reacceleration

properly. First studies using this procedure has been performed by Bertsch, Bertulani and Esbensen [70, 71, 72]. One assumes a potential model for the halo nucleus. For example, a Woods-Saxon potential may be used for the nuclear interaction of the n $+^{10}$ Be, p $+^{7}$ Be or (2n) $+^{9}$ Li systems. In the last case a dineutron model is assumed. To this potential a time-dependent non-relativistic Coulomb interaction is added,

$$V_{coul} = Z_\tau e^2 [\frac{Z_c}{\mid \mathbf{r}_c - \mathbf{R}(t) \mid} + \frac{Z_x}{\mid \mathbf{r}_x - \mathbf{R}(t) \mid} - \frac{Z_a}{R(t)}] \tag{335}$$

where $a = c + x$ is the projectile, $\mathbf{r}_c = -\mathbf{r}A_x/A_a$, and $\mathbf{r}_c = \mathbf{r}(1 - A_x/A_a)$.

The potential above can be expanded into multipoles. Normally, the dipole part of the expansion is the most relevant one. The time dependent wavefunction for the relative motion of $c + x$ is given by

$$\Psi(\mathbf{r}, t) = \frac{1}{r} \sum_{\ell m} u_{\ell m}(r, t) Y_{\ell m}(\widehat{\mathbf{r}}). \tag{(3.9)}$$

Inserting this expansion in the Schrödinger equation and retaining only the dipole expansion of the potential 335 we get

$$\left[\frac{d^2}{dr^2} - \frac{\ell(\ell+1)}{r^2} - \frac{2\mu_{cx}}{\hbar} V_N(r)\right] u_{\ell m}(r, t) + \sum_{\ell' m'} S^{(\ell m)}_{\ell' m'} u_{\ell' m'}(r, t) = -\frac{2\mu_{cx}}{\hbar} \frac{\partial u_{\ell m}}{\partial t} \tag{336}$$

where

$$S^{(\ell m)}_{\ell' m'} = -\frac{2\mu_{cx}}{\hbar} \frac{(-1)^m}{\sqrt{2}} \left[b^2 + v^2 t^2\right]^{-3/2} \sqrt{(2\ell+1)(2\ell'+1)} \begin{pmatrix} \ell & 1 & \ell' \\ 0 & 0 & 0 \end{pmatrix}$$
$$\times \quad \left\{ ib \left[\begin{pmatrix} \ell & 1 & \ell' \\ -m & 1 & -m' \end{pmatrix} + \begin{pmatrix} \ell & 1 & \ell' \\ -m & -1 & -m' \end{pmatrix} \right] + \sqrt{2} vt \begin{pmatrix} \ell & 1 & \ell' \\ -m & 0 & -m' \end{pmatrix} \right\} r. \tag{337}$$

This equation can be solved by a finite difference method. A truncation on the ℓ, m values is needed. Only a few angular momentum states are needed (e.g., up to $\ell = 5$). Denoting $\alpha \equiv (\ell, m)$, the wave function u_α at time $t + \Delta t$ is obtained from the wave function at time t, according to the algorithm [70]

$$u_\alpha(t + \Delta t) = \left[\frac{1}{i\tau} - \Delta^{(2)} + \frac{\Delta t}{2\hbar\tau} V_\alpha\right]^{-1} \left[\frac{1}{i\tau} + \Delta^{(2)} - \frac{\Delta t}{2\hbar\tau} V_\alpha + \frac{\Delta t}{\hbar\tau}\, \widehat{S}\right] u_\alpha(t). \tag{338}$$

In this equation $\tau = \hbar \Delta t / 4\mu_{bx} (\Delta r)^2$ and $\widehat{S} u_\alpha(t) = \sum\limits_{\alpha'} S^{(\alpha)}_{\alpha'} u_{\alpha'}(t)$. Also,

$$V_\alpha(r) = V_N(r) + \frac{\hbar^2 \ell(\ell+1)}{2\mu_{bc} r^2}. \tag{339}$$

The wave functions $u_\alpha(r, t)$ are discretized in a mesh in space, with a mesh-size Δr. The second difference operator $\Delta^{(2)}$ is defined as

$$\Delta^{(2)} u^{(j)}_\alpha = u^{(j+1)}_\alpha(t) + u^{(j-1)}_\alpha(t) - 2u^{(j)}_\alpha(t), \quad \text{with} \;\; u^{(j)}_\alpha \equiv u_\alpha(r_j, t). \tag{340}$$

The 1^{st} operation on the right side of Eq. 338 is trivial. The second one needs special attention (see Supplement C).

The wave function calculated numerically at a very large time will not be influenced by the Coulomb field. The numerical integration can be stopped there. The continuum part of the wave function is extracted by means of the relation (and normalized to unity)

$$\Psi_c(\mathbf{r},t) = [\Psi - \Psi_{gs} < \Psi_{gs} \mid \Psi >] \ \left[1 - |< \Psi_{gs} \mid \Psi >|^2\right]^{-1/2} \tag{341}$$

where Ψ_{gs} is the initial wave function.

This wave function can be projected onto continuum eigenstates of the potential $V_N(r)$ in order to obtain the excitation probability of that state. For illustration lets us use the simplifying assumption that the final states are plane waves. A projection onto these states is equivalent to a Fourier transform of the time dependent wave function. One gets

$$\Psi_c(\mathbf{p}) = \sum_{\ell m} C_{\ell m}(p) Y_{\ell m}(\widehat{\mathbf{p}}) \tag{342}$$

where

$$C_{\ell m}(p) = \sqrt{\frac{2}{\pi}}\, i^{\ell} \int dr\ r\ j_{\ell}(pr) u^{(c)}_{\ell m}(r,t) \tag{343}$$

where j_ℓ is the spherical Bessel function. The probability density for an excitation to a final state with energy E is

$$P(b,E,\Omega) = \frac{1}{2}\left(\frac{2\mu bx}{\hbar^2}\right)^{3/2} \sqrt{E} \mid \Psi_c(\widehat{\mathbf{p}}) \mid^2 . \tag{344}$$

Integrating over Ω :

$$P(b,E) = \frac{1}{2}\left(\frac{2\mu_{bx}}{\hbar^2}\right)^{3/2} \sqrt{E} \sum_{\ell m} \mid C_{\ell m}(p) \mid^2 . \tag{345}$$

In first-order perturbation theory this spectrum would be given by

$$P^{(1)}(b,E) = \frac{4\pi}{9}\left(\frac{2Z_T e^2}{\hbar v}\right)^2 \left(\frac{E}{\hbar v}\right)^2 \ \frac{dB(E1)}{dE} \ \left[K_0^2(x) + K_1^2(x)\right] \tag{346}$$

where the $K's$ are the modified Bessel functions and $x = Eb/\hbar v$. In this case $dB(E1)/dE$ is calculated by using the ground state and continuum states of the same Woods-Saxon potential [4] for $c + x$. To illustrate, we show $P(b,E)$ for ^{8}B(^{7}Be, p)Pb at 50MeV/nucleon in Fig. 27(I). We see that at small impact parameter the coupling between the continuum states is stronger and the reacceleration changes appreciably the form of the spectrum. Due to the reacceleration effect higher order energy states are more populated than in the perturbative calculation.

What matters for experiments is the impact parameter integrated spectrum. From that we can calculate the average energy obtained by reacceleration. This is shown in Figure 27(II). The solid line is the result of the perturbative calculation. The dashed line is based on the semiclassical

[4] In the $p +^7 Be$ case a static Coulomb potential (for homogeneously charged sphere) is added to V_N.

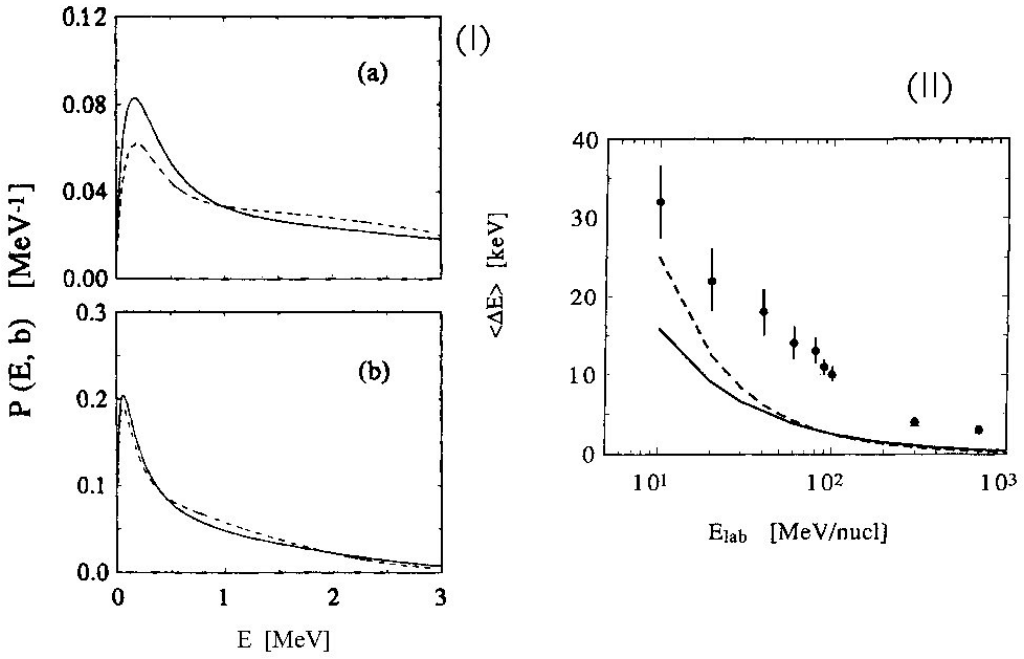

Figure 27: (I) Energy spectrum of the relative motion of p $+^7$ Be in first-order perturbation theory (solid line) and in the non-perturbative approach (dashed) at (a) $b = 15$ fm and (b) $b = 50$ fm. A ^{8}B$+$ ^{208}Pb collision at 50 MeV/nucleon is assumed. (II) Reacceleration energy gained by the fragments in the reaction ^{8}B(^{7}Be, p)Pb as a function of the bombarding energy. The solid line is a the perturbative calculation. The dashed line is based on semiclassical formulas, eqs. 295 - 298. The circles with error bars are the result of a Monte-Carlo classical simulation of the reacceleration energy averaged over impact parameter [79].

formulas, using Eqs. 295-298. The circles with error bars are the result of a Monte-Carlo classical simulation of the reacceleration energy averaged over impact parameter [79]. Here it is assumed that ^{8}B projectiles break-up at the closest distance to the target. The proton and the ^{7}Be are taken as 4 fm apart just after the break-up and are allowed to follow a free Rutherford trajectory afterwards. The relative energy between the fragments at a large distance from the target is then calculated. Different initial orientations between the proton and the ^{7}Be were allowed.

The somewhat different results presented in Fig. 27(II) are inherent to the very different approaches used. The method of solving the Schrödinger equation directly yields the smallest of the results. This can be understood as follows. The methods used to calculate the dashed line and the circles assume that the break-up occurs at the distance of closest approach. This overestimates the reacceleration energy, since in a quantum mechanical approach the proton is first brought to the continuum, then tunnels the Coulomb barrier inducing a time-delay to the reacceleration process. This leads to an effective break-up position which is farther away than the distance of closest

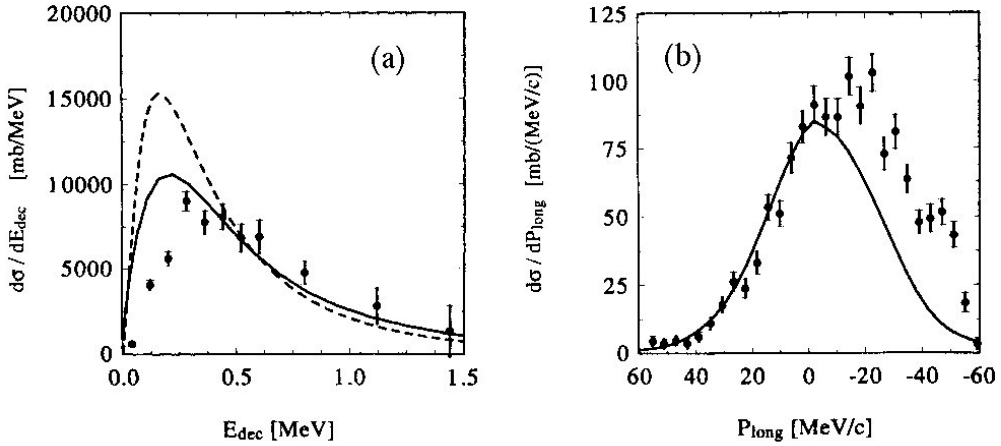

Figure 28: (a) Energy spectrum for the breakup of ^{11}Li at 28 MeV/nucleon. Data points are from [68]. Solid (dashed) line includes (does not include) the reacceleration effect [72]. (b) Longitudinal relative momentum of the neutrons and the ^{9}Li fragments in the breakup of ^{11}Li projectiles at 28 MeV/nucleon. Data are from [68]. Solid curve is a calculation from [72].

approach. One also observes from Fig. 27(II) that the reacceleration effect is more relevant at small laboratory energies.

In Ref. [72] the method of solving numerically the time-dependent Schrödinger equation are compared to the existing data on the energy spectrum of ^{11}Be and ^{11}Li break-up.

In Fig. 27(II) the non-perturbative results are shown as a dashed line. We see that the spectrum is very little influenced by the reacceleration effect. In this case, perturbation theory works very well (as in the ^{8}Be case at $E_{lab} \geq 30$ MeV/nucl.). The same is not true for the break-up of ^{11}Li at 28 MeV/nucleon. This is shown in Fig. 28(a).

The reacceleration effect is very important in this case due to the very large break-up probabilities at small impact parameters. This induces higher order dynamical continuum-continuum interactions which distort the spectrum appreciably. One also observes that although the dynamical corrections modify the spectrum in the right direction the discrepancy with the experiment is appreciable. This might be a deficiency of the cluster model and has to be studied more carefully. Also, the spectrum of the relative longitudinal momentum of the fragments is not in a good agreement with the dynamical calculations of Ref. [72], at least for the higher part of the spectrum. This is shown in the figure 28(b).

Other dynamical calculations have been performed by several authors [80, 81, 82, 78, 83], using similar methods as we discussed so far.

Supplement C

0.22 Solving the t.d. Schrödinger equation

The operations $[]\,u_\alpha$ in the r.h.s. of Eq. 338 is easy. The operation $[]^{-1}\,u'_\alpha$ is more complicated. The problem is to find the vector u in the equation

$$\mathbf{v} = \mathcal{A}^{-1}\,\mathbf{v}, \qquad \text{where} \qquad \mathbf{v} = \mathcal{A}\,\mathbf{u} \tag{347}$$

$\mathbf{u}$ is a vector composed with the $u^{(j)} = u(r_j, t)$ components of the wave-function $u(r, t)$. In Eq. 338 $\mathcal{A}$ is a tri-diagonal operator (matrix). In matrix notation

$$\begin{pmatrix} v_1 \\ v_2 \\ . \\ . \\ . \\ , \\ . \\ v_N \end{pmatrix} = \begin{pmatrix} A_1 & 0 & 0 & . & . & 0 & . \\ A_2^- & A_2 & A_2^+ & 0 & . & . & . \\ 0 & A_3^- & A_3 & A_3^+ & 0 & . & . \\ . & & & & & & \\ . & & & & & & \\ 0 & . & . & . & . & . & A_N \end{pmatrix} \begin{pmatrix} u_1 \\ u_2 \\ u_3 \\ . \\ . \\ . \\ u_N \end{pmatrix}. \tag{348}$$

This involves the following relations

$$A_i^- u_{i-1} + A_i u_i + A_i^+ u_{i+1} = v_i. \tag{349}$$

Assuming a solution of the form

$$u_{i+1} = \alpha_i u_i + \beta_i \tag{350}$$

and inserting in 349 we find the recursion relations for α_i and β_i :

$$\alpha_{i-1} = \gamma_i\, A_i^- \;, \quad \beta_{i-1} = \gamma_i \left(A_i^+ \beta_i - v_i\right) \tag{351}$$

where

$$\gamma_i = -\frac{1}{A_i + \alpha_i A_i^+}. \tag{352}$$

At the end of the lattice we assume $u_N = v_N$. This implies that $\alpha_{N-1} = 0$ and $\beta_{N-1} = v_N$.

For the problem defined by Eq. 338 we have

$$A_k = \frac{1}{i\tau} + 2 + \frac{\Delta t}{2\hbar\tau} v_\alpha^{(k)}, \quad \text{and} \qquad A_k^- = A_k^+ = -1. \tag{353}$$

We can now determine α_i and β_i by running Eqs. 351 backwards from $i = N-2$ down to $i = 1$. Then we use Eq. 350 running forward from $i = 2$ to N, assuming that u_1 at the other extreme of the lattice is given by $u_1 = v_1/A_1$.

Another way to solve the problem 348 for u is by a LU-decomposition, followed by a forward and backward substitution. This method does not need to involve the Dirichlet condition.

Let us assume that the A matrix in 348 can be written as a product of B and U matrix, where

$$A = LU = \begin{pmatrix} b_1 & c_1 & 0 & 0 & . & . \\ a_2 & b_2 & c_2 & 0 & . & . \\ 0 & a_3 & b_3 & c_3 & . & . \\ . & .. & . & .. & . & . \end{pmatrix} \tag{354}$$

$$L = \begin{pmatrix} 1 & 0 & 0 & 0 & . & . \\ \alpha_2 & 1 & 0 & 0 & . & . \\ 0 & \alpha_3 & 1 & 0 & . & . \\ 0 & 0 & \alpha_4 & 1 & . & . \\ . & . & . & . & . & . \\ . & . & . & . & . & . \end{pmatrix} \quad U = \begin{pmatrix} \beta_1 & \alpha_1 & 0 & 0 & . & . \\ 0 & \beta_2 & \gamma_2 & 0 & . & . \\ 0 & 0 & \beta_3 & \gamma_3 & . & . \\ . & . & . & . & & \\ . & . & . & . & & \end{pmatrix}. \tag{355}$$

Then, $AU = V \ \rightarrow L(Uu) = v$, or $Ly = V$. The elements of y are

$$\begin{pmatrix} y_1 \\ y_2 \\ . \\ . \\ . \\ y_N \end{pmatrix} = \begin{pmatrix} \beta_1 & \gamma_1 & 0 & 0 & . & . & . \\ 0 & \beta_2 & \gamma_2 & 0 & . & . & . \\ 0 & 0 & \beta_2 & \gamma_3 & . & . & . \\ 0 & 0 & . & . & . & . & . \end{pmatrix} \begin{pmatrix} u_1 \\ u_2 \\ u_3 \\ . \\ . \\ . \\ u_N \end{pmatrix}. \tag{356}$$

This can be solved by backwards substitution

$$u_N = \frac{y_N}{\beta_N}, \qquad \beta_i u_i + \gamma_i u_{i+1} = y_i \ , \tag{357}$$

or

$$u_i = (y_i - \gamma_1 u_i + 1) \ / \ \beta_i. \tag{358}$$

The other matrix equation

$$\begin{pmatrix} 1 & 0 & 0 & 0 & . & . \\ \alpha_1 & 1 & 0 & 0 & . & . \\ 0 & \alpha_3 & 1 & 0 & . & . \\ 0 & 0 & \alpha_4 & 1 & 0 & . \\ . & . & . & . & & . \end{pmatrix} \begin{pmatrix} y_1 \\ y_2 \\ . \\ . \\ . \\ y_N \end{pmatrix} = \begin{pmatrix} v_1 \\ v_2 \\ . \\ . \\ . \\ v_N \end{pmatrix} \tag{359}$$

can be solved by forward substitution

$$y_1 = v_1, \qquad \alpha_i y_{i-1} + y_i = v_i \ , \tag{360}$$

or

$$y_i = v_i - \alpha_i y_{i-1}. \qquad ((D.15))$$

Now, we need to find α_i and β_i as a function of the original elements of $\mathcal{A}$

$$\begin{pmatrix} 1 & 0 & 0 & 0 & . & . & . \\ \alpha_2 & 1 & 0 & 0 & . & . & \\ 0 & \alpha_3 & 1 & 0 & . & . & \\ . & . & & . & . & & \\ . & . & & . & & . & \\ . & . & & . & & & . \end{pmatrix} \begin{pmatrix} \beta_1 & \gamma_1 & 0 & 0 & 0 & . & . \\ 0 & \beta_2 & \gamma_2 & 0 & 0 & . & . \\ 0 & 0 & \beta_3 & \gamma_3 & & . & . \\ . & . & & & . & & \\ . & . & & & & . & \\ . & . & & & & & \beta_N \end{pmatrix}$$

$$= \begin{pmatrix} b_1 & c_1 & 0 & 0 & 0 & . & . \\ b_2 & b_2 & c_2 & 0 & 0 & . & . \\ 0 & a_3 & b_3 & c_3 & 0 & . & . \\ & . & . & & . & . & \\ & . & . & & . & & . \end{pmatrix}$$

which implies

$$b_1 = \beta_1, \quad b_2 = \alpha_2\gamma_1 + \beta_2, \ \cdots, \ b_i = \gamma_{i-1}\alpha_i + \beta_i.$$

or

$$\beta_i = b_i - \gamma_{i-1}\alpha_i \ , \qquad c_i = \gamma_i. \qquad (361)$$

Also,

$$a_2 = \beta_1\alpha_2, \quad a_3 = \beta_2\alpha_3, \ \cdots, \ a_i = \beta_{i-1}\alpha_i,$$

or

$$\alpha_i = \frac{a_i}{\beta_{i-1}}. \qquad (362)$$

Thus, knowing a_i, b_i and c_i, one can go upwards with this set of equations to solve the problem.

In our particular case,

$$a_i = c_i = -1. \qquad (363)$$

Thus, the above equations simplify to

$$\begin{aligned} \beta_1 &= b_1, & \beta_i &= b_i - \frac{1}{\beta_{i-1}} \ , & i &= 2, ..., N \\ y_1 &= v_1, & y_i &= v_i + \frac{y_{i-1}}{\beta_{i-1}} \ , & i &= 2, ..., N \\ u_N &= \frac{y_N}{\beta_N}, & u_i &= \frac{(y_i + u_{i+1})}{\beta_i} \ , & i &= N-1, ..., 1. \end{aligned} \qquad (364)$$

0.23 Relevance of postacceleration effects and photo-absortpion cross sections

As we have seen in the last section, postacceleration effects are manifest in theoretical calculations, and seem to have some experimental support. However, in most cases the effect is not relevant. There are also some theoretical results which deny the existence of the post-acceleration effects. Let us present a model developed by Baur, Hencken and Trautmann [84]

We consider the breakup of a particle $a = (c+n)$ (deuteron, neutron-halo nucleus) consisting of a loosely bound neutral particle n and the core c (with charge Z_c) in the Coulomb field of a target nucleus with charge Z: $a + Z \to c + n + Z$. As a further simplification the $a = (c + n)$ system is assumed to be bound by a zero range force. The bound-state wave function of the system is given by the wavefunction 238 (here we use N_0 for simplicity). The T-matrix for the reaction can be written as [85]

$$T = \left\langle \chi^{(-)}_{\mathbf{q}_c} \psi_{\mathbf{q}_n} \middle| V_{nc} \middle| \chi^{(+)}_{\mathbf{q}_a} \phi_0 \right\rangle = D_0 \int d^3R \; \chi^{(-)}_{\mathbf{q}_c}(\mathbf{R}) e^{-i\mathbf{q}_n \cdot \mathbf{R}} \chi^{(+)}_{\mathbf{q}_a}(\mathbf{R}), \tag{365}$$

with the "zero range constant" D_0 given by $D_0 = \hbar^2\sqrt{8\pi\eta}/2\mu$. The initial state is given by the incoming Coulomb wave function $\chi^{(+)}_{\mathbf{q}_a}$ with momentum $\mathbf{q}_a$ and the halo wave function ϕ_0. The final state is given by the independent motion of the core described by the outgoing Coulomb wave function $\chi^{(-)}_{\mathbf{q}_c}$ in the Coulomb field of the target nucleus Z with asymptotic momentum $\mathbf{q}_c$ and the free neutron with momentum $\mathbf{q}_n$, described by a plane wave. In these wave functions the Coulomb interaction is taken into account correctly to all orders.

There exists another form of the T-matrix element, which is not equivalent to Eq. 365. It is called the *"prior-form"* [67]. The final state is described by a c.m. motion of the $(c + n)$ system (as a Coulomb wave function) and a relative wave function of the unbound $(c + n)$ system.

The present *"post-form"* description, Eq. 365 includes the effects of "postacceleration". "Postacceleration" arises in a purely classical picture of the breakup process. The nucleus $a = (c+n)$ moves up the Coulomb potential, loosing the appropriate amount of kinetic energy. At the "breakup point", this kinetic energy (minus the binding energy) is supposed to be shared among the fragments according to their mass ratio (assuming that the velocities of c and n are equal). Running down the Coulomb barrier, the charged particle c alone (and not the neutron) gains back the Coulomb energy, resulting in its "postacceleration". Of course this picture is based on the purely classical interpretation of this process, and will be modified in a quantal treatment, where such a "breakup point" does not exist. The semiclassical limit of the theory in this case can be found, e.g., in [86]. A purely classical formula for this postacceleration, where the "breakup point" corresponds to the distance of closest approach is given in [69]. Postacceleration is clearly observed in low energy deuteron breakup, in the (fully quantal) theoretical calculations as well as in the corresponding experiments, see e.g., [87, 88].

The formula Eq. 365 is also useful for the description of the Coulomb dissociation of halo nuclei at high beam energies, see [89]. Within this theory postacceleration effects become negligibly small in the high energy region. This is seen in the numerical calculations [89] and in the analytical

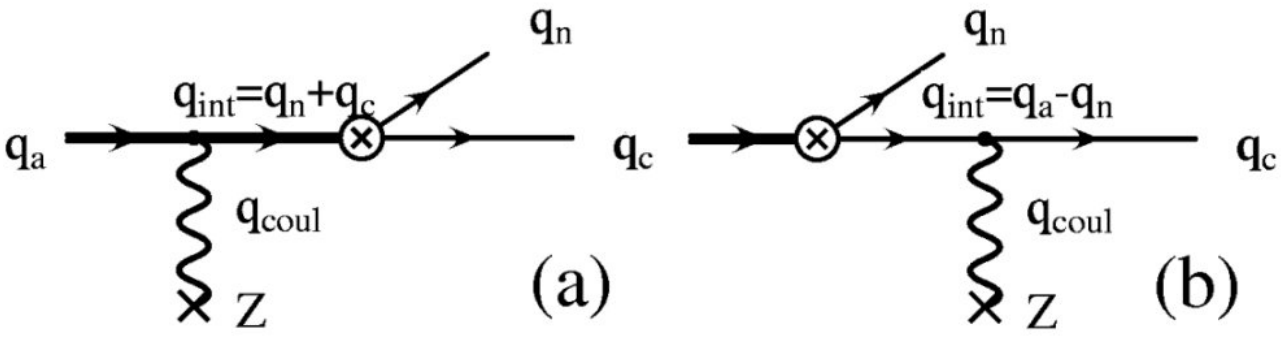

Figure 29: The two bremsstrahlung type of graphs, which describe the Coulomb breakup in the Born approximation. Three-momentum conservation at each vertex determines the intermediate momenta $\mathbf{q}_{\rm int}$.

investigations to be described below. It can, e.g., be applied to ^{11}Be and ^{19}C Coulomb dissociation experiments of Nakamura et al. [56], disregarding the importance of finite range effects.

On the other hand the 1^{st} order semiclassical Coulomb excitation theory was widely applied to the Coulomb dissociation of high energy neutron halo nuclei, see, e.g., [90]. The theory corresponds to the "prior form", mentioned above. The question of higher order electromagnetic effects was studied in [91] within this framework. These effects were found to be small, for zero range as well as finite range wave functions of the $a = (c+n)$-system. It seems interesting to note that postacceleration effects arises through higher order electromagnetic effects in straight line semiclassical theories, see [92]. Through the interference of 1^{st} and 2^{nd} order amplitudes even a "post-deceleration" can arise.

Let us try to establish the relation between the apparently very different post-form and semiclassical theory. It was noticed [90] that in the limit of Coulomb parameters $\eta_a = Z_c Z e^2/\hbar v_a \ll 1$ (i.e. in the Born approximation), where v_a denotes the velocity of particle a ($v_a = \hbar q_a/m_a$), both theories give the same result. Expanding the Coulomb wave functions up to first order in the Coulomb fields one finds

$$T_{\rm Born} = f_{\rm coul} D_0 \left[\frac{1}{q_a^2 - \left[\mathbf{q}_c + \mathbf{q}_n\right]^2} + \frac{m_n}{m_a \left[q_c^2 - \left(\mathbf{q}_n - \mathbf{q}_a\right)^2\right]} \right]. \qquad (366)$$

Here $f_{\rm coul} = 2\eta_a q_a/\left(\mathbf{q}_{\rm coul}\right)^2$ is the usual Coulomb amplitude with the "Coulomb push" $\mathbf{q}_{\rm coul} = \mathbf{q}_a - (\mathbf{q}_c + \mathbf{q}_n)$, for further details see [85]. The two terms in the parenthesis correspond to the two graphs shown in Fig. 29. For small values of $q_{\rm coul}$ the two terms almost cancel and the expansion in $q_{\rm coul}$ was found to be in agreement with the semiclassical result, see [90].

We now show that this agreement is also true in the case of arbitrary values of η_a and η_c. The beam energy must be high (compared to the binding energy E_{bind}) and the two fragments need to

be scattered into forward angles.

This is reminiscent of the result in the theory of bremsstrahlung. Replacing the neutron by a photon the diagrams of Fig. 29 are identical to the bremsstrahlung in lowest order. In this case it was already noticed that the Born result remains valid for arbitrary values of η for high energies and small scattering angles [93]. Here we want to show that the same applies in this case.

The T-matrix can be evaluated analytically in this model due to well known Nordsieck formula [94] (see Eqs. (11)–(13) of [85]). Using this formula one obtains the T-matrix Eq. 365 in terms of a hypergeometric function F as well as its derivative F'. The argument of the hypergeometric function F (and F') is given by [85, 89]:

$$\zeta(\lambda) = \frac{2q_{\rm coul}^2(q_a q_c + \mathbf{q}_a\mathbf{q}_c) - 4(\mathbf{q}_{\rm coul}\mathbf{q}_a + \lambda q_a)(\mathbf{q}_{\rm coul}\mathbf{q}_c - \lambda q_c)}{(q_{\rm coul}^2 - 2\mathbf{q}_{\rm coul}\mathbf{q}_a - 2\lambda q_a)(q_{\rm coul}^2 + 2\mathbf{q}_{\rm coul}\mathbf{q}_c - 2\lambda q_c)}.$$

We observe that (for $\lambda = 0$) this parameter $\zeta(0)$ is found to be negative and $-\zeta(0) \gg 1$ for beam energy large compared to the binding energy and for perpendicular momentum transfers $q_\perp \gg 2\eta_a q_\parallel$ (nonadiabatic case), where $q_\parallel = \omega/v$ with $\hbar\omega = E_{\rm bind} + E_{\rm rel}$ and where the relative energy between c and n is $E_{\rm rel} = \hbar^2 q^2/2\mu$ with the relative momentum given by $\mathbf{q} = (m_c\mathbf{q}_n - m_n\mathbf{q}_c)/m_a$. It was already noticed in the numerical evaluation of the process, due to $-\zeta(0) \gg 1$, that the hypergeometric series does not converge and an analytic continuation had to be used. Here we use this fact to our advantage and make a linear transformation to get the argument of the hypergeometric function close to 0. The transformation used leads to the argument of the hypergeometric function $z = 1/(1-\zeta(0))$ (Eq. 15.3.7 of [95]). In this respect this approach differs from the one used in the bremsstrahlung case, where a transformation giving an argument close to one is used. Using only the lowest order term in the hypergeometric series one obtains after some algebra (up to an overall phase)

$$T \approx 4\pi\ D_0\ f_{\rm coul}\ e^{-\pi\xi/2}\left[e^{-i\phi}\frac{1}{q_a^2 - (\mathbf{q}_n + \mathbf{q}_c)^2} + e^{+i\phi}\frac{m_c}{m_a}\ \frac{1}{q_c^2 - (\mathbf{q}_n - \mathbf{q}_a)^2}\right]. \qquad (367)$$

Hereby, the relative phase is $\phi = \sigma_0(\eta_c) - \sigma_0(\eta_a) - \sigma_0(\xi) - \xi/2\log|\zeta(0)|$. The $\sigma_0(\eta) = \arg\Gamma(1+i\eta)$ are the usual Coulomb phase shifts, and $\xi = \eta_c - \eta_a$. The correspondence to the Born result is clearly seen. One only has an additional prefactor $e^{-\pi\xi/2}$ and a relative phase $e^{\pm i\phi}$ between the two terms. The phase ϕ obviously is higher orders, $\mathcal{O}(\xi)$. Since $v_c \sim v_a$ the quantity ξ is usually very small and so is ϕ for the cases of [56]. The prefactor is also well known in the semiclassical theory, where it accounts for the replacement of the "Coulomb displaced" trajectories with the straight line trajectories. Both corrections vanish in the limit $\xi \to 0$ and the result coincides with the usual Born approximation (even if η_a and η_c are not small).

We have seen that the T-matrix in the case of large Coulomb parameters η_a and η_c corresponds to the Born result (small Coulomb parameter) in the sudden (or nonadiabatic) case $q_\perp \gg 2\eta_a q_\parallel$. We note that the derivation of Eq. (367) only depends on the condition $-\zeta(0) \gg 1$ (and not on the values of the η's). For $\eta_a, \eta_c \gg 1$ one can define a classical path for both a and c in the initial and final state and Eq. (367) can be related to the semiclassical approach.

In many experimental situations the Coulomb push $\mathbf{q}_{\rm coul}$ is small. One can expand Eq. (366)

or Eq. (367) with $\phi = \xi = 0$ for small values of $q_{\rm coul}$. One obtains

$$T = f_{\rm coul} \frac{2D_0}{\pi^2} \frac{m_n^2 m_c}{m_a^3} \frac{2\mathbf{q}\cdot\mathbf{q}_{\rm coul}}{(\kappa^2+q^2)^2}. \tag{368}$$

This result is in remarkable agreement with the usual 1^{st} order treatment of electromagnetic excitation in the semiclassical approximation.

In the semiclassical approach the scattering amplitude is given by the elastic scattering (Rutherford) amplitude times an excitation amplitude $a(b)$, where the impact parameter is related to the $q_\perp$ and η. The absolute square of $a(b)$ gives the breakup probability $P(b)$, in lowest order (LO). It is given by [90, 91]

$$\frac{dP_{\rm LO}}{dq} = \frac{16y^2}{3\pi\eta} \frac{x^4}{(1+x^2)^4},$$

where the variable x is related to the relative momentum between n and c by $x = q/\eta$ and y is a strength parameter given by

$$y = \frac{2ZZ_c m_n e^2}{\hbar v_a m_a b\eta}. \tag{369}$$

This formula shows very interesting scaling properties: Very many experiments, for neutron halo nuclei with different binding energy, beam energy, scattering angles (or $\mathbf{q}_n$ and $\mathbf{q}_c$) all lie on the same universal curve! (Corrections for finite values of $\xi_{\rm eff} = \omega b/v = \xi(\theta) = 2\eta_a q_\parallel/q_\perp$ should also be applied, according to [91].).

Postacceleration effects are also of importance for the use of Coulomb dissociation for the study of radiative capture reactions of astrophysical interest. They could also affect the extraction of photo-neutron cross sections [96] by using the Coulomb dissociation of radioactive nuclear beams. The effect has to be considered for each particular case, in order to access its relevance. For the cases in which Coulomb reacceleration is known to be of minor relevance, the Coulomb excitation of halo nuclei is a powerfull tool to access the information on the photo-absorption cross sections. As an example we show in Figure 30 the dipole strength distributions for ^{6}He as measured by Aumann and collaborators [97]. The agreement with the E1 response, as calculated by Cobis et al.[98] and by Danilin et al. [99] in the three-body framework is quite reasonable.

In Fig. 31 we show the photoneutron cross sections $\sigma_{(\gamma,xn)}$ for ^{16}O [100] (upper-half panel) and for the unstable isotopes ^{20,22}O (lower panels) as extracted from the measured electromagnetic excitation cross section (symbols) [96]. The thresholds for decay channels involving protons (which were not observed in the experiment) are indicated by arrows. For ^{20,22}O the data are compared to the shell model calculations of Sagawa and Suzuki [101].

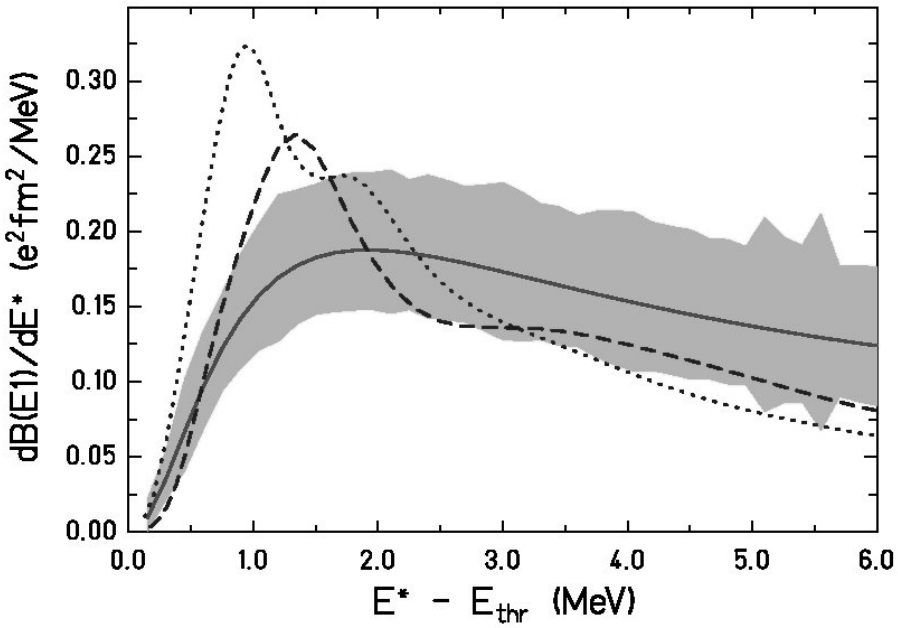

Figure 30: The dipole strength distributions for ^{6}He as measured by Aumann and collaborators [97]. The curves are adapted from Ref. [98] (dotted curve) and from Ref. [99] (dashed curve). The experimentally [97] derived E l-strength distribution and the errors are given by the solid line and the broad, shaded band, respectively. The abscissa is the excitation energy E * minus the two-neutron separation energy E_{th}, , the experimental value of which amounts to 0.975 MeV.

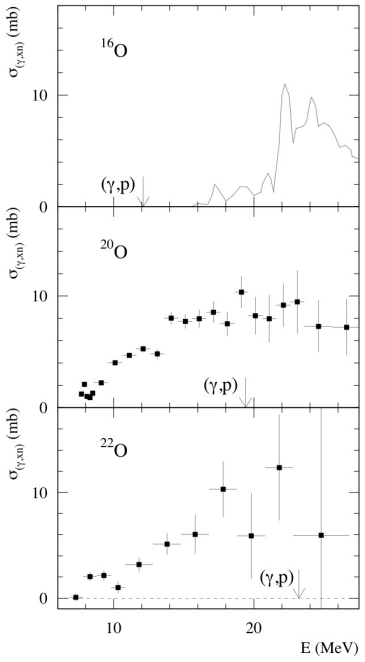

Figure 31: Photoneutron cross sections $\sigma_{(\gamma,xn)}$ for ^{16}O [100] (upper-half panel) and for the unstable isotopes ^{20,22}O (lower panels) as extracted from the measured electromagnetic excitation cross section (symbols) [96]. The thresholds for decay channels involving protons (which were not observed in the experiment) are indicated by arrows. For ^{20,22}O the data are compared to the shell model calculations [101].

Bibliography

[1] K. Alder and A. Winther, *"Coulomb Excitation"* (Academic Press, New York) 1966.

[2] K.Alder and A.Winther, *"Electromagnetic Excitation"* (North-Holland, Amsterdam) 1975.

[3] A. Winther and K. Alder, Nucl. Phys. **A319** (1979) 518.

[4] C.A. Bertulani, L.F. Canto, M.S. Hussein and A.F.R. de Toledo Piza, Phys. Rev. **C53** (1996) 334.

[5] C.A. Bertulani and V. Ponomarev, Phys. Reports **321** (1999) 139.

[6] C.A. Bertulani, Comp. Phys. Comm. **116** (1999) 345.

[7] J.D. Jackson, *"Classical Electrodynamics"* (Wiley, NY) 1975.

[8] C.A. Bertulani and G. Baur, Nucl. Phys. **A442** (1985) 73.

[9] A. Messiah, "*Quantum Mechanics*", North Holland, Amsterdam, 1961.

[10] A.N.F.Aleixo and C.A.Bertulani, Nucl. Phys. **A505** (1989) 448.

[11] L.D.Landau and E.M.Lifshitz, *"The classical theory of fields"*, 4th English ed. (Pergamon, Oxford, 1979) p. 93.

[12] C.E. Aguiar, A.N.F. Aleixo and C.A. Bertulani, Phys. Rev. **C42** (1990) 2180.

[13] M. Abramowitz and I. A. Stegun, *"Handbook of Mathematical Functions"* (National Bureau of Standards, Washington, DC) 1964.

[14] J.M. Eisenberg and W. Greiner, *"Excitation "Mechanisms of the Nuclei"* (North-Holland, Amsterdam), third edition, 1987, p. 227.

[15] G. Baur and C.A. Bertulani, Phys. Lett. **B174** (1986) 23; Nucl. Phys. **A482** (1988) 313; Phys. Rev. **C34** (1986) 1654; Proc. Int. School of Heavy Ion Physics, Erice, Italy, October 1986, Plenum Press, ed. by R.A. Broglia and G.F. Bertsch, p. 331.

[16] D.M. Brink and G.R. Satchler, *"Angular Momentum"* (Clarendon Press, Oxford, 1962).

[17] A. Bohr and B.R. Mottelson, "*Nuclear Structure*", Vol. I, Benjamim, New York, 1969.

[18] W. Bothe and W. Gentner, Z. Phys. **106** (1937) 236.

[19] M. Goldhaber and E. Teller, Phys. Rev. **74** (1948) 1046.

[20] H. Steinwedel and J.H.D. Jensen, Z. Naturforsch. **5a** (1950) 413.

[21] J. Speth and J. Wambach, *Int. Review of Nuclear and Particle Physics*, World Scientific, J. Speth, ed.,Vol. 7, (1991).

[22] F. Bertrand, Annu. Rev. Nucl. Sci. **26** (1976) 457.

[23] C.A. Bertulani and G. Baur, Phys. Rep. **163** (1988) 299.

[24] H. Emling, Prog. Part. Nucl. Phys. **33** (1994) 729.

[25] P. Chomaz and N. Frascaria, Phys. Rep. **252**, 275 (1995).

[26] T. Aumman, P.F. Bortignon and H. Emling, Ann. Rev. Nucl. Part. Sci. **48** (1998) 282.

[27] P.G. Hansen, Nucl. Phys. **A553** (1993) 89c.

[28] C.A. Bertulani, L.F. Canto and M.S. Hussein, Phys. Rep. **226** (1993) 282.

[29] J. Barrette et al., Phys. Lett. **B209** (1988) 182.

[30] J. Beene et al., Phys. Rev. **C41** (1990) 920.

[31] J. Beene, et al., *Int. Nuc. Phys. Conf. on Giant Resonances*, Gull Lake (1993), Nucl. Phys. **A569** (1994) 163c.

[32] M.S. Hussein, R.A. Rego and C.A. Bertulani, Phys. Rep. **201** (1991) 279.

[33] C.A. Bertulani and A. Nathan, Nucl. Phys. **A554** (1993) 158.

[34] I.S. Gradshteyn and I.M. Ryzhik, *"Table of Integrals, Series, and Products"* (Academic Press, New York) 1980.

[35] D. Brink, Ph.D. Thesis, Oxford, 1955, unpublished.

[36] E. Fermi, Z. Phys. **29** (1924) 315; E.J. Williams, Phys. Rev. **45** (1934) 729; C.F. Weiszäcker, Z. Phys. **88** (1934) 612.

[37] C.A. Bertulani and G. Baur, Physics Today, , March 1994, p. 22.

[38] F.E. Bertrand and J.R. Beene, Nucl. Phys. **A520** (1990) 627c.

[39] A. Veyssière, H. Beil, R. Bergère, P. Carlos and A. Leprêtre, Nucl. Phys. **A159** (1970) 561.

[40] J. Raynal, Phys. Rev. **C23** (1981) 2571.

[41] A. M. Nathan, Phys. Rev. **C43** (1991) 2479.

[42] J. Ritman et al., Phys. Rev. Lett. **70** (1993) 533.

[43] R. Schmidt et al., Phys. Rev. Lett. **70** (1993) 1767.

[44] K. Alder and A. Winther, *Coulomb Excitation* (Academic Press, New York) 1966.

[45] K.Alder and A.Winther, *Electromagnetic Excitation* (North-Holland, Amsterdam) 1975.

[46] A. Winther and K. Alder, Nucl. Phys. **A319** (1979) 518.

[47] T. Glasmacher, Annu. Rev. Nucl. Part. Sci. **48** (1998) 1.

[48] C. A. Bertulani and G. Baur, Nucl. Phys. **A442** (1985) 73.

[49] G. Baur and C.A. Bertulani, Nucl. Phys. **A480** (1988) 615.

[50] C.A. Bertulani and A. Nathan, Nucl. Phys. **A554** (1993) 158.

[51] L.F. Canto, A. Romanelli, M.S. Hussein and A.F.R. de Toledo Piza, Phys. Rev. Lett. **72** (1994) 2147.

[52] M.S. Hussein, M.P. Pato, and A.F.R. de Toledo Piza, Phys. Rev. **C51** (1995) 486.

[53] J.M. Eisenberg and W. Greiner, *"Excitation Mechanisms of the Nucleus"* (North-Holland, Amsterdam, 1970).

[54] C.A. Bertulani and A. Sustich, Phys. Rev. **C46** (1992) 2340.

[55] C.A. Bertulani, G. Baur, and M.S. Hussein, Nucl. Phys. **A526** (1991) 751.

[56] T. Nakamura, Phys. Lett. **B331** (1994) 296; T. Nakamura et al., Phys. Rev. Lett. **83** (1999) 1112.

[57] B. Zwieglinski et al., Nucl. Phys. **A315** (1979) 124.

[58] S. Shlomo and G.F. Bertsch, *Nucl. Phys.* **A243** (1975) 507

[59] G.F. Bertsch in *"Computational Nuclear Physics"*, ed. Langanke, Maruhn and Koonin, Springer, p. 75.

[60] G.F. Bertsch and J. Foxwell, Phys. Rev. **C41** (1990) 1300.

[61] S. Nakayama et al., Phys. Rev. Lett. **85** (2000) 262.

[62] N. Teruya, C.A. Bertulani, S. Krewald, H. Dias, and M.S. Hussein, Phys. Rev. **C43** (1991) R2049.

[63] Y. Alhassid, M. Gai and G.F. Bertsch, Phys. Rev. Lett. **49** (1982) 1482.

[64] S.A. Fayans, Phys. Lett. **B267** (1991) 443.

[65] H. Esbensen and G. Bertsch, Nucl. Phys. **A542** (1992) 310.

[66] L.V. Chulkov, B. Jonson and M.V. Zhukov, Europhys. Lett. **24** (1993) 171.

[67] N. Austern, "*Direct Reaction Theory*" (Wiley, New York, 1970).

[68] K. Ieki et al., Phys. Rev. Lett. **70** (1993) 730.

[69] G. Baur, C. A. Bertulani, and D. M. Kalassa, Nucl. Phys. **A550** (1995) 107.

[70] G.F. Bertsch and C.A. Bertulani, Nucl. Phys. **A556** (1993) 136.

[71] C.A. Bertulani and G.F. Bertsch, Phys. Rev. **C49** (1994) 2839.

[72] H. Esbensen, G.F. Bertsch and C.A. Bertulani, Nucl. Phys. **A581** (1995) 107.

[73] C. A. Bertulani and M. S. Hussein, Phys. Rev. Lett. **64** (1990) 1099.

[74] C.A. Bertulani and L.F. Canto, Nucl. Phys. **A539** (1992) 163.

[75] W.E. Press, S.A. Teukolsky, W.T. Vetterling, and B.P. Flannery, "*Numerical Recipes*", Cambridge University Press, 1992.

[76] H. J. Bär and G. Soff, *Physica* **C128** (1985) 225.

[77] A. Romanelli, L.F. Canto, R. Donangelo and P. Lotti, P, Phys. Lett. B558 (1995) 71.

[78] C.A. Bertulani, Z. Phys. **A356** (1996) 293.

[79] C.A. Bertulani, Nucl. Phys. **A587** (1995) 318.

[80] H. Esbensen and G. Bertsch, Phys. Lett. **B359** (1995) 13; Nucl. Phys. **A600** (1996) 37.

[81] T. Kido, K. Yabana and Y. Suzuki, Phys.Rev. **C53** (1996) 2296.

[82] S. Typel, H.H. Wolter and G. Baur, Nucl. Phys. **A613** (1997) 147.

[83] R. Shyam and I.J. Thompson, Phys. Rev. **C59** (1999) 2645.

[84] G. Baur, K. Hencken and D. Trautmann, Proceedings of ENAM2001, 3rd Int.Conference on Exotic Nuclei and Atomic Masses.

[85] G. Baur and D. Trautmann, Nucl. Phys. **A191** (1972) 321.

[86] G. Baur, M. Pauli, and D. Trautmann, Nucl. Phys. **A224** (1974) 477.

[87] G. Baur and D. Trautmann, Phys. Reports **25C** (1976) 293.

[88] G. Baur, F. Roesel, D. Trautmann and R. Shyam, Phys. Rep. **111** (1984) 333.

[89] R. Shyam, P. Banerjee, and G. Baur, Nucl. Phys. **A540** (1992) 341.

[90] G. Baur, K. Hencken, D. Trautmann, S. Typel, and H.H. Wolter, Prog. in Part. and Nucl. Phys. **46** (2001) 99.

[91] S. Typel and G. Baur, Phys. Rev. **C64** (2001) 024601.

[92] S. Typel and G. Baur, Nucl. Phys. **A573** (1994) 486.

[93] L. D. Landau and E. M. Lifschitz, *Lehrbuch der theoretischen Physik IV, Quantenelektrodynamik* (Akademie Verlag, Berlin, 1986).

[94] A. Nordsieck, Phys. Rev. **93** (1954) 785.

[95] M. Abramowitz and I.A. Stegun, *Handbook of Mathematical Functions* (National Bureau of Standards, Washington, DC, 1964)..

[96] A. Leistenschneider et al., Phys. Rev. Lett. **86** (2001) 5442 .

[97] T. Aumann et al., Phys. Rev. **C59** (1999) 1252.

[98] A. Cobis, D. Fedorov and A. Jensen, Phys. Rev. Lett. **79** (1997) 2411.

[99] B.V. Danilin, M.V. Zhukov, J.S. Vaagen and J.M. Bang, Phys. Lett. **B302** (1993) 129.

[100] E. G. Fuller, Phys. Rep. **127** (1985) 187; A. Vessière et al., Nucl. Phys. **A227** (1974) 513; B. L. Berman, At. Data Nucl. Data Tables **15** (1975).319.

[101] H. Sagawa and T. Suzuki, Phys. Rev. **C59** (1999) 3116.